

**MESOPOROUS AND MICROPOROUS METALLO-
SILICATE & ORGANO-SILICATE MOLECULAR
SIEVES : SYNTHESIS, CHARACTERIZATION
AND CATALYTIC PROPERTIES**

A THESIS
SUBMITTED TO THE
UNIVERSITY OF PUNE
FOR THE DEGREE OF
DOCTOR OF PHILOSOPHY
(IN CHEMISTRY)

BY
SUBHASH CHANDRA LAHA

CATALYSIS DIVISION
NATIONAL CHEMICAL LABORATORY
PUNE 411 008
INDIA

MARCH 2002

.....dedicated to my
beloved parents

ACKNOWLEDGEMENTS

I find it difficult for me to write something in short to acknowledge my research guide, Dr. Rajiv Kumar. He has taught me to think, and solve the unconventional problems in a conventional way. His constant inspiration, invaluable guidance and constructive criticism helped a lot to focus my views in the proper perspective. I take this opportunity to express my deepest sense of gratitude and reverence towards him for guiding me in the right direction throughout the course of this work. My deep personal regards are due for him forever.

I am thankful to Dr. A. P. Singh for his constant encouragement both in professional as well as in personal level. My sincere thanks are due to Dr. C. Gopinathan, Dr. S. Sivasanker, Dr. D. Srinivas, Dr. A. A. Belhekar, Dr. S. P. Mirajkar, Dr. H. S. Soni, Dr. S. A. Pardhy, Dr. C. V. V. Satyanarayana, Dr. V. R. K. Murthy, Dr. P. Manikandan, Nalini madam, Violet madam, Seema madam, and all other scientific and non-scientific staff of Catalysis Division for their help and encouragement.

The invaluable help I received from Dr. S. R. Sainkar for SEM, Dr. R. Parischa, Dr. R. Gonnade and Dr. M. Bhadbhade for TEM, Dr. S. Ganapathy and Dr. P. Rajamohanam for NMR, and Mr. Bhujang for drawing is also appreciated.

It gives me great pleasure to thank my labmates, Priyoda, Deenu, Chitta, Anirban, Senapati, Mahesh, Raina and Rajesh for their constant help, encouragement and the nice time I had with them.

I would like to thank my friends Tapas, Chandranath, Pranab, Shrabanti, Kaushik, Sachin, Sushama, Vandana, Venkatesh, Chidam, Muthu, Thomas, Shiju, Pai, Anand, Suresh, Bennur, Balakrishna, Tresa, Biju, Subarnoda, Saptarshida, Mahuadi, Bikash, Kausik, Atashi, Arijit, Sarbani, Anjan, Sujata, Somnath, Debasish, Arindam, Kousik, Tarun, Anuradha, Bibhas, Debudut, Saikat, Sumit, Samanta, Prabal, Utpal, Dilip, Sukhen, Rajaram, Kshudiram, Sumanda and Boudi, Shubho, Annyt, Babu, Aditya, Lahada, Majida, Anuji, Pandey and Jitu for their inspiration, encouragement and help.

I would like to express my profound gratitude to Dr. A. V. Ramaswamy, Head, Catalysis Division, not only formally for allowing me to use all the available facilities in

the division but also personally for many stimulating discussions and guidance throughout the course of this investigation.

It gives me great pleasure to thank my parents, sister and grandmother for their love, unflinching support, tremendous patience, trust and encouragement during many years of studies that they have shown to me in their own special way. They have been my constant source of strength and determination, and have brought a great deal of happiness to my life.

I would like to confess that even though I try my best, it is not possible for me to acknowledge and thank all those known and unknown faces individually for their direct and indirect contribution for the successful completion of this work. I am grateful to all of you for your kind cooperation.

Finally, my thanks are due to Council of Scientific and Industrial Research, Government of India, for awarding me the research fellowship, and to Dr. Paul Ratnasamy, Director, National Chemical Laboratory, Pune for allowing me to carry out my research and extending all possible infrastructural facilities at NCL, and to submit this work in the form of a thesis for the award of the Ph. D. degree.

Subhash Chandra Laha

Table of Contents

List of Contents	i
List of Figures	vi
List of Schemes	xi
List of Tables	xii
Abbreviations	xiv

1. INTRODUCTION

1.1. GENERAL BACKGROUND AND INTRODUCTION	1
1.2 SYNTHESIS AND MECHANISMS FOR THE FORMATION OF MESOPOROUS MATERIALS	4
1.2.1. Liquid Crystal Templating (LCT) mechanism	4
1.2.2. Silicate Rod Assembly	5
1.2.3. Charge Density Matching and Folding Sheets	6
1.2.4. Silicatropic Liquid Crystals	7
1.2.5. Generalized Liquid Crystal Templating Mechanism	8
1.2.5.1. <i>Electrostatic Interaction</i>	8
1.2.5.2. <i>Hydrogen Bonding Interaction</i>	9
1.2.5.3. <i>Covalent Interactions</i>	10
1.3. METAL-SUBSTITUTED MESOPOROUS MOLECULAR SIEVES	10
1.4. MESOPOROUS SILICATES AS SUPPORT/HOST	10
1.4.1. Immobilization of Metals/Metal Complexes in Mesoporous Silicates	10
1.4.2. Covalently Anchored Organo-Functionalized Mesoporous Silicates	11
1.4.2.1. <i>In situ Synthetic Methods</i>	11
1.4.2.2. <i>Post Synthetic Methods</i>	11
1.5 CONTROL OF CRYSTAL AND PORE SIZES	12
1.6. CONTROL OF MORPHOLOGY	13
1.7. PHYSICO-CHEMICAL CHARACTERIZATION	13
1.7.1. X-ray Diffraction	14
1.7.2. Adsorption Measurements	14

1.7.3.	Diffuse Reflectance UV-Vis Spectroscopy	15
1.7.4.	Fourier-Transform Infrared (FTIR) Spectroscopy	15
1.7.5.	Nuclear Magnetic resonance (NMR) Spectroscopy	16
1.7.6.	Electron Paramagnetic Resonance (EPR) Spectroscopy	16
1.7.7.	Scanning Electron Microscopy (SEM)	16
1.7.8.	Transmission Electron Microscopy (TEM)	17
1.7.9.	Thermal Analysis (TG-DTA)	17
1.8.	CATALYTIC APPLICATIONS AND PROSPECT	17
1.8.1.	Acid Catalysis	18
1.8.2.	Redox Catalysis	19
1.9.	SCOPE AND OBJECTIVES OF THE THESIS	21
1.10.	OUTLINE OF THE THESIS	24
1.11.	REFERENCES	26
2.	SYNTHESIS	
2.1.	EXPERIMENTAL	36
2.1.1.	Materials	36
2.1.2.	Synthesis of MCM-41 Type Mesoporous Materials	36
2.1.2.1.	<i>Synthesis of Si-MCM-41</i>	37
2.1.2.2.	<i>Synthesis of Al-MCM-41</i>	38
2.1.2.3.	<i>Synthesis of Ti- and V-MCM-41</i>	39
2.1.2.4.	<i>Synthesis of Ce-containing MCM-41 Type Mesoporous Materials</i>	40
2.1.2.4.1.	Synthesis of Ce-MCM-41	40
2.1.2.4.2.	Synthesis of Ce-impregnated MCM-41	41
2.1.2.4.3.	Synthesis of Ce-exchanged MCM-41	41
2.1.2.4.4.	Synthesis of amorphous silica-ceria	41
2.1.2.3.	<i>Synthesis of Organo-functionalized MCM-41</i>	41
2.1.3.	Synthesis of TS-1 and TS-2	43
2.1.3.1.	<i>Synthesis of TS-1</i>	43
2.1.3.2.	<i>Synthesis of TS-2</i>	44
2.2.	RESULTS AND DISCUSSION	45
2.2.1.	Synthesis of Si-MCM-41	45
2.2.1.1.	<i>Effect of time</i>	45

2.2.1.1.	<i>Effect of different promoters</i>	48
2.2.1.1.	<i>Effect of promoter concentrations</i>	49
2.2.1.1.	<i>Effect of different sources of phosphate (PO_4^{3-}) promoter</i>	50
2.3.	REFERENCES	52
3.	CHARACTERIZATION	
3.1.	EXPERIMENTAL	53
3.1.1.	X-ray Diffraction	53
3.1.2.	Chemical Analyses	53
3.1.3.	Adsorption Measurements	54
3.1.4.	Diffuse Reflectance UV-Vis Spectroscopy	54
3.1.5.	Fourier-Transform Infrared (FTIR) Spectroscopy	54
3.1.6.	Pyridine and Ammonia Sorption	54
3.1.7.	Nuclear Magnetic Resonance (NMR) Spectroscopy	55
3.1.8.	Electron Paramagnetic Resonance (EPR) Spectroscopy	55
3.1.9.	Scanning Electron Microscopy (SEM)	56
3.1.10.	Transmission Electron Microscopy (TEM)	56
3.1.11.	Thermal Analysis (TG-DTA)	56
3.2.	RESULTS AND DISCUSSION	57
3.2.1.	MCM-41 Type Mesoporous Materials	57
3.2.1.1.	<i>Si-MCM-41</i>	57
3.2.1.2.	<i>Al-MCM-41</i>	61
3.2.1.2.1.	FTIR spectra of chemisorbed pyridine	65
3.2.1.3.	<i>Ti- and V-MCM-41</i>	67
3.2.1.3.1.	Diffuse Reflectance UV-Vis Spectroscopy	67
3.2.1.3.2.	IR Spectroscopy	69
3.2.1.3.3.	^{51}V MAS NMR	69
3.2.1.3.4.	Diffuse Reflectance UV-Vis Spectroscopy of Ti-MCM-41-P (50) : Interaction with aqueous hydrogen peroxide (HP) and urea-hydrogen peroxide (UHP)	69
3.2.1.3.5.	EPR Spectroscopy of Ti-MCM-41-P (50) : Interaction with HP and UHP	72

3.2.1.4.	<i>Ce-MCM-41</i>	73
3.2.1.4.1.	Powder X-ray Diffraction	73
3.2.1.4.2.	N ₂ adsorption	75
3.2.1.4.3.	Diffuse Reflectance UV-Vis Spectroscopy	78
3.2.1.4.4.	FTIR Spectroscopy	79
3.2.1.4.5.	FTIR Spectra of Chemisorbed Pyridine	82
3.2.1.4.6.	FTIR Spectra of Chemisorbed Ammonia	83
3.2.1.4.7.	¹³ C CP MAS NMR	85
3.2.1.4.8.	²⁹ Si MAS NMR	87
3.2.1.4.9.	SEM and EDX	89
3.2.1.4.10.	TEM	89
3.2.1.4.11.	TG-DTA	92
3.2.1.5.	<i>Organo-functionalized MCM-41</i>	93
3.2.1.5.1.	Powder X-ray Diffraction	93
3.2.1.5.2.	C, H, N and S analysis	93
3.2.1.5.3.	N ₂ adsorption	94
3.2.1.5.4.	Diffuse Reflectance IR Spectroscopy	96
3.2.1.5.5.	¹³ C CP MAS NMR	97
3.2.1.5.6.	²⁹ Si CP MAS NMR	98
3.2.2.	TS-1 and TS-2	100
3.2.2.1.	<i>Diffuse Reflectance UV-Vis Spectroscopy : Interaction with HP and UHP</i>	101
3.2.2.2.	<i>EPR Spectroscopy : Interaction with HP and UHP</i>	102
3.3.	REFERENCES	105
4.	CATALYTIC PROPERTIES	
4.1.	ACID CATALYZED REACTIONS	108
4.1.1.	Experimental	108
4.1.1.1.	<i>Isopropylation of Naphthalene</i>	108
4.1.1.2.	<i>Dehydration of Cyclohexanol</i>	109
4.1.1.3.	<i>Acylation of Alcohols, Amines, Thiols and Phenols</i>	109
4.1.2.	Results and Discussion	110
4.1.2.1.	<i>Isopropylation of Naphthalene over Al-MCM-41</i>	110
4.1.2.2.	<i>Dehydration of Cyclohexanol over Ce-MCM-41</i>	111

4.1.2.3.	<i>Acylation of Alcohols, Amines, Thiols and Phenols over Ce-MCM-41</i>	112
4.2.	OXIDATION REACTIONS	120
4.2.1.	Experimental	120
4.2.1.1.	<i>Hydroxylation of 1-Naphthol</i>	120
4.2.1.2.	<i>Epoxidation Reactions</i>	121
4.2.2.	Results and Discussion	121
4.2.2.1.	<i>Hydroxylation of 1-Naphthol over V-, Ti- and Ce-MCM-41</i>	121
4.2.2.2.	<i>Epoxidation Reactions</i>	126
4.2.2.2.1.	Epoxidation of Cyclohexene over Ti-MCM-41 and V-MCM-41	126
4.2.2.2.2.	Epoxidation of Styrene and Allylbenzene over TS-1 and TS-2	128
4.2.2.2.3.	Epoxidation of Allyl alcohol, Allyl chloride, Allyl bromide and Methylallyl chloride over TS-1	137
4.2.2.2.4.	Epoxidation of 1-Hexene and Cyclohexene over TS-1 and TS-2	139
4.2.2.2.5.	Explanation for high epoxide selectivity over titano-silicate/U+HP or UHP systems	141
4.3.	REFERENCES	143
5.	SUMMARY AND CONCLUSIONS	144

List of Figures

Figure 1.1	Number of publications on ordered mesoporous materials as found by Chemical Abstracts on Compact Disks (CA on CD) of the American Chemical Society using different keywords (MCM-41 or FSM-16 or SBA-15 or mesoporous materials or ordered mesoporous oxides or ordered mesoporous materials).	3
Figure 2.1	Change of X-ray diffraction pattern with time (h) in hydrothermal synthesis of as-synthesized Si-MCM-41-P prepared in the presence of promoter (NaH_2PO_4).	46
Figure 2.2	^{29}Si MAS NMR spectra of as-synthesized Si-MCM-41-S (without promoter) and Si-MCM-41-P (with promoter) samples measured at different time interval (h) and corresponding calcined (end) samples. $Q_2 : Q_3 : Q_4$ ratios of different samples were calculated using Jandel Scientific PeakFit deconvolution program.	47
Figure 2.3	Correlation between the synthesis time and the charge/radius ($Z/r, \text{\AA}^{-1}$) ratio of the central cation of the promoter in the synthesis of Si-MCM-41.	48
Figure 2.4	Effect of promoter (NaH_2PO_4) concentration on the synthesis time of Si-MCM-41-P.	49
Figure 3.1	Nitrogen adsorption-desorption isotherm and pore size distribution (inset) for Si-MCM-41-P. The pore size distribution is calculated by plotting derivative of pore volume and pore radius (DV_p/DR_p) against pore diameter (P. D.).	59
Figure 3.2	Framework IR spectra of calcined Si-MCM-41-P (a), Al-MCM-41-P (50) (b), Ti-MCM-41-P (50) (c) and V-MCM-41-P (50) (d).	61
Figure 3.3	^{13}C CP MAS NMR spectra of CTA^+ ions in solution (CDCl_3) and as-synthesized Si-MCM-41-P, Al-MCM-41-P (50), Ti-MCM-41-P (50) and V-MCM-41-P (50). The triplet observed at <i>ca.</i> 77 ppm for CTABr is due to solvent (CDCl_3).	62
Figure 3.4	Scanning electron micrographs of calcined Si-MCM-41-P having different types of particle morphology : (a) worm type and (b) hexagonal type.	63

Figure 3.5	Transmission electron micrographs of calcined Si-MCM-41-P (a) and Ti-MCM-41-P (50) (b).	63
Figure 3.6	X-ray diffraction pattern of as-synthesized Si-MCM-41-P, Al-MCM-41-P (50), Ti-MCM-41-P (50) and V-MCM-41-P (50).	64
Figure 3.7	^{27}Al MAS NMR spectra of calcined Al-MCM-41-S (50) (a) and Al-MCM-41-P (50) (b).	65
Figure 3.8	FTIR spectra of chemisorbed pyridine on Al-MCM-41-P (50) sample at desorption temperatures of 373 (a), 473 (b), 573 (c) and 673 K (d).	66
Figure 3.9	Diffuse reflectance UV-Vis spectra of calcined V-MCM-41-P (50) and Ti-MCM-41-P (50).	68
Figure 3.10	^{51}V MAS NMR spectra of calcined V-MCM-41-S (50) (a) and V-MCM-41-P (50) (b).	70
Figure 3.11	Diffuse reflectance UV-Vis spectra of calcined Ti-MCM-41-P (50) (a), Ti-MCM-41-P (50) + UHP (b), Ti-MCM-41-P (50) + H_2O (c), Ti-MCM-41-P (50) + UHP + Acetone (d) and Ti-MCM-41-P (50) + aqueous H_2O_2 (e).	71
Figure 3.12	EPR spectra of Ti-MCM-41-P (50) + UHP (A) and Ti-MCM-41-P (50) + HP (B).	72
Figure 3.13	X-ray diffraction patterns of as-synthesized (a) Si-MCM-41, (b) Ce-MCM-41-R (160), (c) Ce-MCM-41-R (80), (d) Ce-MCM-41-R (40), (e) Ce-MCM-41-R (20), (f) Ce-exchanged MCM-41.	74
Figure 3.14	Nitrogen adsorption-desorption isotherm and pore size distribution (inset) for Ce-MCM-41-R (40).	76
Figure 3.15	Diffuse reflectance UV-Vis spectra of calcined (a) Ce-MCM-41-R (20), (b) Ce-MCM-41-R (40), (c) Ce-MCM-41-R (80), (d) Ce-MCM-41-R (160), (e) Ce-exchanged MCM-41 and (f) $\text{SiO}_2\text{-CeO}_2$ (20).	79
Figure 3.16	IR spectra in the framework and the hydroxyl vibration region of calcined (a) Si-MCM-41, (b) Ce-MCM-41-R (160), (c) Ce-MCM-41-R (80), (d) Ce-MCM-41-R (40) and (e) Ce-MCM-41-R (20).	81
Figure 3.17	FTIR spectra of chemisorbed pyridine on Ce-MCM-41-R (40) at desorption temperatures of 373 (a), 423 (b), 473 (c) and 523 K (d).	83

Figure 3.18	FTIR spectra of Ce-MCM-41-R (40) in the 1800-1300 cm^{-1} region after being exposed to gaseous NH_3 for 30 min (a) and at desorption temperatures of 373 (b), 423 (c), 473 (d) and 523 K (e).	84
Figure 3.19	FTIR spectra of Ce-MCM-41-R (40) in the 3500-2700 cm^{-1} region after being exposed to gaseous NH_3 for 30 min.	85
Figure 3.20	^{13}C CP MAS NMR spectra of as-synthesized (a) Ce-MCM-41-R (40), (b) Si-MCM-41 and (c) CTMA ⁺ ions in solution (CDCl_3).	87
Figure 3.21	^{29}Si MAS NMR spectra of calcined (a) Ce-MCM-41-R (40) and (b) Si-MCM-41.	88
Figure 3.22	Scanning electron micrographs of calcined Ce-MCM-41-R (40) sample having different types of particle morphology : (a) winding worm type, (b) hexagonal type and (c) unique hexagonal rod type.	90
Figure 3.23	Transmission electron micrographs of calcined Ce-MCM-41-R (80) sample : (a) parallel fringes (side-on view), (b) hexagonal array (viewed along the pore direction) and (c) selected area electron diffraction pattern of (b).	91
Figure 3.24	TGA-DTA curves of as-synthesized (a) Si-MCM-41 and (b) Ce-MCM-41-R (40).	92
Figure 3.25	X-ray diffraction patterns of as-synthesized HS-MCM-41 (A), H_2N -MCM-41 (B), HS- H_2N -MCM-41 (C), HS-Al-MCM-41 (D) and Vinyl-MCM-41 (E).	94
Figure 3.26	IR spectra of H_2N -MCM-41 and HS-MCM-41 after removal of the template (surfactant) by acid-solvent extraction.	96
Figure 3.27	^{13}C CP MAS NMR spectrum of template free HS-MCM-41.	97
Figure 3.28	^{13}C CP MAS NMR spectrum of template free H_2N -MCM-41.	98
Figure 3.29	^{29}Si CP MAS NMR spectrum of template free HS-MCM-41.	99
Figure 3.30	^{29}Si CP MAS NMR spectrum of template free H_2N -MCM-41.	100
Figure 3.31	Comparison of diffuse reflectance UV-Vis spectra of different TS-1 (Figure 1A) and TS-2 (Figure 1B) samples: calcined TS-1 and TS-2 (curves 'a' and 'f'), TS-1/TS-2 + UHP (curves 'b' and 'g'), TS-1/TS-2 + H_2O (curves 'c' and 'h'), TS-1/TS-2 + UHP + Acetone (curves 'd' and 'i') and TS-1/TS-2 + aqueous H_2O_2 (curves 'e' and 'j').	102

- Figure 3.32 Comparison of EPR spectra of different TS-1 + UHP (A), TS-1 + aqueous H₂O₂ (B), TS-2 + UHP (C) and TS-2 + aqueous H₂O₂ (D). 103
- Figure 4.1 Comparison of catalytic activity and selectivity of Al-MCM-41-S and Al-MCM-41-P samples. S_{1-IPN} = Selectivity of 1-isopropyl-naphthalene; S_{2-IPN} = Selectivity of 2-isopropyl-naphthalene; S_{DIPNs} = Selectivity of diisopropyl-naphthalenes. 110
- Figure 4.2 Activity of Ce-MCM-41 samples in the dehydration of cyclohexanol to cyclohexene. () Ce-MCM-41-R, (?) Ce-MCM-41-P (40), (?) Ce-MCM-41-A (40), (?) Ce-EX-MCM-41, (o) Ce-Im-MCM-41 (20) and (x) SiO₂-CeO₂ (20). 111
- Figure 4.3 Effect of reaction temperature on the epoxidation of styrene. Reaction conditions: Catalyst TS-1 (20 wt% with respect to styrene); styrene : H₂O₂ (mol/mol) = 4.0; styrene : acetone (wt/wt) = 1.0; reaction time = 12 h. (A) Comparison of styrene conversion with different H₂O₂ sources: (i) HP, (?) U+HP, and (?) UHP. (B) Comparison of selectivities for styrene oxide (solid symbol) and benzaldehyde + phenylacetaldehyde (open symbol) with different H₂O₂ sources: (i ?) HP, (? ?) U+HP, and (? Δ) UHP. 131
- Figure 4.4 Effect of reaction time on the epoxidation of styrene. Reaction conditions: Temperature = 313 K; catalyst TS-1 (20 wt% with respect to styrene); styrene : H₂O₂ (mol/mol) = 4.0; styrene : acetone (wt/wt) = 1.0. (A) Comparison of styrene conversion with different H₂O₂ sources: (i) HP, (?) U+HP, and (?) UHP. (B) Comparison of selectivities for styrene oxide (solid symbol) and benzaldehyde + phenylacetaldehyde (open symbol) with different H₂O₂ sources: (i ?) HP, (? ?) U+HP, and (? Δ) UHP. 132
- Figure 4.5 Effect of styrene to H₂O₂ molar ratios on the epoxidation of styrene. Reaction conditions: Temperature = 313 K; catalyst TS-1 (20 wt% with respect to styrene); styrene : acetone (wt/wt) = 1.0; reaction time = 12 h. (i) Styrene conversion, (?) styrene oxide (SO) selectivity and (?) benzaldehyde + phenylacetaldehyde (B + P) selectivity. 133

- Figure 4.6 Effect of acetone to styrene weight ratios on the epoxidation of styrene. Reaction conditions: Temperature = 313 K; catalyst TS-1 (20 wt% with respect to styrene); styrene : H₂O₂ (mol/mol) = 40; reaction time = 12 h. (◊) Styrene conversion, (○) styrene oxide (SO) selectivity and (□) benzaldehyde + phenylacetaldehyde (B + P) selectivity. 135
- Figure 4.7 Effect of catalyst concentration on the epoxidation of styrene. Reaction conditions: Temperature = 313 K; styrene : H₂O₂ (mol/mol) = 4.0; styrene : acetone (wt/wt) = 1.0; reaction time = 12 h. (◊) Styrene conversion, (○) styrene oxide (SO) selectivity and (□) benzaldehyde + phenylacetaldehyde (B + P) selectivity. 136
- Figure 4.8 Effect of urea to H₂O₂ molar ratios on the epoxidation of styrene. Reaction conditions: Temperature = 313 K; catalyst TS-1 (20 wt% with respect to styrene); styrene : H₂O₂ (mol/mol) = 4.0; styrene : acetone (wt/wt) = 1.0; reaction time = 12 h. (◊) Styrene conversion, (○) styrene oxide (SO) selectivity and (□) benzaldehyde + phenylacetaldehyde (B + P) selectivity. 137

List of Schemes

- Scheme 1.1 Liquid crystal templating mechanism proposed for the formation of MCM-41: (A) liquid crystal phase initiated and (B) silicate anion initiated. 5
- Scheme 1.2 Silicate rod assembly proposed for the formation of MCM-41: (1) and (2) involve the random ordering of rod-like micelles and interaction with silicate species; (3) represents the spontaneous packing of the rods and (4) is the remaining condensation of silicate species upon final heating of the organic/inorganic composites. 6
- Scheme 1.3 Mechanisms proposed for the transformation of surfactant-silicate systems from lamellar to hexagonal mesophases. (A) Hexagonal mesophase obtained by charge density matching and (B) folding of kanemite silicate sheets around intercalated surfactant molecules formed the hexagonal mesostructure. 7
- Scheme 1.4 The model (cooperative organization) for the formation of silicatropic liquid crystal phase/silicate-surfactant mesophases. (A) represents the organic and inorganic precursor solutions, (B) represents the preliminary interaction of the two precursor solutions after mixing, and (C) represents the multidentate interaction of the oligomeric silicate units with the surfactant molecules. 8
- Scheme 4.1 Different cyclic Ti-species active for epoxidation reactions. 141

List of Tables

Table 1.1	Pore-size regimes and representative porous silica based materials.	2
Table 1.2	Oxidation catalysis reported over mesoporous metallo-silicate molecular sieves.	20
Table 2.1	Chemical compositions of the synthesis gel mixtures ($\text{Si}/\text{M} = 50$) and effect of promoter in the synthesis time of Si, Al, Ti and V-MCM-41 samples.	39
Table 2.2	Chemical composition of the synthesis gel mixture of organo-functionalized MCM-41 samples.	42
Table 2.3	Effect of NaCl and different sources of phosphate (PO_4^{3-}) promoter in the pH, synthesis time, and solid yield of different Si-MCM-41 samples.	50
Table 3.1	Effect of promoter in the synthesis time and results of elemental analysis, d_{100} spacing and unit cell parameter a_0 of M-MCM-41 (M = Si, Al, Ti and V) samples.	57
Table 3.2	Effect of NaCl and different sources of phosphate (PO_4^{3-}) promoter on the physico-chemical properties of different Si-MCM-41 samples.	58
Table 3.3	Nitrogen sorption pore diameter, framework wall thickness (FWT), BET surface area and average particle size of M-MCM-41 (M = Si, Al, Ti and V) samples.	60
Table 3.4	Results of elemental analysis, d_{100} spacing and unit cell parameter (a_0) of M-MCM-41 (M = Si and Ce) samples.	75
Table 3.5	Nitrogen sorption pore diameter, pore volume, FWT and BET surface area of M-MCM-41 (M = Si and Ce) samples.	77
Table 3.6	Band assignments in the IR spectra of Si-MCM-41 and Ce-MCM-41-R (20).	82
Table 3.7	IR spectroscopic assignments of vibrational modes and wavenumbers for bands formed upon chemisorption of NH_3 on Ce-MCM-41-R (40).	86
Table 3.8	Theoretical and observed organic composition of the organo-functionalized MCM-41 samples.	95
Table 3.9	BET surface area and pore size distribution of organo-functionalized MCM-41 samples.	95

Table 4.1	Acylation of alcohols and polyols with acetic anhydride as acylating agent over cerium containing MCM-41.	113
Table 4.2	Acylation of amines and thiols with acetic anhydride as acylating agent over cerium containing MCM-41.	115
Table 4.3	Chemoselective acylation of amino alcohol and mercapto alcohol with acetic anhydride as acylating agent over cerium containing MCM-41.	116
Table 4.4	Acylation of 1-hexanol with different acylating agents over cerium containing MCM-41.	117
Table 4.5	Activity of different cerium containing MCM-41 samples in the acylation of 1-hexanol with acetic anhydride.	119
Table 4.6	Activity of Different Metal Containing MCM-41 Samples (Ce, Ti and Zr) in the Acylation of <i>n</i> -Hexanol with Acetic Anhydride.	120
Table 4.7	Comparison of the catalytic activity and selectivity of V-MCM-41-S, V-MCM-41-P and Ti-MCM-41-P samples in the hydroxylation of 1-naphthol.	123
Table 4.8	Activity of the Ce-MCM-41 samples in the hydroxylation of 1-naphthol with H ₂ O ₂ .	124
Table 4.9	Activity of the Ce-MCM-41 samples in the hydroxylation of 1-naphthol with <i>tert</i> -butyl hydroperoxide (TBHP).	125
Table 4.10	Comparison of the catalytic activity and selectivity of Ti-MCM-41-S, Ti-MCM-41-P and V-MCM-P samples in the epoxidation of cyclohexene.	127
Table 4.11	Effect of different oxidants on epoxidation of styrene and allylbenzene over TS-1 and TS-2.	129
Table 4.12	Effect of solvent on epoxidation of styrene with UHP over TS-1.	134
Table 4.13	Effect of different oxidants on epoxidation of allyl alcohol, allyl chloride, allyl bromide and methylallyl chloride over TS-1.	138
Table 4.14	Effect of different oxidants on epoxidation of 1-hexene and cyclohexene over TS-1 and TS-2.	140

Abbreviations

1,2-DHN	1,2-Dihydroxynaphthalene
1,2-NQ	1,2-Naphthoquinone
1,4-DHN	1,4-Dihydroxynaphthalene
1,4-NQ	1,4-Naphthoquinone
1-IPN	1-Isopropyl naphthalene
2-IPN	2-Isopropyl naphthalene
APTS	3-Aminopropyltrimethoxysilane
BD	Benzaldehyde
BET	Brunauer-Emmett-Teller
CO	Cyclohexene oxide
C-OL	Cyclohexenol
CP MAS NMR	Cross polarization magic angle spinning nuclear magnetic resonance
CTABr	Cetyltrimethylammonium bromide
CX	Cyclohexene
DIOLS	2-Phenyl-1,2-propanediol/styrene diol/1,2-hexanediol/1,2-cyclohexanediol
DIPNs	Diisopropyl naphthalenes
DTA	Differential Thermal Analysis
EDX	Energy dispersive X-ray
EP	Epoxy allylbenzene/styrene oxide
EPR	Electron paramagnetic resonance
FID	Flame ionization detector
FTIR	Fourier transform infrared
GC	Gas chromatography
GC-IR	Gas chromatography-Infrared
GC-MS	Gas chromatography-Mass spectrometry
IPA	Isopropyl alcohol
MAS NMR	Magic angle spinning nuclear magnetic resonance
MCM-41	Mobile crystalline materials -41
MeOH	Methyl alcohol
MPTS	3-Mercaptopropyltrimethoxysilane
P	Promoter

PAD	Phenylacetaldehyde
S	Standard conditions
SEM	Scanning electron microscopy
TBAOH	Tetrabutylammonium hydroxide
TBHP	<i>tert</i> -Butyl hydroperoxide
TBOT	Tetrabutyl orthotitanate
TEM	Transmission electron microscopy
TEOS	Tetraethyl orthosilicate
TG	Thermogravimetry
TGA	Thermogravimetric analysis
TLC	Thin layer chromatography
TMAOH	Tetramethylammonium hydroxide
TOF	Turn over frequency
TPAOH	Tetrapropylammonium hydroxide
TS-1	Titano-silicalite-1
TS-2	Titano-silicalite-2
U+HP	Urea+hydrogen peroxide
UHP	Urea-hydrogen peroxide
UV-Vis	Ultraviolet-visible
VTES	Vinyltriethoxysilane
XRD	X-ray diffraction

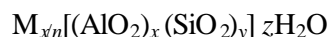
CHAPTER 1

INTRODUCTION

1.1. GENERAL BACKGROUND AND INTRODUCTION

Zeolites are crystalline microporous silica based solids, which are used extensively in adsorption and catalytic processes. The practical importance of these materials has led the studies focused on the synthesis, characterization and applications of different types of zeolites and related materials such that they form an important part of material science, inorganic chemistry and of course catalysis.¹⁻⁸

Traditionally, zeolites (aluminosilicates) are classified as crystalline materials in which Si and Al are tetrahedrally coordinated by oxygen atoms in a three-dimensional network. The crystallographic unit cell of the zeolites may be represented as:



where M is a charge compensating cation with valency n . The ratio x/y may have any value ranging from zero to one. The number of water molecules, which can be reversibly adsorbed and desorbed in the zeolite pores, is represented by z . The presence of trivalent Al atoms in the lattice develops a unit negative charge per Al atom in the framework, which is compensated by a cation such as proton (H^+) producing acidity in zeolites.

However, a variety of trivalent (B, Ga, Fe, As etc.)⁹⁻¹² and tetravalent (Ti, Ge, V, Sn, Zr etc.)¹³⁻¹⁸ transition and non-transition metal ions have been incorporated in a variety of different zeolite structures, MFI being the most preferred structure for heteroatom incorporation.

Different architectural features of zeolites and related materials generating different types of shape-selectivities (product, reactant and transition state),¹⁹⁻²¹ and their relatively high stability towards thermal, hydrothermal and chemical treatments have also been well studied leading to their use as catalysts for oil refining, petrochemistry and organic synthesis in the production of fine and specialty chemicals. Moreover, zeolites and related molecular sieves have earned the reputation of 'green catalysts' due to several important environmental factors

e.g. waste minimization, simple operation, easy work-up, regeneration and reuse of the catalysts for several times etc.

However, the main restriction of microporous zeolitic materials is the size constraints of *ca.* 0.75 nm and therefore not suitable for catalytic transformations involving organic molecules having kinetic diameters above 0.75 nm. The catalytic transformation of molecules with kinetic diameters larger than 0.75 nm, especially important for the preparation of fine chemicals, requires zeolitic materials with larger pore diameters. Hence, there has been an ever-growing interest in expanding the pore sizes of the zeolitic materials from micropore to mesopore region. In Table 1.1 different porous materials, along with typical examples, are classified.

Table 1.1
Pore-size regimes and representative porous silica based materials

Type and pore size (nm)	Examples	Actual size range ^a (nm)
Microporous (<2)	Zeolites	0.45 × 0.45 (LTA, 8 MR),
		0.54 × 0.56 (MFI, 10 MR),
		0.74 × 0.74 (FAU, 12 MR)
		0.75 × 1.0 (UTD-1, 14 MR)
Mesoporous (2-50)	Aerogels	>10
	Pillared layer clays	1, 10 ^b
	M41S	2-10
Macroporous (> 50)	Glasses	>50

^aMR = membered ring opening.

^bBimodal pore-size distribution.

The synthesis of mesoporous molecular sieves called M41S is one of the most exciting discoveries in the field of materials synthesis in the last decade.²²⁻²⁴ The M41S family is

classified into three members: MCM-41 (hexagonal), MCM-48 (cubic) and MCM-50 (lamellar). These mesoporous silicate and aluminosilicate materials, with well-defined pore sizes of 2-10 nm, break past the pore size constraint of microporous zeolites. Very high surface areas ($>700 \text{ m}^2\text{g}^{-1}$) and the control of pore sizes are among the many desirable properties that have made such materials the focus of great interest. The synthesis of these materials opens definitive new possibilities for preparing catalysts with uniform pores in the mesoporous region, which will allow the ingress and egress of relatively large molecules in their mesopores for catalytic transformations. Obviously, an explosion of research activity has occurred within a few years (Figure 1.1). This includes new investigations on different aspects such as synthesis procedures, synthesis mechanisms, heteroatom insertion, stability, physico-chemical characterization, adsorption, and catalytic applications etc.²⁵⁻²⁹

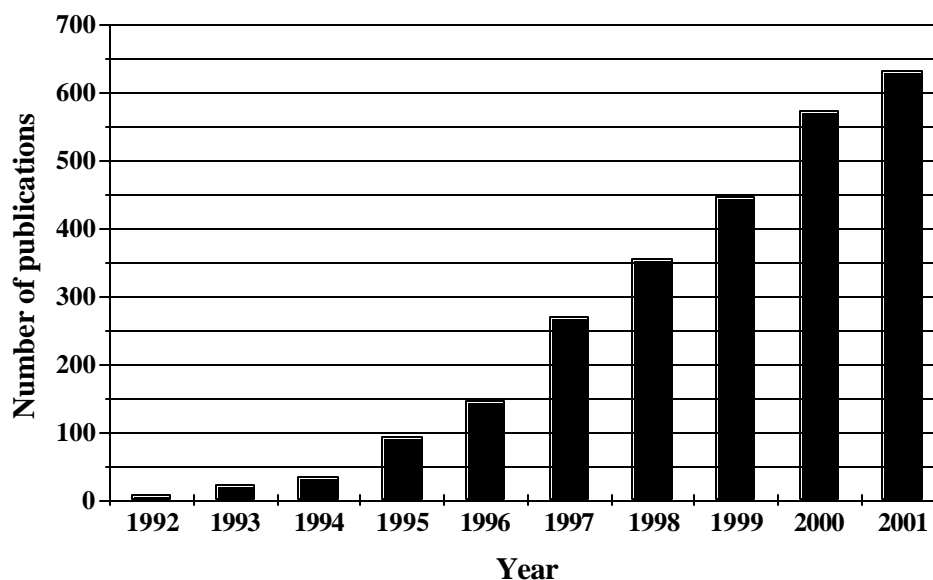


Figure 1.1 Number of publications on ordered mesoporous materials as found by Chemical Abstracts on Compact Disks (CA on CD) of the American Chemical Society using different keywords (MCM-41 or FSM-16 or SBA-15 or mesoporous materials or ordered mesoporous oxides or ordered mesoporous materials).

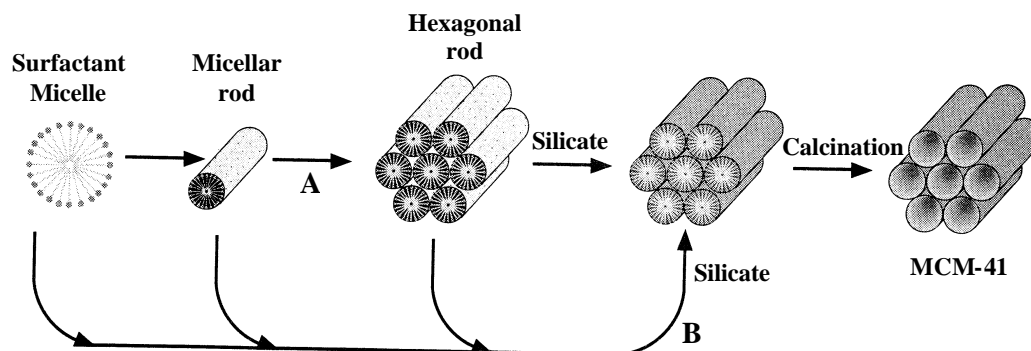
1.2. SYNTHESIS AND MECHANISMS FOR THE FORMATION OF MESOPOROUS MATERIALS

A number of models have been proposed in order to explain the mechanism of formation of mesoporous materials by various synthesis routes. All these models are based on the presence and the role of surfactants in solution to guide the formation of inorganic mesostructures. In solution, surfactants having two parts within the same molecule (hydrophilic head group and long chain hydrophobic tail group) will aggregate and self-organize in such a way as to minimize contact between the incompatible ends. The type of interaction between the surfactant and the inorganic precursor under different synthesis conditions needs careful attention and is a subject of much discussion.

1.2.1. Liquid Crystal Templating (LCT) Mechanism

In order to explain the synthesis mechanism, Mobil researchers proposed a liquid crystal templating (LCT) mechanism, based on the similarity between liquid crystalline surfactant assemblies (i.e. lyotropic phases) and M41S.^{22,23} The mesostructure formation depends on the hydrocarbon chain length of the surfactant tail group,³⁰ the effect of variation of the surfactant concentration and the additional organic swelling agents. The lowest concentration at which surfactant molecules aggregate to form spherical isotropic micelles is called critical micelle concentration (CMC_1). Further increase in the surfactant concentration initiates aggregation of spherical into cylindrical or rod-like micelles (CMC_2). There are three main liquid crystalline phases with hexagonal, cubic and lamellar structures. The hexagonal phase is the result of hexagonal packing of cylindrical micelles, the lamellar phase corresponds to the formation of surfactant bilayers and the cubic phase may be regarded as a bicontinuous structure. Two mechanistic pathways were postulated for the formation of M41S type materials :

- (A) The structure is defined by the organization of surfactant molecules into lyotropic liquid crystal (LC) phase, which serves as template for the formation of the MCM-41 structure. The first step of the synthesis is the formation of a micellar rod around the surfactant micelle which will produce a hexagonal array of rods, followed by incorporation of an inorganic array around the rod-like structures in the second step (Scheme 1.1).
- (B) Highly sensitive liquid crystal structures formed in surfactant solutions may also interact with the silicate species directly which results in the ordering of the subsequent silicate-enclatherated surfactant micelles to form MCM-41 structure.



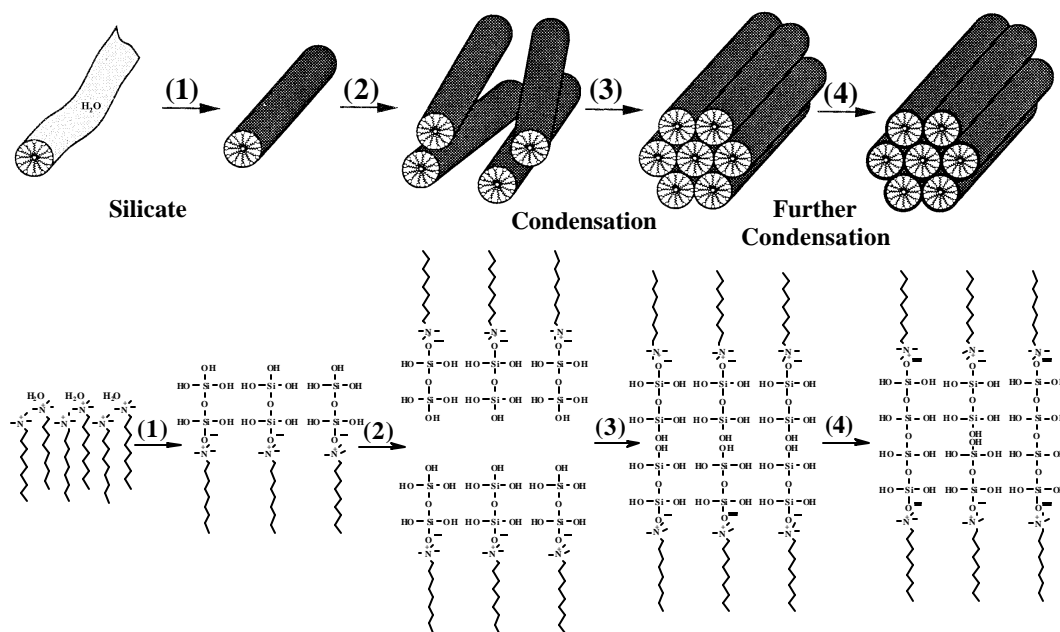
Scheme 1.1 Liquid crystal templating mechanism proposed for the formation of MCM-41: (A) liquid crystal phase initiated and (B) silicate anion initiated.^{22,23}

So, the negatively charged inorganic components preferentially interacted with the positively charged ammonium head groups of the surfactants and condensed into a solid. However, it was clearly shown²⁴ that pathway A (Scheme 1.1) did not take place because the surfactant concentrations used were far below the critical micelle concentration (CMC_2) required for hexagonal LC formation.

1.2.2. Silicate Rod Assembly

Davis and co-workers³¹ by carrying out *in situ* ^{14}N NMR spectroscopy concluded that the liquid crystalline phase is not present in the synthesis medium during the formation of MCM-

41, and consequently, this phase cannot be the structure-directing agent for the synthesis of the mesoporous materials (Scheme 1.2).



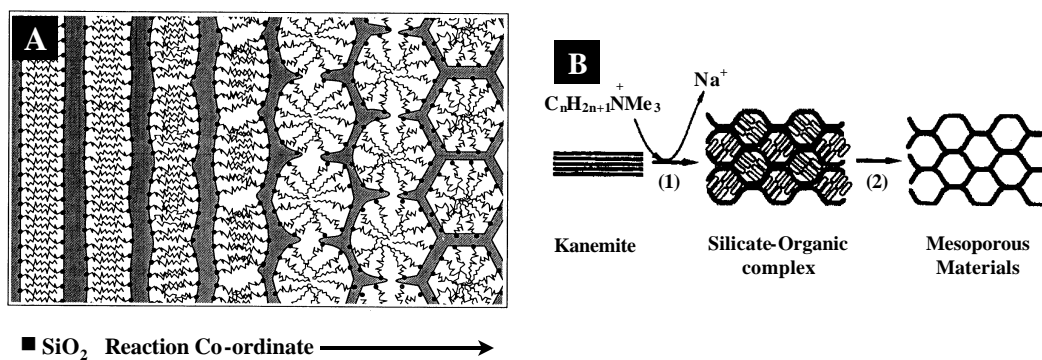
Scheme 1.2 Silicate rod assembly proposed for the formation of MCM-41: (1) and (2) involve the random ordering of rod-like micelles and interaction with silicate species; (3) represents the spontaneous packing of the rods and (4) is the remaining condensation of silicate species upon final heating of the organic/inorganic composites.³¹

1.2.3. Charge Density Matching and Folding Sheets

Both the ‘charge density matching’ and ‘folding sheets’ mechanistic models are based on the transformation of lamellar phase to hexagonal one. The ‘charge density matching’ model proposed by Monnier et al.³² and Stucky et al.³³ suggested that the condensation of initially formed silicate species by the electrostatic attraction between the anionic silicates and the cationic surfactant head groups, reduces the charge density and therefore, curvature was

introduced into the layers to maintain the charge density balance with the surfactant head groups, which transformed the lamellar mesostructure into the hexagonal one (Scheme 1.3A).

Similarly, Inagaki et al.³⁴ proposed the ‘folding sheets mechanism’ and suggested that the incorporation of surfactants by ion-exchange of interlayer Na^+ ions into the highly flexible sodium silicate sheets of kanemite resulted in folding of the silicate sheets around the surfactants which ultimately condensed into a hexagonal mesostructure (FSM-16) similar to MCM-41 (Scheme 1.3B).

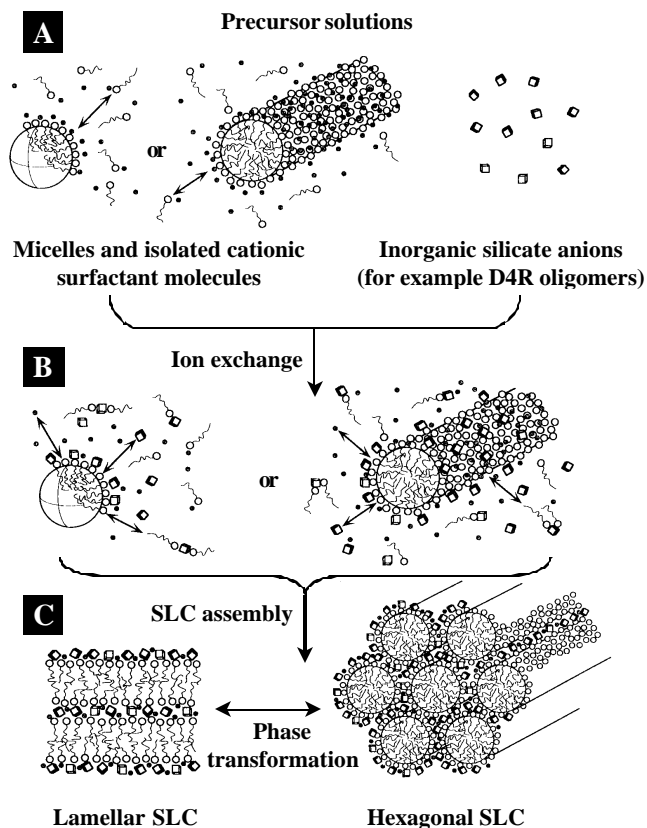


Scheme 1.3 Mechanisms proposed for the transformation of surfactant-silicate systems from lamellar to hexagonal mesophases. (A) Hexagonal mesophase obtained by charge density matching^{32,33} and (B) folding of kanemite silicate sheets around intercalated surfactant molecules formed the hexagonal mesostructure.³⁴

1.2.4. Silicatropic Liquid Crystals

Firouzi and co-workers^{35,36} showed that the properties and structure of a particular system were not determined by the long-range ordered organic arrays, but by the dynamic interplay among ion-pair inorganic and organic species. The silicate anions ion-exchanged with the surfactant halide counter ions formed the ‘silicatropic liquid crystal’ (SLC) phase (Scheme 1.4), which exhibited very similar behavior to that of typical lyotropic systems and finally

condensed irreversibly into MCM-41. The various stages of synthesis were monitored by means of small angle neutron scattering (SANS).



Scheme 1.4 The model (cooperative organization) for the formation of silicotropic liquid crystal phase/silicate-surfactant mesophases. (A) represents the organic and inorganic precursor solutions, (B) represents the preliminary interaction of the two precursor solutions after mixing, and (C) represents the multidentate interaction of the oligomeric silicate units with the surfactant molecules.^{35,36}

1.2.5. Generalized Liquid Crystal Templating Mechanism

1.2.5.1. Electrostatic Interaction

A generalized mechanism for the formation of mesostructured materials based on the specific type of electrostatic interaction between a given inorganic precursor I and surfactant

head group S (similar to that of Scheme 1.4) was proposed by Huo and co-workers.^{37,38} In this way, cationic quaternary ammonium surfactants (S^+) are used for the structuring of anionic inorganic silicate species (I), which could be categorized as the S^+I^- pathway. On the other hand, anionic surfactants (S) are employed for structuring cationic inorganic species (I^+) (S^-I^+ mesostructures). Organic-inorganic combinations with identically charged partners are also possible, but then the formation of the mesostructure is mediated by the counter-charged ions, which must be present in stoichiometric amounts ($S^+X^-I^+$ (X is a counter anion) and $S^-M^+I^-$ (M^+ is a metal cation) mesostructures).

1.2.5.2. Hydrogen Bonding Interaction

Neutral amine template surfactants (S^0) and hydroxylated TEOS (I^0) have been used by Tanev and Pinnavaia³⁹⁻⁴¹ to prepare hexagonal mesoporous silicas (HMS) that have thicker pore walls, high thermal stability and smaller crystallite size but, have higher amounts of interparticle mesoporosity and lower degree of long-range ordering of pores than MCM-41 materials. At high concentrations, the non-ionic head groups (N^0) of polyethylene oxide⁴² and ethylene glycol hexadecyl ether⁴³ can also act as structure directors like the amine head group (S^0).

1.2.5.3. Covalent Interactions

In a different synthetic approach, Ying and co-workers have successfully synthesized hexagonally packed mesoporous metal oxide materials completely stable to surfactant removal through a ligand-assisted templating (LAT) mechanism.⁴⁴ The surfactants were pre-treated with the metal alkoxides precursor in the absence of water to form metal-ligated surfactants by nitrogen-metal bond formation between the surfactant head group and the metal alkoxide precursor. The control of mesostructure phases was found possible by adjustment of the metal/surfactant ratio. The existence of covalent interaction is concluded by NMR spectroscopic studies.

1.3. METAL-SUBSTITUTED MESOPOROUS MOLECULAR SIEVES

In order to generate potential catalytic activities, the incorporation of heteroatoms into the inert framework or walls of pure siliceous mesoporous materials is an important route to modify the nature of the framework and make them catalytically active. In general, it is observed that the incorporation of tetrahedrally coordinated aluminum on the walls during the synthesis decreases the order in the material⁴⁵ and the degree of incorporation depends on the aluminum precursor⁴⁶ and method of preparation.⁴⁵ The incorporation of trivalent metal ions such as Al,^{45,46} B,⁴⁷ Ga,⁴⁸ Fe⁴⁹ etc. in the walls of silica network mesostructure produces framework negative charges that can be compensated by protons providing acid sites and therefore, such materials are important from the point of view of acid catalysis. The incorporation of transition metal elements such as Ti,^{50,51} V,⁵² Cr,⁵³ Mn,⁵⁴ Fe,⁵⁵ Co,⁵⁶ Sn,⁵⁷ Mo,⁵⁸ Zr⁵⁹ etc. is also important to prepare mesoporous catalysts with redox catalytic properties.

1.4. MESOPOROUS SILICATES AS SUPPORT/HOST

1.4.1. Immobilization of Metals/Metal Complexes in Mesoporous Silicates

The post-synthesis immobilization of metals and organometallic complexes on the surface of mesoporous silicates allows the preparation of multifunctional molecular sieves with desired catalytic properties. Mesoporosity and very high surface area of mesoporous materials (particularly MCM-41) have been largely used for the immobilization of different metals as well as bulky organometallic complexes. The processes for metal immobilization include wet impregnation,⁶⁰ vapor deposition,⁶¹ treatment with $(\text{NH}_4)_2\text{MF}_6$ ($\text{M} = \text{Si}^{4+}, \text{Ti}^{4+}$, etc.)⁶² and metal alkoxides,⁶³ ion exchange with metal salts^{64,65} etc.

The immobilization of metal complex is mostly done by ion exchange followed by the complexation with ligand⁶⁶ and also by direct incorporation of the metal complex in the mesoporous hexagonal channels of MCM-41.⁶⁷

1.4.2. Covalently Anchored Organo-Functionalized Mesoporous Silicates

The advantages of inorganic-organic hybrid materials arise from the fact that inorganic components can provide mechanical, thermal or structural stability, while the organic features are more readily modified for specific applications in catalysis, separation or sensing.⁶⁸ The presence of large amount of silanol groups $[(\text{-O-})_3\text{SiOH}]$ in MCM-41 and HMS materials attracted the researchers primarily for anchoring the organic functional groups using the concept of organic functionalization in silica gel and then those organic functional groups or ligands were used for anchoring different types of metal complexes with or without modification of the parent functional groups.

1.4.2.1. In situ Synthetic Methods

Organically functionalized mesoporous silicas were prepared conveniently at room temperature⁶⁹ or at higher temperature⁷⁰ by the co-condensation of tetraalkoxysilane (Si(OR)_4) and organosiloxanes ($\text{R}^1\text{-Si(OR)}_3$) in the presence of surfactant (template) and auxiliary chemicals. Thus, a variety of inorganic-organic hybrid materials, where the organic functional groups are attached covalently with the silica surface of MCM-41 through Si-C bonds, are very important for their various potential applications. An acidic solvent extraction technique is generally used to remove the surfactant from the product to yield an organo-functionalized ordered porous silica material.^{69,70}

1.4.2.2. Post Synthetic Methods

Organo functional groups were also introduced to the pore surface of mesoporous silica as the terminal groups for organic monolayers by post synthesis modification. The treatment

of mesoporous silica with organosiloxane precursors produces hybrid inorganic-organic materials by hydrolysis and finally condensation of organosiloxane groups.⁷¹

Although the organic functional groups have been introduced into mesoporous silica in both ways, *in situ* and post synthetic methods, organometallic complexes attached covalently to the pore surface are introduced only by post synthesis modifications.^{72,73}

1.5. CONTROL OF CRYSTAL AND PORE SIZES

Extensive research efforts have been undertaken to control the crystal size, pore dimensions and pore sizes. The control of crystal size and pore dimensions are also important factors, particularly for MCM-41 with unidirectional channels. High quality hexagonal mesoporous materials of good thermal stability and smaller crystal sizes were obtained by heating precursor gels in the microwave at 150 °C for 1 h or even less.⁷⁴ The disordered mesoporous material, KIT-1, interconnected in a three-dimensional and fully disordered way is also of interest from the catalytic point of view.⁷⁵

One of the most interesting and useful features of M41S family is the flexibility to synthesize these materials with different pore diameters (2-10 nm). This can be achieved in three different ways: (i) by varying the chain length of hydrophobic alkyl group (8 to 22 carbon atoms) in the surfactant molecules,²³ (ii) by adding organic swelling agents such as 1,3,5-trimethylbenzene,²³ alkanes of different chain length,⁷⁶ etc. which will increase the micellar size by solvation of the added hydrophobic molecules in the hydrophobic region of the micelles, and (iii) by adjusting the composition of the gel and the crystallization variables.⁷⁷

In a different approach, Sun and Ying⁷⁸ were able to control pore sizes between 0.5-2 nm by the use of short-chain alkylamines as supramolecular templates, allowing for systematic bridging of the mesoporous and microporous regimes. The ligand-assisted templating (LAT)

technique was further modified by them to produce microporous Nb-TMS6 with the use of α,ω -dialkylamines.⁷⁹

1.6. CONTROL OF MORPHOLOGY

The morphology of originally obtained MCM-41 type mesoporous materials^{22,23} is consists of aggregates and loose agglomerates of small particles. However, for many applications in catalysis, chemical sensing or as optical devices, well-defined morphologies are required. The research has been focused to obtain thin films, fibers, spheres and monoliths. Huo et al.³⁷ and Yang et al.⁸⁰ have used acid medium (S^+XI^+) for the preparation of a large variety of differently curved and highly interesting morphologies. Thin films have been prepared at the air/water⁸¹ and oil/water⁸² interface as free-standing films, on both the mica⁸³ and the graphite⁸⁴ surfaces and by using dip- or spin-coating⁸⁵ techniques. While, the preparations of fiber morphologies were carried out in oil-in-water emulsions⁸² and in aqueous phase⁸⁶ under acidic (S^+XI^+) conditions, the syntheses of hollow⁸² as well as hard spheres⁸⁷ of mesoporous silicas were carried out by emulsion biphasic chemistry. Monolithic periodic mesoporous silicas prepared by different systems using ionic and non-ionic surfactants^{43,88} are also very important for several applications. An interesting morphology of 'tubules-within-a-tubule' hierachiral order has been reported by Lin and Mou.⁸⁹

1.7. PHYSICO-CHEMICAL CHARACTERIZATION

A number of techniques have been used to characterize different types of microporous and mesoporous zeolites and related molecular sieve materials. Each technique is unique by itself and provides important information for the understanding of different structural features of a particular microporous or mesoporous material. Among all, the most commonly used

spectroscopic (powder X-ray diffraction (XRD), energy dispersive X-ray analysis (EDX), diffuse reflectance UV-Vis, FTIR, solid state magic angle spinning (MAS) NMR, and electron paramagnetic resonance (EPR) etc.), microscopic (scanning electron microscopy (SEM), and transmission electron microscopy (TEM) etc.), volumetric (adsorption and surface area analysis by BET method), and thermogravimetric (thermogravimetry-differential thermal analysis (TG-DTA)) methods are essential for thorough characterization of these materials.

1.7.1. X-ray Diffraction

Powder X-ray diffraction is the most important and commonly used tool to identify and measure the uniqueness of structure, phase purity, degree of crystallinity and unit cell parameters of crystallite materials. Microporous solids show characteristic peaks in the 2θ range of $5-50^\circ$ whereas the mesoporous materials exhibit characteristic peaks in the low angle region between $1.5-10^\circ$ (2θ). Isomorphous substitution of a heteroatom in the framework of the molecular sieves can be easily predicted by calculating the changes in the unit cell parameters and unit cell volume. This is one of the indirect ways to confirm isomorphous substitution. The unit cell dimensions determined by XRD is also used to calculate the framework wall thickness (FWT) of hexagonal channels in MCM-41 materials.

1.7.2. Adsorption Measurements

The ability to adsorb selective molecules of comparable sizes through the pores into the channels of molecular sieves made them interesting and useful in the field of heterogeneous catalysis. The sorption properties of molecular sieves provide information about the hydrophobic/hydrophilic character, pore size distribution and pore volume as well as surface area. The adsorption of nitrogen measured by Brunauer-Emmett-Teller (BET) equation at low

pressure (10^{-4} Torr) and liquification temperature of N_2 (77 K) is the standard method for the determination of surface area, pore volumes and pore size distribution of molecular sieves.⁹⁰

1.7.3. Diffuse Reflectance UV-Vis Spectroscopy

The diffuse reflectance UV-Vis spectroscopy is known to be a very sensitive and useful technique for the identification and characterization of the metal ion coordination and its existence in the framework or extra-framework position of metal containing molecular sieves. The position of “ligand-to-metal charge transfer” (L→M) band depends on the ligand field symmetry surrounding the metal center and the electronic transitions from ligand-to-metal require higher energy for a tetra-coordinated metal ion than for a hexa-coordinated one. For most of the isomorphously substituted microporous and mesoporous metallo-silicate (particularly Ti- and V-containing) molecular sieves, transitions in the UV region (200-400 nm) are of prime interest.

1.7.4. Fourier-Transform Infrared (FTIR) Spectroscopy

The FTIR spectroscopy in the framework region ($400-1300\text{ cm}^{-1}$) provides additional information about the structural details including isomorphous substitution in molecular sieves, whereas the hydroxyl region ($3000-4000\text{ cm}^{-1}$) contributes for the determination of different (Brönsted and Lewis) acid sites⁹¹ and silanol groups.⁹² The band at 960 cm^{-1} in the framework region is very important and generally attributed to the incorporation of metal ions in the framework of silica matrix particularly for Ti-containing molecular sieves.⁹³ Acidic and basic properties as well as its strength in molecular sieves can also be determined by FTIR spectroscopy using CO_2 , ammonia, pyridine, triphenylphosphine etc. as the probe molecules.⁹⁴

1.7.5. Nuclear Magnetic resonance (NMR) Spectroscopy

Nuclear magnetic resonance spectroscopy, both in the liquid and the solid state, is a very important tool for understanding the structure of zeolites and determining the active species at the molecular level during synthesis (*in situ*) and also to characterize the local environment of framework metal ions in solids. Lippama et al.⁹⁵ showed that ²⁹Si MAS NMR spectra are very sensitive to the nature and chemical environment of the atoms. MAS NMR of ²⁷Al, ⁵¹V, etc. has also been extensively studied to characterize the incorporation of heteroatom in the framework by determining the local environment of Al, Ga, V, etc. in corresponding metallosilicate molecular sieves.^{96,97} The ¹³C CP MAS NMR spectra of as-synthesized molecular sieves give us information about the incorporation of intact organic structure directing agents inside the channels of these materials.

1.7.6. Electron Paramagnetic Resonance (EPR) Spectroscopy

Electron paramagnetic resonance spectroscopy is the resonance absorption of the electromagnetic (microwave) radiation by magnetically split states of unpaired electrons. It is a very important tool for determining the oxidation states and incorporation of paramagnetic metal ions in the framework or extra-framework position in metallosilicate molecular sieves. This technique provides important information about the redox sites and paramagnetic charge-transfer complex.

1.7.7. Scanning Electron Microscopy (SEM)

This is another important tool for morphological characterization of microporous and mesoporous molecular sieve materials. Different types of morphology of the synthesized materials as well as the presence of any amorphous phase in the samples can be characterized using this technique. The major advantage of SEM is that bulk samples can also be studied directly by this technique.

1.7.8. Transmission Electron Microscopy (TEM)

The topographic information obtained by TEM at near atomic resolution has been a key method for the structural characterization and identification of the various phases of mesoporous materials, i.e. hexagonal (MCM-41), cubic (MCM-48) and lamellar (MCM-50) phases. Both the cylindrical and the hexagonal pore structures with similar XRD pattern as that of MCM-41 materials have been observed by high resolution TEM.⁹⁸ However, the hexagonal shape is energetically most favorable, since this the only way to maintain a constant wall thickness which in turn maximizes surfactant-silicate surface interaction.⁹⁹

1.7.9. Thermal Analysis (TG-DTA)

The thermoanalytical technique has been widely used to get information on the thermal stability of microporous and mesoporous molecular sieves. Further, it provides information about the temperature programmed desorption of physisorbed water, oxidative decomposition of the occluded organic materials and dehydroxylation of SiOH groups in the channels of molecular sieves. Moreover, any phase transformations can also be detected from differential thermal analysis (DTA).

1.8. CATALYTIC APPLICATIONS AND PROSPECT

The unique physical properties (e.g. high specific surface area, large pore size etc.) of MCM-41 have made these materials highly desirable hosts for the fixation of large active complexes. Due to large void space the diffusional restrictions of reactants/products are absent and therefore, these materials are quite suitable for catalytic applications involving bulky molecules.

Initially, the catalytic studies with mesoporous molecular sieves focused mainly on acid catalysis and redox reactions. Since then, a wide variety of applications including deposition

of heteroatom onto the surface of mesoporous walls have been established and the field is still expanding rapidly. More recently, research has been devoted for the fixation of catalytically active complexes onto the walls of the MCM-41 porous framework to combine the advantages of homogeneous catalysis with a heterogeneous catalyst support.

1.8.1. Acid Catalysis

Although it has been thought that MCM-41 will extend the applications of zeolites for bulky molecules whose diffusion is strongly impeded in zeolites (e.g. USY), the higher intrinsic activity observed for USY (139 times) than MCM-41 in *n*-heptane (small reactant) cracking is not only due to larger amount of Brønsted acid sites, but also stronger acid sites present in the zeolite. It has been established by now that most of the Brønsted acid sites in Al-MCM-41 materials are of weak-medium strength and produces only mild acidity. Hence, the Al-MCM-41 materials are found to be quite useful for carrying out reactions such as hydroisomerization, mild hydrocracking (MHC), hydrodesulfurization (HDS), hydrodenitrogenation (HDN), demetalization, olefin oligomerization etc., which require a catalyst with mild acidity.¹⁰⁰

The advantages of mesoporous materials in the synthesis of fine chemicals have got paramount importance due to fast diffusion of large reactants as well as products through the pores, which substantially minimize the formation of unwanted secondary products. A good example for the shape selective alkylation of 2,4-di-*tert*-butylphenol with cinnamyl alcohol, carried out on AlMCM-41, demonstrates that unlike large pore HY zeolite, benzopyran is the major product since there is no diffusional problems in MCM-41.¹⁰¹ The mild acidity combined with the mesopores in MCM-41 materials made them useful catalysts especially for the preparation of fine chemicals by carrying out reactions such as tetrahydropyranylation¹⁰² of bulky alcohols and phenols e.g. cholesterol (protection of hydroxyl functionality in peptide, nucleotide, carbohydrate and steroid chemistry),

acylation¹⁰³ (synthetic fragrances and pharmaceuticals), acetalization¹⁰⁴ (pharmaceuticals, fragrances and detergents), Beckman rearrangements,¹⁰⁵ glycosidation,¹⁰⁶ etc.

Catalytic applications of metal (Ni, Mo, Co, Pt, Pd, W etc.) supported MCM-41 materials are very useful for certain acid catalysis. Examples include gasoil hydrocracking by NiMo-Al-MCM-41,¹⁰⁰ hydrogenation and hydrocracking by sulfided CoMo-Al-MCM-41,¹⁰⁷ isomerization of 1-hexane by Pt-Al-MCM-41,^{108,109} n-butane cracking by phosphotungstic acid (H₃PW₁₂O₄₀)-modified MCM-41¹¹⁰ and Heck reactions by Pd-TMS11 material^{111,112} etc.

1.8.2. Redox Catalysis

Metallo-silicate molecular sieves particularly titano-silicates with MFI or MEL topologies (e.g. TS-1 or TS-2) have been extensively investigated for selective oxidation reactions^{7,113} (e.g. epoxidation, hydroxylation, oxyfunctionalization of alkanes, ammoxidation, sulfoxidation and various other types of oxidations). However, very high catalytic activity and selectivity of these molecular sieves have been effectively used only in the oxidation of small molecules due to small pore size of these materials (0.53 × 0.55 nm). As a result of that a considerable amount of research was dedicated for the preparation of large pore metallo-silicate molecular sieves (e.g. Ti-beta with BEA structure (0.76 × 0.64 nm)) in which bigger molecules (e.g. long chain aliphatic olefins) can also be accommodated inside the pores for selective oxidation reactions.¹¹⁴⁻¹¹⁶

Mesoporous Ti-MCM-41⁵⁰ and Ti-HMS⁵¹ were used for the epoxidation of norbornene with *tert*-butyl hydroperoxide (TBHP) and oxidation of 2,6-di-*tert*-butylphenol (2,6-DTBP) with aqueous H₂O₂, respectively. Although the intrinsic activity of Ti-MCM-41 is lower than that of TS-1 and Ti-beta particularly for the epoxidation of small molecules with aqueous H₂O₂, it showed higher catalytic activity in the epoxidation of bulkier norbornene with TBHP. Moreover, higher catalytic activity of Ti-HMS than Ti-MCM-41 in the liquid phase

peroxide oxidation of bulkier reactants e.g. 2,6-DTBP is explained on the basis of high textural mesoporosity of Ti-HMS, which has less diffusional limitation than Ti-MCM-41.

Table 1.2
Oxidation catalysis reported over mesoporous metallo-silicate molecular sieves

No.	Catalysts	Reaction	Reference
1.	V-MCM-41	Oxyfunctionalization of alkanes, hydroxylation of 1-naphthol and epoxidation of cyclooctene with H ₂ O ₂ , isobutyraldehyde/dioxygen (IBA/O ₂) and TBHP	25, 52, 117, 118
2.	V-HMS	Oxidation of 2,6-DTBP with H ₂ O ₂ and TBHP	119
3.	Cr-MCM-41	Oxidation of 1-naphthol, phenol and aniline with H ₂ O ₂	53, 120
4.	Mn-MCM-41	Oxidation of cyclohexane and propene to CO ₂	118, 121
5.	Fe-MCM-41	Oxidation of cyclohexane	118
6.	Co-MCM-41	Oxidation of cyclohexane	118
7.	Sn-MCM-41	Hydroxylation of phenol and 1-naphthol with H ₂ O ₂ and epoxidation of norbornene with TBHP	122
8.	Sn-HMS	Lactide ring-opening polymerization	123
9.	Mo-MCM-41	Oxidation of cyclohexanol and cyclohexane with H ₂ O ₂	118, 124
10.	Zr-MCM-41	Oxidation of cholesterol and 1-naphthol with TBHP	125, 126
11.	Ti-MCM-41 ^a	Epoxidation of <i>cis</i> -cyclooctene with TBHP	127

^a Polymer embedded.

Moreover, the possibilities have been expanded by the incorporation of Ti into the framework of AlMCM-41 to prepare a bifunctional acid-oxidation catalyst. It has been shown that Ti-Al-MCM-41 was able to catalyze multistep oxidation of linalool (epoxidation

followed by acid-catalyzed intramolecular ring opening of the epoxide) to cyclic furan and pyran hydroxy ethers in one pot and using TBHP as oxidant.¹²⁸

The catalytic activity of metal deposited/immobilized on MCM-41 was evaluated in epoxidation of propene and selective oxidation of propane to acetone and of isobutene to *t*-butanol with a H₂-O₂ mixture under flow (Au/Ti-MCM-41),¹²⁹ oxidation of 2,6-di-*tert*-butylphenol (Cu/MCM-41),¹³⁰ oxidation of carbon monoxide (Pt/MCM-41),¹³¹ reduction of NO_x by propene (Pt, Rh, and Co/MCM-41)¹³² etc. Immobilized enzymes were used for different stereoselective hydrolysis reactions.^{133,134} Whereas immobilized as well as anchored organometallic complexes attached onto the walls of MCM-41 have been used in the selective oxidation of 1-hexane and cyclohexane with TBHP and H₂O₂,¹³⁵⁻¹³⁷ the epoxidation of norbornene and hydroxylation of 1-naphthol with TBHP,¹³⁸ enantioselective epoxidation of styrene and α -methylstyrene,¹³⁹ stereospecific propene polymerization,¹⁴⁰ and asymmetric borohydride reduction of ketones.¹⁴¹

1.9. SCOPE AND OBJECTIVES OF THE THESIS

In the present investigation, the synthesis, characterization and catalytic applications of MCM-41 type mesoporous materials (all silica, Al, Ti, V and Ce-MCM-41) and organo-functionalized MCM-41 materials are discussed in detail. For comparative purpose, microporous TS-1 and TS-2 have also been synthesized, characterized and used for selective epoxidation reactions.

It has been observed that the addition of catalytic amount of promoter oxyanions to the synthesis precursor mixture of zeolites and silica based microporous materials reduces the crystallization time considerably.^{142,143} This motivated us to check whether the addition of catalytic amount of promoter oxyanions can decrease the synthesis time in the case of MCM-41 type materials or not. The results obtained with MCM-41 materials show that the effect is

quite general and is applicable not only to Si-MCM-41 but also to Al-MCM-41, Ti-MCM-41 and V-MCM-41 materials.¹⁴⁴

The incorporation of various heteroatoms into the framework or the walls of MCM-41 has been systematically studied, characterized and also used as catalysts to show their catalytic activity. However, the reports on the incorporation of cerium in mesoporous molecular sieves are, at best scanty. Recently, a brief report about cerium silicate analogues of MFI, BEA and MTW is published.¹⁴⁵ It is expected that the size incompatibility between Ce^{4+} and Si^{4+} ions will produce longer $=\text{Si-O-Ce}=\text{}$ bonds causing large bond angle strain in Ce-substituted silica network and therefore, the incorporation of Ce in microporous metallo-silicate molecular sieves is expected to be rather difficult. However, the incorporation of Ce in the framework of MCM-41 is more likely because of the greater flexibility of the silica network. Further, the incorporation of Ce, an early member of lanthanides, in the MCM-41 silica network is expected to impart dual catalytic activity in heterogeneous acid as well as in redox catalysis. Hence it was thought interesting to study in detail the incorporation of Ce in MCM-41 and to evaluate its catalytic activity in acid catalyzed and redox reactions.¹⁴⁶

The organo-functionalized MCM-41 type materials can be used as solid ligands for metal ions, forming anchored metal complex onto the walls of MCM-41. Whereas bifunctional organo-functionalized MCM-41 can be potentially used to prepare a class of mixed-metal complexes in a single inert matrix with desired catalytic properties. In fact, using organo-functionalized MCM-41 as support, a very high degree of regioselectivity and enantiomeric excess was observed in the allylic amination of cinnamyl acetate with benzylamine.¹⁴⁷ Further, a novel use of these mesoporous organo-inorganic composites was recently demonstrated for size selective entrapment and stabilization of gold nanoparticles from a mixture of gold and silver colloidal nanoparticles in solution.¹⁴⁸ These advantages attracted our attention for the functionalization and anchoring of metal complexes onto the walls of

MCM-41 with the aim to exploit the heterogeneity of these materials as a substitute of homogeneous systems.^{149,150}

Although the titano-silicate molecular sieves are efficient catalysts for various selective oxidation reactions using aqueous hydrogen peroxide as oxidant, in the epoxidation of various olefinic compounds the epoxide selectivity is reduced due to the formation of isomerized and/or cleaved secondary products as the oxirane ring is quite prone to acid catalyzed isomerization and hydrolysis in the presence of water (coming from aqueous H_2O_2). In order to circumvent this problem anhydrous source of hydrogen peroxide namely urea-hydrogen-peroxide adduct (UHP), which slowly releases *anhydrous* H_2O_2 into solution¹⁵¹ has been used for the epoxidation of a variety of olefinic compounds in the presence of Ti-MCM-41, TS-1 and TS-2 as redox catalysts producing excellent epoxide yields.^{144,152,153} The addition of urea in aqueous H_2O_2 (U+HP, urea and aqueous H_2O_2 added separately for the *in situ* formation of UHP) also shows significant effect on the selectivity of epoxides. This motivated us to carry out epoxidation of styrene with aqueous H_2O_2 in the presence of varying amount of urea separately added to the reaction mixture.¹⁵²

Since UHP releases *anhydrous* H_2O_2 , it may provide interesting information on the nature of the active sites in Ti-MCM-41, TS-1 and TS-2 using diffuse reflectance UV-Vis and EPR techniques, which could not be observed using aqueous hydrogen peroxide.¹⁵⁴⁻¹⁵⁶ This motivated us to use anhydrous urea-hydrogen peroxide (UHP) adduct as the source of H_2O_2 in which the absence of water molecules will not increase and/or equalize the coordination number of different Ti-species during the formation of Ti-superoxo compounds. Direct spectroscopic evidences for the formation of different Ti-superoxo complexes by the solid-solid interaction between Ti-MCM-41/TS-1/TS-2 and urea-hydrogen peroxide adduct were obtained from the characteristic continuous absorption band in the UV-Vis region (300-500

nm) and the anisotropic EPR spectra for the superoxide radical attached to Ti(IV) centers on Ti-MCM-41, TS-1 and TS-2.^{152,153}

1.10. OUTLINE OF THE THESIS

The thesis has been divided into five chapters.

Chapter 1 presents the general introduction and literature review about various chemical aspects of porous (both microporous and mesoporous) molecular sieve materials. Different synthesis parameters and mechanistic aspects of the micellar mediated synthesis, characterization techniques and catalytic applications of ordered mesoporous materials are discussed in brief. The scope and objectives of the present investigation is outlined at the end of this chapter.

Chapter 2 describes the synthesis of various molecular sieve materials prepared during this investigation. This includes :

1. Synthesis of Si-MCM-41, Al-MCM-41, Ti-MCM-41 and V-MCM-41 type mesoporous materials in the presence and in the absence of promoter by varying different synthetic parameters and promoter concentration.
2. Synthesis of Ce-MCM-41 type mesoporous materials by varying different synthetic parameters.
3. Synthesis of different organo-functionalized MCM-41 materials by *in situ* and post synthetic methods.
4. Synthesis of TS-1 and TS-2.

This chapter also includes a detailed discussion on the results obtained for the promoter-induced synthesis of Si-MCM-41 using different promoters and promoter concentrations.

Chapter 3 deals with the discussion of experimental results of physico-chemical characterization of all the above-mentioned samples by spectroscopic (XRD, EDX, DR-UV-

Vis, FTIR, MAS NMR, and EPR etc.), microscopic (SEM, and TEM etc.), volumetric (surface area measurements), and thermogravimetric (TG-DTA) methods.

Chapter 4 gives an account of selective catalytic applications of the molecular sieve materials synthesized during this investigation. This includes :

1. Acid catalyzed reactions
 - (i) Isopropylation of naphthalene over Al-MCM-41 samples.
 - (ii) Dehydration of cyclohexanol over Ce-MCM-41 samples.
 - (iii) Chemoselective acylation of alcohols, amines, phenols and thiols over Ce-MCM-41 samples.
2. Oxidation reactions
 - (i) Hydroxylation of 1-naphthol catalyzed by V-MCM-41, Ti-MCM-41 and Ce-MCM-41.
 - (ii) Epoxidation of cyclohexene over Ti-MCM-41 and V-MCM-41.
 - (iii) Epoxidation of a variety of olefinic compounds over TS-1 and TS-2.

Chapter 5 summarizes and concludes the results obtained and the basic finding of the present work.

1.11. REFERENCES

1. Barrer, R. M., “*Hydrothermal Chemistry of Zeolites*” Academic Press, New York, (1982).
2. Breck, D. W., “*Zeolite Molecular Sieves*”, Wiley, New York (1974).
3. Szostak, R., “*Molecular Sieves: Principles of Synthesis and Identifications*”, Van Nostrand Reinhold, New York (1989).
4. Davis, M. E., *Acc. Chem. Res.* **26**, 111 (1993).
5. Schultz, P. G., *Angew. Chem. Int. Ed. Engl.* **28**, 1283 (1989).
6. Corma, A., *Chem. Rev.* **95**, 559 (1995).
7. Arends, I. W. C. E., Sheldon, R. A., Wallau, M., and Schuchardt, U., *Angew. Chem. Int. Ed. Engl.* **36**, 1144 (1997).
8. Thomas, J. M., *Angew. Chem. Int. Ed.* **38**, 3588 (1999).
9. Taramasso, M., Forlani, O., Manara, G., and Notari, B., *U. K. Pat.* 2023562 (1979).
10. Meyers, B. L., Ely, S. R., Kutz, N. A., Kudak, J. A., and Van den Bossche, E., *J. Catal.* **91**, 352 (1985).
11. McNicol, B. D., and Pott, G. T., *J. Catal.* **25**, 223 (1972).
12. Bhaumik, A., and Kumar, R., *J. Chem. Soc. Chem. Commun.* 349 (1995).
13. Kumar, R., and Ratnasamy, P., *Catal. Lett.* **22**, 227 (1993)
14. Gabelica, Z., and Guth, J. L., *Stud. Surf. Sci. Catal.* **49 A**, 421 (1994).
15. Taramaso, M., Perego, G., and Notari, B., *U. S. Pat.* 4410501 (1983).
16. Thangaraj, A., Kumar, R., Mirajkar, S. P., and Ratnasamy, P., *J. Catal.* **130**, 1 (1991).
17. Ramasawamy, A. V., Sivasanker, S., and Ratnasamy, P., *Catal. Lett.* **22**, 236 (1993).
18. Rakshe, B., Ramasawamy, V., and Ramasawamy, A. V., *J. Catal.* **163**, 501 (1996).
19. Csicsery, S. M., *Zeolites* **4**, 202 (1984).
20. Csicsery, S. M., *Pure Appl. Chem.* **58**, 841 (1986).

21. Ratnasamy, P., and Kumar, R., *Stud. Surf. Sci. Catal.* **97**, 367 (1995).
22. Kresge, C. T., Leonowicz, M. E., Roth, W. J., Vartulli, J. C., and Beck, J. S., *Nature* **359**, 710 (1992).
23. Beck, J. S., Vartulli, J. C., Roth, W. J., Leonowicz, M. E., Kresge, C. T., Schmitt, K. D., Chu, C. T.-W., Olson, D. H., Sheppard, E. W., McCullen, S. B., Higgins, J. B., and Schlenker, J. L., *J. Am. Chem. Soc.* **114**, 10834 (1992).
24. Vartulli, J. C., Kresge, C. T., Leonowicz, M. E., Chu, A. S., McCullen, S. B., Johnson, I. D., and Sheppard, E. W., *Chem. Mater.* **6**, 2070 (1994).
25. Sayari, A., *Chem. Mater.* **8**, 1840 (1996).
26. Stucky, G. D., Q. Huo, Q., Firouzi, A., Chmelka, B. F., Schacht, S., Martin, I. G. V., and Schüth, F., *Stud. Surf. Sci. Catal.* **105**, 3 (1997).
27. Corma, A., *Chem. Rev.* **97**, 2373 (1997).
28. Ying, J. Y., Mehnert, C. P., and Wong, M. S., *Angew. Chem. Int. Ed.* **38**, 56 (1999).
29. Ciesla, U., and Schüth, F., *Microporous Mesoporous Mater.* **27**, 131 (1999).
30. Beck, J. S., Vartulli, J. C., Kennedy, G. J., Kresge, C. T., Roth, W. J., and Schramm, S. E., *Chem. Mater.* **6**, 1816 (1994).
31. Chen, C.-Y., Burkett, S. L., Li, H.-X., and Davis, M. E., *Microporous Mater.* **2**, 27 (1993).
32. Monnier, A., Schüth, F., Huo, Q., Kumar, D., Margolese, D., Maxwell, R. S., Stucky, G. D., Krishnamurty, M., Petroff, P., Firouzi, A., Janicke, M., and Chmelka, B. F., *Science* **261**, 1299 (1993).
33. Stucky, G. D., Monnier, A., Schüth, F., Huo, Q., Margolese, D. I., Kumar, D., Krishnamurty, M., Petroff, P., Firouzi, A., Janicke, M., and Chmelka, B. F., *Mol. Cryst. Liq. Cryst.* **240**, 187 (1994).
34. Inagaki, S., Fukushima, Y., and Kuroda, K., *J. Chem. Soc., Chem. Commun.* 680 (1993).

35. Firouzi, A., Kumar, D., Bull, L. M., Besier, T., Sieger, P., Huo, Q., Walker, S. A., Zasadzinski, J. A., Glinka, C., Nicol, J., Margolese, D., Stucky, G. D., and Chmelka, B. F., *Science* **267**, 1138 (1995).
36. Firouzi, A., Atef, F., Oertli, A. G., Stucky, G. D., and Chmelka, B. F., *J. Am. Chem. Soc.* **119**, 3596 (1997).
37. Huo, Q., Margolese, D. I., Ciesla, U., Feng, P., Sieger, P., Leon, R., Petroff, P., Schüth, F., and Stucky, G. D., *Nature* **368**, 317 (1994).
38. Huo, Q., Margolese, D. I., Ciesla, U., Demuth, D. G., Feng, P., Gier, T. E., Sieger, P., Firouzi, A., Chmelka, B. F., Schüth, F., and Stucky, G. D., *Chem. Mater.* **6**, 1176 (1994).
39. Tanev, P. T., and Pinnavaia, T. J., *Science* **267**, 865 (1995).
40. Tanev, P. T., and Pinnavaia, T. J., *Science* **271**, 1267 (1996).
41. Zhang, W., Fröba, M., Wang, J., Tanev, P. T., Wong, J., and Pinnavaia, T. J., *J. Am. Chem. Soc.* **118**, 9164 (1996).
42. Bagshaw, S. A., Prouzet, S. A., and Pinnavaia, T. J., *Science* **269**, 1242 (1995).
43. Attard, G. S., Glyde, J. C., and Goltner, C. G., *Nature* **378**, 366 (1995).
44. D. M. Antonelli, D. M., Ying, J. Y., *Angew. Chem. Int. Ed. Engl.* **35**, 426 (1996).
45. Ryoo, R., Ko, C. H., and Howe, R. F., *Chem. Mater.* **9**, 1607 (1997).
46. Luan, Z., Cheng, Ch. F., Zhou, W., and Klinowski, J., *J. Phys. Chem.* **99**, 1018 (1995).
47. Sayari, A., Danumah, C., and Moudrakovski, I. L., *Chem. Mater.* **7**, 813 (1995).
48. Cheng, C.-F., He, H., Zhou, W., Klinowski, J., Gonçalves, J. A. S., and Gladden, L. F., *J. Phys. Chem.* **100**, 390 (1996).
49. Tuel, A., and Gontier, S., *Chem. Mater.* **8**, 114 (1996).
50. Corma, A., Navarro, M. T., and Pariente, J. P., *J. Chem. Soc. Chem. Commun.* 147 (1994).

51. Tanev, P. T., Chibwe, M., and Pinnavaia, T. J., *Nature* **368**, 321 (1994).
52. Reddy, K. M., Moudrakovski, I., and Sayari, A., *J. Chem. Soc. Chem. Commun.* 1059 (1994).
53. Ulagappan, N., and Rao, C. N. R., *Chem. Commun.* 1047 (1996).
54. Zhao, D., and Goldfarb, D., *J. Chem. Soc. Chem. Commun.* 875 (1995).
55. Yuan, Z. Y., Liu, S. Q., Chen, T. H., Wang, J. Z. and Li, H. X., *J. Chem. Soc., Chem. Commun.* 973 (1995).
56. Jentys, A., Pham, N. H., Vinek, H., Englisch, M., and Lercher, J. A., *Microporous Mater.* **6**, 13 (1996).
57. Das, T. K., Chaudhari, K., Chandwadkar, A. J., and Sivasanker, S., *J. Chem. Soc. Chem. Commun.* 2495 (1995).
58. Rana, R. K., and Viswanathan, B., *Catal. Lett.* **52**, 25 (1998).
59. Tuel, A., Gontier, S., and Teissier, R., *J. Chem. Soc., Chem. Commun.* 651 (1996).
60. Corma, A., Martínez, A., Martínez-Soria, V., and Monton, J. B., *J. Catal.* **153**, 25 (1995).
61. Grubert, G., Rathousky, J., Schulz-Ekloff, G., Wark, M., and Zukal, A., *Microporous Mesoporous Mater.* **22**, 225 (1998).
62. Velarde, A. M., Bartl, P., Niessen, T. E. W., Hoelderich, W. F., *J. Mol. Catal. A: Chem.* **157**, 225 (2000).
63. Ahn, W. S., Lee, D. H., Kim, T. J., Kim, J. H., Seo, G., and Ryoo, R., *Appl. Catal., A* **181**, 39 (1999).
64. Ryoo, R., Kim, Mi J., Kim, J. M., and Jun, S., *Chem. Commun.* 2225 (1997).
65. Shen, S-C., and Kawi, S., *Chem. Lett.* 1293 (1999).
66. Liu, C., Ye, X., and Wu, Y., *Catal. Lett.* **36**, 263 (1996).
67. Maschmeyer, T., Rey, F., Sankar, G., and Thomas, J. M., *Nature* **378**, 159 (1995).

-
68. Schubert, U., *New J. Chem.* **18**, 1049 (1994).
 69. Burkett, S. L., Sims, S. D., and Mann, S., *Chem. Commun.* 1367 (1996).
 70. Lim, M. H., Blanford, C. F., and Stein, A., *J. Am. Chem. Soc.* **119**, 4090 (1997).
 71. Brunel, D., *Microporous Mesoporous Mater.*, **27**, 329 (1999).
 72. Sutra, P., and Brunel, D., *J. Chem. Soc., Chem. Commun.* 2485 (1996).
 73. Carvalho, W. A., Wallau, M., and Schuchardt, U., *J. Mol. Catal. A* **144**, 91 (1999).
 74. Wu, C.G., and Bein, T., *J. Chem. Soc., Chem. Commun.* 925 (1995).
 75. Ryoo, R., Kim, J. M., Ko, C. H., and Shin, C. H., *J. Phys. Chem.* **100**, 17718 (1996).
 76. Ulagappan, N., and Rao, C. N. R., *J. Chem. Soc., Chem. Commun.* 2759 (1996).
 77. Khushalani, D., Kuperman, A., Ozin, G. A., Tanaka, K., Garcés, J., Olken, M. M., and Kuperman, A., *Adv. Mater.* **7**, 842 (1996).
 78. Sun, T., Ying, J. Y., *Nature* **389**, 704 (1997).
 79. Sun, T., Ying, J. Y., *Angew. Chem. Int. Ed.* **37**, 664 (1998).
 80. Yang, H., Coombs, N., and Ozin, G. A., *Nature* **386**, 692 (1997).
 81. Yang, H., Coombs, N., Sokolov, I., and Ozin, G., *Nature* **381**, 589 (1996).
 82. Schacht, S., Huo, Q., Voight-Martin, I. G., Stucky, G. D., and Schüth, F., *Science* **273**, 768 (1996).
 83. Yang, H., Kuperman, A., Coombs, N., Mamiche-Afara, S., and Ozin, G. A., *Nature* **379**, 703 (1996).
 84. Aksay, I. A., Trau, M., Manne, S., Homma, I., Yao, N., Zhou, L., Fenter, P., Eisenberger, P. M., and Gruner, S. M., *Science* **273**, 892 (1996).
 85. Ogawa, M., *J. Chem. Soc., Chem. Commun.* 1149 (1996).
 86. Huo, Q., Zhao, D., Feng, J., Weston, K., Burratto, S. K., Stucky, G. D., Schacht, S., and Schüth, F., *Adv. Mater.* **9**, 974 (1997).
 87. Huo, Q., Feng, J., Schüth, F., and Stucky, G. D., *Chem. Mater.* **9**, 14 (1997).

-
88. Anderson, M. T., Martin, J. E., Odinek, J. G., Newcomer, P. P., and Wilcoxon, J. P., *Microporous Mater.* **10**, 13 (1997).
 89. Lin, H.-P., and Mou, C.-Y., *Science* **273**, 765 (1996).
 90. Brunauer, S., Emmett, P. H., and Teller, E., *J. Am. Chem. Soc.*, **60**, 309 (1938).
 91. Freyhardt, C. C., Tsapatsis, M., Lobo, R. F., Balkus Jr., and Davis, M. E., *Nature* **381**, 295 (1996).
 92. Jacobs, P. A., and Martier, W. Y., *Zeolites* **2**, 226 (1982).
 93. Notari, B., *Stud. Surf. Sci. Catal.* **37**, 413 (1987).
 94. Ryczkowski, J., *Catal. Today* **68**, 263 (2001).
 95. Lippama, E., Magi, M., Samoson, A., Tarmak, M., and Engelhardt, G., *J. Am. Chem. Soc.* **103**, 4992 (1981).
 96. Fyfe, C. A., Gobbi, G. C., Klinowski, J., Thomas, J. M., and Ramdas, S., *Nature* **296**, 530 (1982).
 97. Reddy, K. M., Moudrakovski, I., and Sayari, A., *J. Chem. Soc., Chem. Commun.* 1059 (1994).
 98. Chenite, A., Page, Y. L., and Sayari, A., *Chem. Mater.* **7**, 1015 (1995).
 99. Alfredsson, V., Keung, M., Monnier, A., Stucky G. D., Unger, and K. K., Schüth, F., *J. chem. Soc, Chem. Commun.* 921 (1994).
 100. Corma, A., Martínez, A., Martínez-Soria, V., and Monton, J. B., *J. Catal.* **153**, 25 (1995).
 101. Armengol, E., Cano, M. L., Corma, A., García, H., and Navarro, M. T., *J. Chem. Soc., Chem. Commun.* 519 (1995).
 102. Kloetstra, K. R., and Van Bekkum, H., *J. Chem. Res.* 26 (1995).
 103. Gunnewegh, E. A., Gopie, S. S., and Van Bekkum, H., *J. Mol. Catal. A: Chem.* **106**, 151 (1996).

104. Climent, M. J., Corma, A., Iborra, S., Navarro, M. C., and Primo, J., *J. Catal.* **161**, 786 (1996).
105. Dai, L.-X., Koyama, K., and Tatsumi, T., *Catal. Lett.* **53**, 211 (1998).
106. Climent, M. J., Corma, A., Iborra, S., Miquel, S., Primo, J., and Rey, F., *J. Catal.* **183**, 76 (1999).
107. Song, S., and Reddy, K. M., *Appl. Catal. A: General* **176**, 1 (1999).
108. Del Rossi, K. J., Hatzikos, G. H., and Huss, A. Jr., *U. S. Patent* 5,256,277 (1993).
109. Chaudhari, K., Das, T. K., Chandwadkar, A. J., and Sivasanker, S., *J. Catal.* **186**, 81 (1999).
110. Kresge, C. T., Marler, D. O., Rav, G. S., and Rose, B. H., *U. S. Patent* 5,366,945 (1994).
111. Mehnert, C. P., and Ying, J. Y., *Chem. Commun.* 2215 (1997).
112. Mehnert, C. P., Weaver, D. W., and Ying, J. Y., *J. Am. Chem. Soc.* **120**, 12289 (1998).
113. Kumar, P., Kumar, R., and Pandey, B., *Synlett* 289 (1995).
114. Cambor, M. A., Corma, A., Martínez, A., and Pérez-Pariente, J., *J. Chem. Soc., Chem. Commun.* 8 (1992).
115. Corma, A., Esteve, P., Martínez, A., and Valencia, S., *J. Catal.* **152**, 18 (1995).
116. Blasco, T., Cambor, M. A., Corma, A., Esteve, P., Martínez, A., Prieto, C., and Valencia, S., *J. Chem. Soc., Chem. Commun.* 2367 (1996).
117. Neumann, R., and Khenkin, A. M., *Chem. Commun.* 2643 (1996).
118. Carvalho, W. A., Varaldo, P. B., Wallau, M., and Schuchardt, U., *Zeolites* **18**, 408 (1997).
119. Reddy, J. S., and Sayari, A., *J. Chem. Soc. Chem. Commun.* 2231 (1995).
120. Das, T. K., Chaudhari, K., Nandan, E., Chandwadkar, A. J., Sudalai, A., Ravindranathan and Sivasanker, S., *Tet. Lett.* **38**, 3631 (1997).

121. Burch, R., Cruise, N., Gleeson, D., and Tsang, S. C., *J. Chem. Soc. Chem. Commun.* 1495 (1995).
122. Chaudhari, K., Das, T. K., Rajmohanam, P. R., Lazar, K., Sivasanker, S., and Chandwadkar, A. J., *J. Catal.* **183**, 281 (1999).
123. Abdel-Fattah, T. M., and Pinnavaia, T. J., *J. Chem. Soc., Chem. Commun.* 665 (1996).
124. Rana, R. K., and Viswanathan, B., *Catal. Lett.* **52**, 25 (1998).
125. Vercruyse, K. A., Klingeleers, D. M., Colling, T., and Jacobs, P. A., *Stud. Surf. Sci. Catal.*, **117**, 469 (1998).
126. Chaudhari, K., Bal, R., Srinivas, D., Chandwadkar, A. J., and Sivasanker, S., *Microporous Mesoporous Mater.* **50**, 209 (2001).
127. Vankelecom, I., Vercruyse, K., Moens, N., Parton, R., Reddy, J. S., and Jacobs, P. A., *Chem. Commun.* 137 (1997).
128. Corma, A., Iglesias, M., and Sanchez, F., *J. Chem. Soc., Chem. Commun.* 1635 (1995).
129. Kalvachev, Y. A., Hayashi, T., Tsubota, S., and Haruta, M., *J. Catal.*, **186**, 228 (1999).
130. Fujiyama, H., Kohara, I., Iwai, K., Nishiyama, S., Tsuruya, S., and Masai, M., *J. Catal.* **188**, 417 (1999).
131. Junges, U., Jacobs, W., Voight-Martin, I., Krutzsch, B., and Schüth, F., *J. Chem. Soc., Chem. Commun.* 2283 (1995).
132. Schiesser, W., Vinek, H., and Jentys, A., *Catal. Lett.* **54**, 189 (1999).
133. Diaz, J. F., Balkus, K. J. Jr., *J. Mol. Catal. B: Enzym.* **2**, 115 (1996).
134. He, J., Li, X., Evans, D. G., Duan, X., and Li, C., *J. Mol. Catal. B: Enzym.* **11**, 45 (2000).
135. Carvalho, W. A., Wallau, M., and Schuchardt, U., *J. Mol. Catal. A: Chem.* **144**, 91 (1999).
136. Ernst, S., and Selle, M., *Microporous Mesoporous Mater.* **27**, 355 (1999).

137. Maschmeyer, T., Oldroyd, R. D., Sankar, G., Thomas, J. M., Shannon, I. J., Klepetko, J. A., Masters, A. F., Beattie, J. K., and Catlow, C. R. A., *Angew. Chem., Int. Ed. Engl.* **36**, 1639 (1997).
138. Koner, S., Chaudhari, K., Das, T. K., and Sivasanker, S., *J. Mol. Catal. A: Chem.* **150**, 295 (1999).
139. Kim, G.-J., and Shin, J.-H., *Tetrahedron Lett.* **40**, 6827 (1999).
140. Tudor, J., and O'Hare, D., *Chem. Commun.* 603 (1997).
141. Raynor, S. A., Thomas, J. M., Raja, R., Johnson, B. F. G., Bell, R. G., and Mantle, M. D., *Chem. Commun.* 1925 (2000).
142. Kumar, R., Bhaumik, A., Ahedi, R. K., and Ganapathy, S., *Nature* **381**, 298 (1996).
143. Kumar, R., Mukherjee, P., Pandey, R. K., Rajmohan P., and Bhaumik, A., *Microporous Mesoporous Mater.* **22**, 23 (1998).
144. Laha, S. C., and Kumar, R., *Microporous Mesoporous Mater.* (in press).
145. Guo, H., Wang, X., and Zou, B., *Cuihua Xuebao (Eng)* **18**, 185 (1997).
146. Laha, S. C., Mukherjee, P., Sainkar S. R., and Kumar, R., *J. Catal.* (in press).
147. Johnson, B. F. G., Raynor, S. A., Shephard, D. S., Mashmeyer, T., Thomas, J. M., Sankar, G., Bromley, S., Oldroyd, R., Gladden, L., and Mantle, M. D., *Chem. Commun.* 1167 (1999).
148. Mukherjee, P., Sastry, M., and Kumar, R., *PhysChemComm* **4**, (2000).
149. Laha, S. C., Mukherjee, P., and Kumar, R., *Bull. Mater. Sci.* **22**, 623 (1999).
150. Mukherjee, P., Laha, S. C., Mandal, D., and Kumar, R., *Stud. Surf. Sci. Catal.* **129**, 283 (2000).
151. Gonsalves, A. M. A. R., Johnstone, R. A. W., Pereira, M. M., and Shaw, J., *J. Chem. Research (S)* 208 (1991).
152. Laha, S. C., and Kumar, R., *J. Catal.* **204**, 64 (2001).

153. Laha, S. C., and Kumar, R., *J. Catal* (in press).
154. Bengoa, J. F., Gallegos, N. G., Marchetti, S. G., Alvarez, A. M., Cagnoli, M. V., and Yeramían, A. A., *Microporous Mesoporous Mater.* **24**, 163 (1998).
155. Geobaldo, F., Bordiga, S., Zecchina, A., Giamello, E., Leofanti, G., and Petrini, E., *Catal. Lett.* **16**, 109 (1992).
156. Chaudhari, K., Srinivas, D., and Ratnasamy, P., *J. Catal* **203**, 25 (2001).

CHAPTER 2

SYNTHESIS

2. SYNTHESIS

Different synthesis routes and mechanisms proposed for the formation of mesoporous materials are reviewed in Chapter I. These are mainly based on the fact that the surfactant molecules will self-organize and interact with the silicate species to yield mesoporous materials. It is therefore logical to say that any synthetic parameter, which will assist and/or nucleate the self-organization of surfactant molecules (e.g. addition of catalytic amount of promoter in the precursor synthesis mixture) for the formation of mesoporous materials, will certainly decrease the synthesis time considerably.

The present chapter deals with the detailed description for synthesis of mesoporous silicate, metallo-silicate,¹ and organo-silicate materials²⁻⁴ obtained in the presence and/or the absence of promoters based on the procedures as described in the literature. It also includes a brief description for the synthesis of microporous medium pore TS-1^{5,6} and TS-2,⁷ incorporated in the present thesis mainly for comparative purpose.

2.1. EXPERIMENTAL

2.1.1. Materials

Materials used for the synthesis of mesoporous and microporous silicate, metallo-silicate, and organo-silicate materials are tabulated in Appendix A (Table A.1). The chemicals were used as received without any further purification if not mentioned specifically.

2.1.2. Synthesis of MCM-41 Type Mesoporous Materials

Generally, the synthesis of mesoporous materials are carried out hydrothermally in an autoclave under autogeneous pressure using a surfactant like cetyltrimethylammonium halide/hydroxide as template and sodium hydroxide and/or tetramethylammonium hydroxide

as mineralizer. Moreover, MCM-41 type mesoporous materials can also be synthesized by refluxing the gel mixture at atmospheric pressure under stirring.¹

During the present work, pure-silicate (Si-MCM-41), alumino-silicate (Al-MCM-41), titano-silicate (Ti-MCM-41) and vanado-silicate (V-MCM-41) type mesoporous materials were synthesized in the presence as well as in the absence of promoter. The synthesis of Si-MCM-41 was studied in detail to investigate the effect of different promoters, promoter concentration and other synthetic parameters mainly in the presence of phosphate (PO_4^{3-}) as promoter.

Hydrothermal syntheses of various Ce-MCM-41 samples were carried out by different methods. The synthesis of Ce-impregnated MCM-41 (Si/Ce = 40), Ce-exchanged MCM-41 (Si/Ce = 40) and physical mixture of amorphous silica-ceria (Si/Ce = 40) samples were also carried out for comparison of their activity with Ce-MCM-41 samples.

Organo-functionalized MCM-41 samples were also synthesized by *in situ* method using tetraalkoxysilane ($\text{Si}(\text{OR})_4$) and organosiloxane ($\text{R}^1\text{-Si}(\text{OR})_3$) as the two silica sources. In the case of post synthetic method, Si-MCM-41 was treated with organosiloxane to get the organo-functionalized MCM-41.

2.1.2.1. Synthesis of Si-MCM-41

The syntheses of Si-MCM-41 samples were carried out using Na_2SiO_3 and SiO_2 in a molar ratio $\text{Na}_2\text{SiO}_3/\text{SiO}_2 = 0.124 : 1$ as different silica sources. In a typical preparation, the two different silica sources, Na_2SiO_3 and SiO_2 were suspended in an aqueous solution of TMAOH and subsequently combined with an aqueous solution of CTABr. Finally, an aqueous solution of NaH_2PO_4 was added as promoter to the synthesis mixture. The typical molar gel composition of Si-MCM-41-P ('P' corresponds to promoter) sample was 1 SiO_2 : 0.11 Na_2O : 0.08 TMAOH : 0.21 CTABr : 125 H_2O : 0.1 NaH_2PO_4 . For the synthesis of standard Si-MCM-41-S ('S' corresponds to standard procedure) sample in the absence of

promoter, an aqueous solution of NaCl instead of NaH₂PO₄ was added to the synthesis mixture to maintain the same Na⁺/SiO₂ molar ratio as in the case of Si-MCM-41-P sample. A standard Si-MCM-41-S₀ sample was also prepared in the absence of both promoter and NaCl, keeping otherwise the same gel composition. The molar gel composition of different Si-MCM-41 samples is presented in Table 2.1. The Si-MCM-41-S₀, Si-MCM-41-S and Si-MCM-41-P samples were synthesized by refluxing the gel mixtures at atmospheric pressure under stirring at a constant temperature of 373 K for a period of 816 h. Different Si-MCM-41 samples were also prepared by varying the synthesis time, Na⁺/SiO₂ ratio, promoter concentrations etc. and also by using sodium salts of different sources of phosphate promoter (e.g. Na₂HPO₄, Na₃PO₄) and different promoter oxyanions (e.g. NO₃⁻, AsO₄³⁻, SO₄²⁻, BrO₃⁻ and IO₃⁻) etc. The solid products thus obtained were washed thoroughly first with deionized water and then with acetone, dried at 353 K and calcined in flowing air at 813 K for 8 h.

2.1.2.2. Synthesis of Al-MCM-41

The syntheses of Al-MCM-41 samples were carried out using NaAlO₂ as the aluminum source. For the synthesis of Al-MCM-41-P sample, an aqueous solution of NaAlO₂ was added to the mixture of Na₂SiO₃, SiO₂ (Na₂SiO₃/SiO₂ (mol/mol) = 0.124 : 1) and aqueous TMAOH under stirring. Then, aqueous solutions of CTABr and NaH₂PO₄ were added to the synthesis mixture and stirred for 15 minutes after each addition. The final molar gel composition of Al-MCM-41-P sample was 1 SiO₂ : 0.01 Al₂O₃ : 0.12 Na₂O : 0.08 TMAOH : 0.21 CTABr : 125 H₂O : 0.1 NaH₂PO₄. For the synthesis of standard Al-MCM-41-S sample in the absence of promoter, an aqueous solution of NaCl instead of NaH₂PO₄ was added to the synthesis mixture to maintain the same Na⁺/SiO₂ molar ratio as in the case of Al-MCM-41-P sample. The final gel mixtures were refluxed under stirring for a period of 12-24 h as shown in Table 2.1. The solid products were collected by filtration, washed thoroughly with deionized water and acetone, dried at 353 K and calcined in flowing air at 813 K for 8 h.

Table 2.1
Chemical compositions of the synthesis gel mixtures (Si/M = 50)^a and effect of promoter in the synthesis time of Si-, Al-, Ti- and V-MCM-41 samples

Sample ^b	Molar gel composition						pH	Synthesis time (h)
	CTABr	Na ₂ O ^c	TMAOH	H ₂ O	P ^d	NaCl		
Si-MCM-41-S ₀	0.21	0.11	0.08	125	-	-	11.2	16
Si-MCM-41-S	0.21	0.11	0.08	125	-	0.1	11.2	16
Si-MCM-41-P	0.21	0.11	0.08	125	0.1	-	10.9	08
Al-MCM-41-S	0.21	0.12	0.08	125	-	0.1	11.2	24
Al-MCM-41-P	0.21	0.12	0.08	125	0.1	-	11.2	12
Ti-MCM-41-S	0.21	-	0.4	125	-	-	11.2	16
Ti-MCM-41-P	0.21	-	0.4	125	0.1	-	11.1	08
V-MCM-41-S	0.21	-	0.4	125	-	-	11.2	16
V-MCM-41-P	0.21	-	0.4	125	0.1	-	11.1	08

^aM : Metal; Al for Al-MCM-41, Ti for Ti-MCM-41 and V for V-MCM-41.

^b S₀, S and P denote samples synthesized in the absence of both promoter & NaCl, in the presence of NaCl only (standard condition) and in the presence of promoter, respectively.

^cIncludes Na coming from Na₂SiO₃ and NaAlO₂.

^dP : Promoter; NaH₂PO₄ used for Si and Al-MCM-41; H₃PO₄ used for Ti- and V-MCM-41.

2.1.2.3. Synthesis of Ti- and V-MCM-41

For the synthesis of Ti- and V-MCM-41 materials, TBOT and VOSO₄·3H₂O were used as the metal ion sources, whereas H₃PO₄ and fumed SiO₂ were used as promoter and silica source, respectively. Since, in the synthesis of Ti- and V-MCM-41-P samples, H₃PO₄, an acid was used as promoter; excess TMAOH was used to maintain the pH of the gel mixtures. In a

typical preparation of Ti-MCM-41-P sample, TBOT in *dry* isopropanol was added very slowly to the mixture of fumed SiO₂ and TMAOH. Then, aqueous solutions of CTABr and H₃PO₄ were added to the synthesis mixture. The final molar gel composition of Ti-MCM-41-P sample was 1 SiO₂ : 0.02 TiO₂ : 0.4 TMAOH : 0.21 CTABr : 125 H₂O : 0.1 H₃PO₄. The standard Ti-MCM-41-S sample was prepared in the absence of promoter using the gel composition as given in Table 2.1.

The synthesis of two V-MCM-41 (V-MCM-41-P and V-MCM-41-S) samples were also carried out, both in the presence and in the absence of promoter, in the same way as that of Ti-MCM-41 samples except that an aqueous solution VOSO₄·3H₂O was added in place of an alcoholic solution of TBOT.

2.1.2.4. Synthesis of Ce-containing MCM-41 Type Mesoporous Materials

2.1.2.4.1. Synthesis of Ce-MCM-41

The hydrothermal syntheses of Ce-MCM-41 samples were mainly carried out under reflux condition at atmospheric pressure. However, the syntheses were also carried out in autoclave under autogeneous pressure in stirring as well as in static conditions. The molar gel compositions of the synthesis gels were 1 SiO₂ : x CeO₂ : 0.30 TMAOH : 0.25 CTABr : 125 H₂O, where $x = 0, 0.00625, 0.0125, 0.025$ and 0.05 .

In a typical synthesis of Ce-MCM-41 sample, 3.0 g of fumed silica was slowly added to 5.47 g of TMAOH in 10.0 g water under vigorous stirring. Subsequently, an aqueous solution of ceric sulfate (0.505 g dissolved in 10.0 g water) was added followed by the addition of 4.55 g of CTABr dissolved in 30.0 g water. The remaining 58.4 g of water was added and the stirring was continued for 15 minutes. Finally, the synthesis gel was taken in a glass flask (250 ml capacity) and *refluxed* for 48 h under stirring. The materials thus obtained were filtered, washed thoroughly first with deionized water and then with acetone and dried at 353 K. All the samples were calcined at 813 K for 8 h in presence of air. While, Ce-MCM-41

samples with Si/Ce ratios of 160, 80, 40 and 20 were prepared under reflux condition, the Ce-MCM-41 samples with Si/Ce = 40 were also prepared in autoclave under autogeneous pressure in static condition as well as in stirring condition (Parr reactor) at 200 rpm both at 373 K for 48 h, for comparison purpose. All the samples resembled a light yellow color.

2.1.2.4.2. Synthesis of Ce-impregnated MCM-41

2.0 g of calcined Si-MCM-41 sample was added to a solution of 0.336 g $\text{CeSO}_4 \cdot 4\text{H}_2\text{O}$ dissolved in 10.0 g water to prepare Ce-impregnated MCM-41 with Si/Ce = 20. The mixture was then mixed thoroughly and heated on a water bath to dryness. The dried impregnated sample was then calcined at 773 K for 6 h.

2.1.2.4.3. Synthesis of Ce-exchanged MCM-41

1.0 g of calcined Si-MCM-41 sample was added to a solution of 0.126 g $\text{CeSO}_4 \cdot 4\text{H}_2\text{O}$ dissolved in 25.0 g water to prepare Ce-exchanged MCM-41. The mixture was stirred at room temperature for 24 h and then the exchanged material was filtered, washed thoroughly with deionized water, dried at 373 K and calcined at 773 K for 6 h.

2.1.2.4.4. Synthesis of amorphous silica-ceria

Amorphous silica-ceria (Si/Ce = 20) sample was prepared for comparison of its catalytic activity with Ce-MCM-41 samples. The synthesis of amorphous silica-ceria (Si/Ce = 20) was carried out by adding 0.28 g cerium (IV) oxide and 2.0 g fumed silica in 10.0 g water. Then the mixture was stirred at room temperature for 15 min. and heated on a water bath to dryness. The dried amorphous silica-ceria sample was calcined at 773 K for 6 h.

2.1.2.5. Synthesis of Organo-Functionalized MCM-41

The syntheses of various organo-functionalized MCM-41 materials were carried out by *in situ* as well as post synthetic methods. For *in situ* synthesis of 3-aminopropyl- and 3-mercaptopropyl-functionalized-MCM-41 materials, 3-X-propyltrimethoxysilane (XPTS) was

used along with TEOS in a 1 : 2.5 molar ratio as the silica sources (X = NH₂ or SH). The gel composition was 1.0 XPTS : 2.5 TEOS : 0.42 CTABr : 0.96 NaOH : 272 H₂O : 66 MeOH. Methanol was used in the initial gel mixture to reduce and control the fast hydrolysis of XPTS. Similarly, vinyl-MCM-41 was also prepared using the gel composition as 1.0 TEOS : 0.1 VTES : 0.15 CTABr : 0.38 NaOH : 125 H₂O (VTES = vinyltriethoxysilane). The bifunctional HS-H₂N-MCM-41 and HS-Al-MCM-41 were prepared in a same way as the corresponding monofunctional MCM-41 materials, using the gel composition as given in Table 2.2. For the SH-Al-MCM-41 sample SiO₂ : Al₂O₃ molar ratio was 1 : 0.025. All the synthesis gel mixtures were first stirred at room temperature for 12 h to remove methanol and then heated in autoclave at 368 K for 36 h under static condition. The products obtained were filtered, washed several times with distilled water and acetone, and then dried at ambient

Table 2.2
Chemical composition of the synthesis gel mixture of organo-functionalized MCM-41 samples

Sample	Molar Gel Composition ^a							
	TEOS	APTS	MPTS	VTES	CTA	NaOH	H ₂ O	MeOH
A : HS-MCM-41	2.5	-	1.0	-	0.42	0.96	272	66
B : H ₂ N-MCM-41	2.5	1.0	-	-	0.42	0.96	272	66
C : HS-H ₂ N-MCM-41	1.0	0.125	0.125	-	0.17	0.38	109	26
D : HS-Al-MCM-41	1.0	-	0.1	-	0.17	0.38	109	26
E : Vinyl-MCM-41	1.0	-	-	0.1	0.15	0.38	125	-

^a TEOS, tetraethyl orthosilicate; APTS, 3-aminopropyltrimethoxysilane; MPTS, 3-mercaptopropyltrimethoxysilane; VTES, vinyltriethoxysilane; CTA, cetyltrimethylammonium bromide; MeOH, methanol.

temperature under vacuum. From all organo-functionalized MCM-41 samples, surfactant was removed by solvent extraction containing methanol, water and HCl. In a typical extraction process, 85 g of methanol and 3.25 g of HCl (35.4 wt.%) were used for 24 h under reflux for the removal of surfactant from 1.0 g of the solid product.

H₂N-MCM-41 and HS-MCM-41 were also synthesized by post synthesis modification. In a typical synthesis of H₂N-MCM-41 or HS-MCM-41 sample, 1.0 g of activated Si-MCM-41 was taken in 25 ml *dry* toluene and to this stirred suspension, 0.60 g of APTS or 0.66 g of MPTS diluted in 25 ml of *dry* toluene was added very slowly through a syringe under N₂ atmosphere at room temperature (298 K). After complete addition of APTS or MPTS, the mixture was refluxed at 353 K for 24 h in N₂ atmosphere. The functionalized H₂N-MCM-41 or HS-MCM-41 was filtered and washed with *dry* toluene followed by acetone and dried at ambient temperature under vacuum.

2.1.3. Synthesis of TS-1 and TS-2

Titanium-silicate molecular sieves, TS-1 and TS-2, were prepared by employing the concept of promoter-induced synthesis of zeolitic materials. In the synthesis of TS-1 and TS-2, TEOS, TBOT and H₃PO₄ were used as silica source, titanium source and promoter, respectively.

2.1.3.1. Synthesis of TS-1

In a typical preparation of TS-1 sample, 20.8 g of TEOS was slowly added to 50.8 g of TPAOH under vigorous stirring for 2 h. Next, a solution containing 1.13 g of TBOT dissolved in 5.7 g *dry* isopropanol (IPA) was added slowly to the above clear solution of TPA-silicate under vigorous stirring. The gel mixture was further stirred for 30 min. and then an aqueous solution of 0.77 g H₃PO₄ diluted by 4.4 g water was added very slowly under vigorous stirring, which was continued for one more hour. The final molar gel composition

for the TS-1 sample was 1 TEOS : 0.5 TPAOH : 0.033 TBOT : 0.067 H₃PO₄ : 25 H₂O. The gel mixture was heated in a stainless steel autoclave at 433 K for 6 h under autogeneous pressure and agitation (60-65 rpm). After crystallization, the solid product was collected by centrifugation, washed thoroughly first with deionized water and dilute acid solution (containing 2 wt.% H₂SO₄ and 5 wt.% H₂O₂) and then with deionized water, dried at 393 K for 4 h and calcined at 813 K in air for 12 h.

2.1.3.2. Synthesis of TS-2

The TS-2 sample was also prepared similarly using TBAOH as the organic templating agent. In a typical preparation, 20.8 g of TEOS was added to a solution of 15.0 g TBAOH diluted with 15.0 g water under vigorous stirring for 1 h. The mixture was stirred for another 1 h. To the above clear solution of TBA-silicate, a solution of 1.13 g of TBOT dissolved in 5.7 g *dry* isopropanol (IPA) was added slowly under vigorous stirring. Stirring was continued for another 1 h and then a solution of 7.7 g TBAOH diluted with 5.0 g water was added slowly under vigorous stirring. Finally, an aqueous solution of 0.77 g H₃PO₄ diluted by 11.4 g water was added very slowly and stirring was continued for one more hour. The final molar gel composition for the TS-2 sample was 1 TEOS : 0.35 TBAOH : 0.033 TBOT : 0.067 H₃PO₄ : 25 H₂O. The crystallization of the sample was carried out in a stainless steel autoclave at 433 K for 6 h under agitation (60-65 rpm). After crystallization the solid product was collected by filtration and thoroughly washed. The TS-2 sample then dried at 393 K for 4 h and calcined at 813 K in air for 12 h.

2.2. RESULTS AND DISCUSSION

2.2.1. Synthesis of Si-MCM-41

The effects of different promoter oxyanions and their corresponding oxyacids of group IV, V, VI and VII elements affecting the synthesis mechanism has been examined by preparing different samples in the presence and the absence of promoters.

2.2.1.1. Effect of time

It has been reported that the diffraction pattern of the hexagonal mesostructure was detected within 1 h.^{8,9} However, the material with final degree of long-range ordering and thermal stability was attained only after several hours (≥ 16 h). In the preparation of Si-MCM-41-P sample, we have also observed that the mesostructure was formed within 1 h of the hydrothermal treatment as shown by XRD profile in Figure 2.1. However, the broad peak becomes narrower and d_{100} value shifted to higher value with increase in the synthesis time. The regularity of the products with narrower pore size distribution and the solid yield also increased with increasing synthesis time. Well-ordered Si-MCM-41 in the absence of promoter (Si-MCM-41-S) is obtained after 16 h whereas the same in the presence of promoter (Si-MCM-41-P) is obtained in 8 h only (Table 2.1).

Similar observations were made from the ^{29}Si MAS NMR spectra of as-synthesized Si-MCM-41-S and Si-MCM-41-P samples measured at different time interval. It is observed that the intensity of more condensed $(\text{SiO})_4\text{Si}$ (Q_4) species observed at *ca.* -110 ppm increases at the expense of less condensed $(\text{SiO})_3\text{SiOH}$ (Q_3) and $(\text{SiO})_2\text{Si}(\text{OH})_2$ (Q_2) species observed at *ca.* -100 and -90 ppm, respectively. The Q_3/Q_4 ratio, which is generally used to determine the degree of condensation of solid silicate product, decreases with increasing synthesis time due to condensation of Q_3 to Q_4 species (Figure 2.2). Since, MCM-41 is an ordered array of amorphous silicate material and therefore, it contains substantial amount of defect sites (Q_3

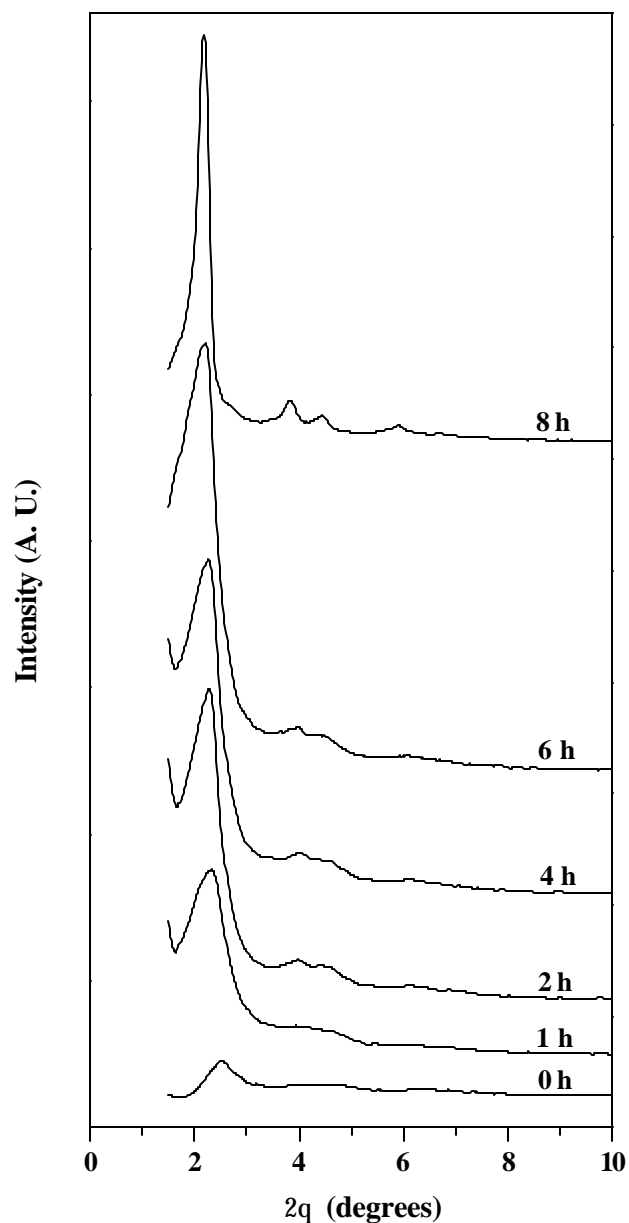


Figure 2.1 Change of X-ray diffraction pattern with time (h) in hydrothermal synthesis of as-synthesized Si-MCM-41-P prepared in the presence of promoter (NaH₂PO₄).

species) even in the final product in accordance with the reports of earlier workers.^{10,11} Nevertheless, the Q₃/Q₄ ratio for Si-MCM-41-P samples is always lower than that of Si-MCM-41-S samples both in as-synthesized and in calcined form (Figure 2.2). The ²⁹Si MAS NMR spectra of calcined Si-MCM-41-S and Si-MCM-41-P samples show substantial

condensation of Q₃ to Q₄ species during calcination. The Q₃ : Q₄ ratios of Si-MCM-41-S (16 h) sample was measured as 56 : 44 (1.27) and 23 : 77 (0.30) before and after calcination, respectively. The corresponding values of Q₃/Q₄ ratio of Si-MCM-41-P sample were 43 : 57 (0.75) and 14 : 86 (0.16) before and after calcination.

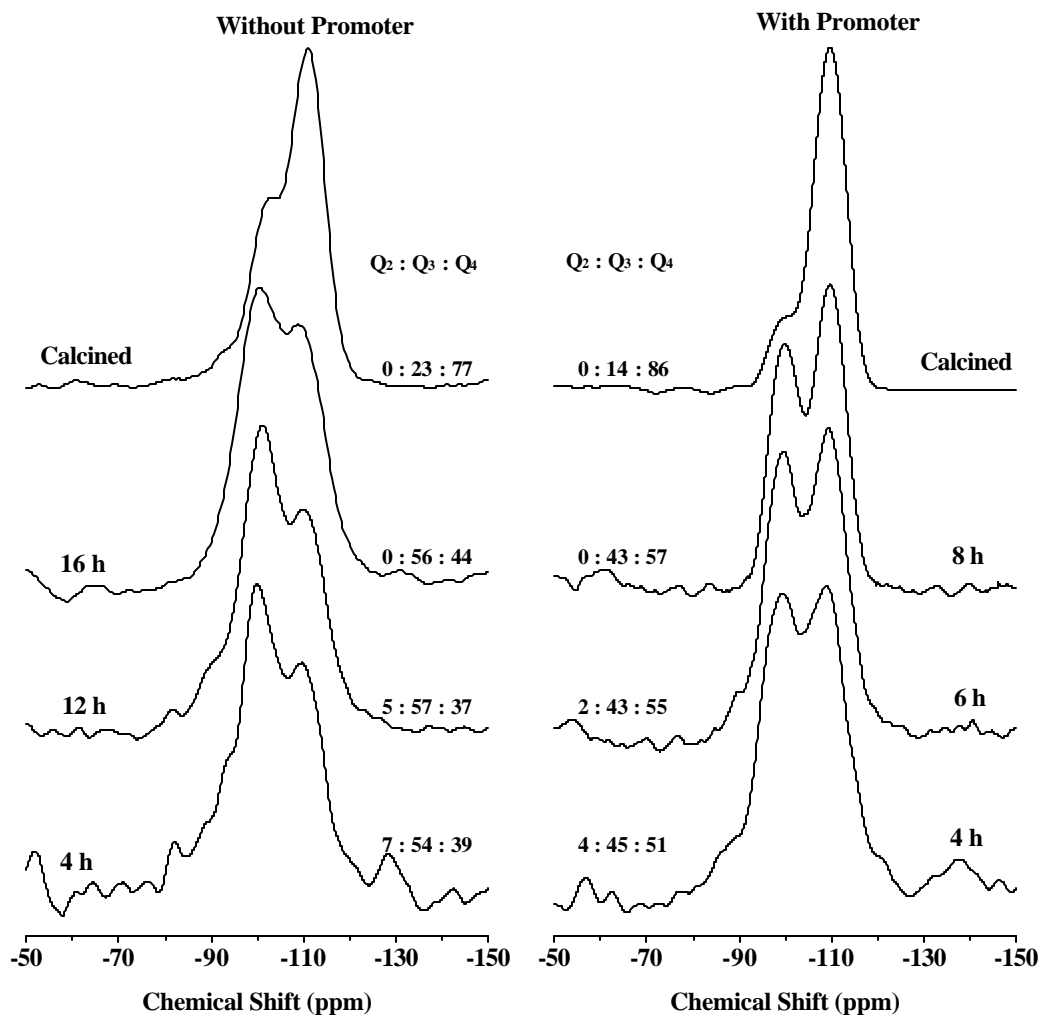


Figure 2.2 ²⁹Si MAS NMR spectra of as-synthesized Si-MCM-41-S (without promoter) and Si-MCM-41-P (with promoter) samples measured at different time interval (h) and corresponding calcined (end) samples. Q₂ : Q₃ : Q₄ ratios of different samples were calculated using Jandel Scientific PeakFit deconvolution program.

2.2.1.2. Effect of different promoters

The effect of different promoters in the synthesis of Si-MCM-41 materials is shown in Figure 2.3. It is observed that the synthesis of Si-MCM-41 materials in the presence of promoter is faster (< 16 h) than in its absence for obtaining ordered MCM-41 materials. It is also observed that at same promoters concentrations, the synthesis time to obtain well-ordered MCM-41 material decreases with increase in the charge/radius (Z/r) ratio of the central cation of the corresponding promoter oxyanion, as it has been observed in the case of zeolites.^{5,6}

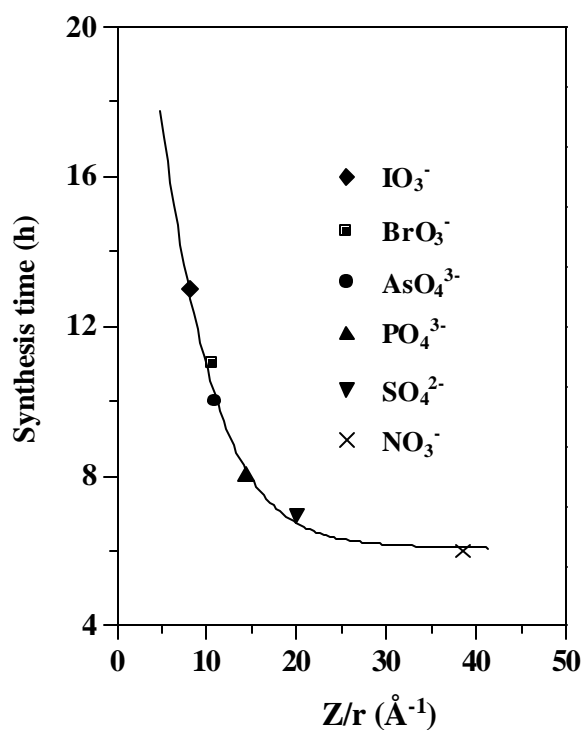


Figure 2.3 Correlation between the synthesis time and the charge/radius (Z/r , \AA^{-1}) ratio of the central cation of the promoter in the synthesis of Si-MCM-41.

Thus, at same promoter concentration, the effect of different promoters in the synthesis of MCM-41 materials depends on the polarizing ability of promoter oxyanion. Higher polarizing ability of the promoter central cation leads to shorter synthesis time. However, the decrease in

the synthesis time is proportional to the increase in the Z/r value of the central cation of promoter up to a certain limit. Further increase in the Z/r value of the central cation of promoter (as in the case of NO_3^- and SO_4^{2-}) did not decrease the synthesis time proportionately and practically it reaches to a limiting value (Figure 2.3).

2.2.1.3. Effect of promoter concentrations

The graphical co-relation between promoter concentration (NaH_2PO_4) and synthesis time is given in Figure 2.4. It is observed that with an increase in phosphate (PO_4^{3-}) concentration in the synthesis gel, the synthesis time decreases and reaches a limiting value at $\text{P/Si} = 0.15$. No significant change is observed upon further increasing the promoter concentration. This indicates that an optimum range of promoter concentration is required for the promoter-

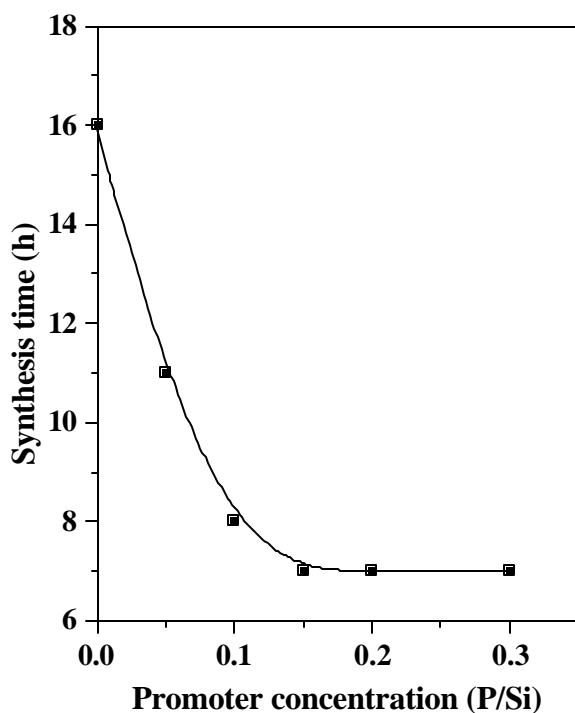


Figure 2.4 Effect of promoter (NaH_2PO_4) concentration on the synthesis time of Si-MCM-41-P.

induced synthesis of Si-MCM-41 materials. Similar results were obtained for Si-MCM-41 with Na_2HPO_4 and also for Al-, Ti- and V-MCM-41 with NaH_2PO_4 .

2.2.1.4. Effect of different sources of phosphate (PO_4^{3-}) promoter

To determine the effect of different sources of phosphate (PO_4^{3-}) promoter (Table 2.3), three different sodium salts of phosphate (NaH_2PO_4 , Na_2HPO_4 and Na_3PO_4) were used for the synthesis of Si-MCM-41-P materials and compared with the Si-MCM-41-S samples prepared in its absence. The Na^+/SiO_2 ratio was maintained by adding appropriate amount of NaCl in

Table 2.3
Effect of NaCl and different sources of phosphate (PO_4^{3-}) promoter in the pH, synthesis time, and solid yield of different Si-MCM-41 samples

Sample ^a	NaCl or Promoter	Na^+/SiO_2	pH		Synthesis time (h)	Solid yield (%) ^b
			$pH_{initial}$	pH_{final}		
Si-MCM-41-S	NaCl	0.1	11.2	11.0	16	85
Si-MCM-41-S'	NaCl	0.2	11.2	11.0	16	83
Si-MCM-41-S''	NaCl	0.3	11.2	11.0	16	82
Si-MCM-41-P	NaH_2PO_4	0.1	10.9	10.8	08	90
Si-MCM-41-P'	Na_2HPO_4	0.2	11.2	11.0	08	90
Si-MCM-41-P''	Na_3PO_4	0.3	11.2	11.0	08	92

^a S symbols (S \Rightarrow 1 equivalent of NaCl, S' \Rightarrow 2 equivalent of NaCl and S'' \Rightarrow 3 equivalent of NaCl) and P symbols (P, NaH_2PO_4 ; P', Na_2HPO_4 ; and P'', Na_3PO_4) denote samples synthesized in the presence of NaCl only (standard condition) and in the presence of promoter, respectively.

^b Based on SiO_2 taken in the gel mixture.

later case. The pH of the three syntheses gels containing three promoters, under otherwise same reaction conditions, is slightly different due to difference in basicity of the three salts as given in Table 2.3. The range of pH value for all the samples was 11 ± 0.2 . However, the same synthesis time and comparable solid yield of Si-MCM-41-P, Si-MCM-41-P' and Si-MCM-41-P'' samples synthesized in the presence of these promoters (although at slightly different pHs) clearly indicate that the fast syntheses of these materials are solely due to the presence of promoter. The slight difference in pH does not have any significant contributing effect. It is also important to note that the solid yield of Si-MCM-41-P samples (prepared in the presence of promoter) is higher than that of Si-MCM-41-S samples (without promoter) prepared under same synthesis conditions.

2.3. REFERENCES

1. Carvalho, W. A., Varaldo, P. B., Wallau, M., and Schuchardt, U., *Zeolites* **18**, 408 (1997).
2. Burkett, S. L., Sims, S. D., and Mann, S., *Chem. Commun.* 1367 (1996).
3. Lim, M. H., Blanford, C. F., and Stein, A., *J. Am. Chem. Soc.* **119**, 4090 (1997).
4. Brunel, D., *Microporous Mesoporous Mater.* **27**, 329 (1999).
5. Kumar, R., Bhaumik, A., Ahedi, R. K., and Ganapathy, S., *Nature* **381**, 298 (1996).
6. Kumar, R., Mukherjee, P., Pandey, R. K., Rajmohan P., and Bhaumik, A., *Microporous and Mesoporous Mater.* **22**, 23 (1998).
7. Reddy, J. S., and Kumar, R., *Zeolites* **12**, 95 (1995).
8. Chen, C. Y., Li, H. X., and Davis, M. E., *Microporous Mater.* **2**, 17 (1993).
9. Monnier, A., Schüth, F., Hio, Q., Kumar, D., Margolese, D., Maxwell, R. S., Stucky, G. D., Krishnamurty, M., Petroff, P., Firouzi, A., Janicke, M., and Chmelka, B. F., *Science* **261**, 1299 (1993).
10. Beck, J. S., Vartulli, J. C., Roth, W. J., Leonowicz, M. E., Kresge, C. T., Schmitt, K. D., Chu, C. T.-W., Olson, D. H., Sheppard, E. W., McCullen, S. B., Higgins, J. B., and Schlenker, J. L., *J. Am. Chem. Soc.* **114**, 10834 (1992).
11. Park, D. H., Cheng, C. F., He, H., and Klinowski, J., *J. Mater. Chem.* **7**, 159 (1997).

CHAPTER 3

CHARACTERIZATION

3. CHARACTERIZATION

In this chapter the experimental details and the results of different spectroscopic (powder X-ray diffraction (XRD), energy dispersive X-ray analysis (EDX), diffuse reflectance UV-Vis, FTIR, solid state magic angle spinning (MAS) NMR, and electron paramagnetic resonance (EPR)), microscopic (scanning electron microscopy (SEM), and transmission electron microscopy (TEM)), volumetric (adsorption and surface area analysis by BET method), and thermogravimetric (thermogravimetry-differential thermal analysis (TG-DTA)) characterization of various mesoporous and microporous materials, synthesized as described in Chapter 2, are presented and discussed.

3.1. EXPERIMENTAL

3.1.1. X-ray Diffraction

The powder X-ray diffractograms of as-synthesized and calcined samples were recorded either on a Rigaku D MAX III VC or Rigaku Miniflex diffractometer using a Ni-filtered monochromatic Cu K_{α} radiation ($\lambda = 1.5406 \text{ \AA}$). The microporous materials were scanned between 5-50° (2 θ) whereas the spectra of mesoporous materials were recorded in the 2 θ range 1.5-10°. The scanning rate was 1°/min in all cases. The samples were prepared as thin layers on glass/aluminum slides, prior to scanning.

3.1.2. Chemical Analyses

The chemical compositions of as-synthesized and calcined samples were determined mainly by microanalysis of organic groups/molecules (C, H, N and S) and EDX analysis of different metal atoms (Si, Al, Ti, V, and Ce etc.). The elemental (C, H, N and S) analyses were carried out on a Carlo Erba EA1108 elemental analyzer. The EDX analyses of calcined

samples were recorded on a Kevex equipment attached with Jeol JSM-5200 scanning microscope.

3.1.3. Adsorption Measurements

The specific surface area, pore size and pore volume of calcined samples were determined by BET method from N₂ adsorption isotherms using a commercial volumetric adsorption apparatus (Omnisorb 100 CX, Coulter Corporation, USA). Approximately, 150-200 mg calcined sample was first degassed at 673 K for 5 h at 10⁻⁵ Torr and then slowly cooled to room temperature under vacuum and the anhydrous weight of the sample was taken. Finally, the sample was cooled to 77 K using liquid nitrogen and the adsorption of nitrogen was carried out at different equilibrium pressures.

3.1.4. Diffuse Reflectance UV-Vis Spectroscopy

The diffuse reflectance UV-Vis spectra were recorded in the range 200-600 nm with a Shimadzu UV-2101 PC spectrometer equipped with a diffuse reflectance attachment using solid sample holder. The base line correction was made using barium sulfate as the reference standard.

3.1.5. Fourier-Transform Infrared (FTIR) Spectroscopy

The FTIR spectra were recorded in the 400-4000 cm⁻¹ range on a Shimadzu FTIR-8201 PC in Nujol on KBr disc. To avoid the bands of hydrocarbon coming from nujol, FTIR spectra of organo-functionalized MCM-41 samples were recorded in the diffuse reflectance mode as KBr pellets.

3.1.6. Pyridine and Ammonia Sorption

FTIR spectra of adsorbed pyridine and of ammonia were recorded using a specially designed all silica *in situ* controlled environment cell. The spectra were recorded using

Nicolet 60 SXB or Shimadzu 8300 spectrometer with a resolution of 2 cm^{-1} averaging over 500 scans. In Nicolet 60 SXB spectrometer, the samples were activated under vacuum (10^{-6} Torr) at 673 K for 3 h and then cooled to 373 K before recording the spectra. Then the samples were allowed to adsorb pyridine at an equilibrium pressure of 20 mm of Hg for 30 min. Excess and physisorbed pyridine was removed by evacuation for 1 h before recording the spectra of chemisorbed pyridine at 373 K. In this way, the samples were heated to 423, 473, 523, 573 and 673 K successively under vacuum for 1 h at each temperature before recording the spectra. Similarly, ammonia gas (10 vol.% in helium) was passed through the samples loaded on Shimadzu 8300 spectrometer at 373 K and the spectrum was recorded. Then excess and physisorbed ammonia was removed by purging nitrogen for 1 h before recording the spectra of chemisorbed ammonia. The samples were further heated to 423, 473 and 523 K successively under flowing nitrogen for 1 h at each temperature before recording the spectra.

3.1.7. Nuclear Magnetic Resonance (NMR) Spectroscopy

The solid-state MAS and CP MAS NMR spectra were recorded on Bruker MSL 300 or DRX 500 NMR spectrometers. The finely powdered samples were placed in 7.0 mm zirconia rotor and spun at 2.5-3.5 kHz (MSL 300) or 7-8 kHz (DRX 500). The chemical shifts were referred with respect to adamantane CH carbon ($\delta = 28.7$ ppm from TMS), $\text{Al}(\text{H}_2\text{O})_6^{3+}$ ($\delta = 0.0$ ppm), tetraethyl orthosilicate ($\delta = -82.4$ ppm from TMS) and VOCl_3 ($\delta = 0.0$ ppm) for ^{13}C , ^{27}Al , ^{29}Si and ^{51}V , respectively.

3.1.8. Electron Paramagnetic Resonance (EPR) Spectroscopy

The EPR spectra of the samples were recorded on a Bruker EMX spectrometer operating at X-band frequency and 100 kHz field modulation. EPR measurements were done on Ti-MCM-41, TS-1 and TS-2 and samples (50 mg) reacted with solid urea-hydrogen peroxide

(UHP; 100 mg) or 45 wt.% aqueous hydrogen peroxide (HP; 100 mg). The low temperature measurements were carried out at 77 K using a Bruker BVT 3000 variable temperature set-up. The spin Hamiltonian parameters were determined by simulating the EPR spectra using the Simfonia software package.

3.1.9. Scanning Electron Microscopy (SEM)

The SEM micrographs of the samples were determined either on a JEOL JSM-5200 or Leica Stereoscan 440 scanning electron microscope. The samples were loaded on stubs and sputtered with thin gold film to prevent surface charging and also to protect from thermal damage from the electron beam, prior to scanning.

3.1.10. Transmission Electron Microscopy (TEM)

The TEM images were scanned on a JEOL JEM-1200EX instrument with 100 kV of acceleration voltage. The samples were dispersed on Cu-grid coated with thin polymeric film. The dispersed samples were then coated with carbon to avoid vaporization of the samples under high vacuum and in the presence of high-energy electron beam.

3.1.11. Thermal Analysis (TG-DTA)

The thermogravimetry and differential thermal analyses (TG-DTA) of the as-synthesized samples were carried out on a Setaram TG-DTA 92 instrument under a flow of air (2.5 liter/h) with a heating rate of 10 K/min. between 298 and 1000 K. The base line correction was made using inert α -alumina as the reference sample.

3.2. RESULTS AND DISCUSSION

3.2.1. MCM-41 Type Mesoporous Materials

3.2.1.1. Si-MCM-41

The physical properties of Si-MCM-41 samples prepared in the presence and absence of promoter are similar. The synthesis time, Si/M molar ratio and XRD data of well-ordered Si-MCM-41, Al-MCM-41, Ti-MCM-41 and V-MCM-41 samples are given in Tables 3.1 and 3.2.

Table 3.1

Effect of promoter in the synthesis time and results of elemental analysis, d_{100} spacing and unit cell parameter a_0 of M-MCM-41 (M = Si, Al, Ti and V) samples

Sample ^a	Synthesis time (h)	(Si/M) _{gel}	(Si/M) _{solid}	d_{100} (Å)	a_0 (Å) ^b
Si-MCM-41-S ₀	16	-	-	38.2	44.1
Si-MCM-41-S	16	-	-	38.2	44.1
Si-MCM-41-P	08	-	-	37.9	43.8
Al-MCM-41-S (50)	24	50	48	37.9	43.8
Al-MCM-41-P (50)	12	50	49	37.5	43.3
Ti-MCM-41-S (50)	16	50	51	39.4	45.5
Ti-MCM-41-P (50)	08	50	52	39.4	45.5
V-MCM-41-S (50)	16	50	66	39.4	45.5
V-MCM-41-P (50)	08	50	64	39.1	45.1

^a S₀, S and P denote samples synthesized (i) in the absence of both promoter and NaCl (S₀), (ii) in the presence of NaCl only (standard condition) (S), and (iii) in the presence of promoter (P), respectively.

^b Calculated by the equation, $a_0 = 2 d_{100}/\sqrt{3}$.

Table 3.2
Effect of NaCl and different sources of phosphate (PO_4^{3-}) promoter on the physico-chemical properties of different Si-MCM-41 samples

Sample ^a	d_{100} (Å)	BET surface area (m^2g^{-1})	Pore diameter (Å)
Si-MCM-41-S	38.2	1296	27.6
Si-MCM-41-S'	38.1	1252	27.4
Si-MCM-41-S''	38.1	1202	27.1
Si-MCM-41-P	37.9	1480	27.0
Si-MCM-41-P'	38.1	1376	27.1
Si-MCM-41-P''	38.0	1167	26.7

^a S symbols (S \Rightarrow 1 equivalent of NaCl, S' \Rightarrow 2 equivalent of NaCl and S'' \Rightarrow 3 equivalent of NaCl) and P symbols (P, NaH_2PO_4 ; P', Na_2HPO_4 ; and P'', Na_3PO_4) denote samples synthesized in the presence of NaCl only (standard condition) and in the presence of promoter, respectively.

The BET surface area also increases with an increase in the synthesis time. The inflection in the N_2 isotherm around $P/P_0 = 0.25-0.4$ becomes sharper indicating narrower and uniform pore size distribution.¹ Typical N_2 adsorption isotherm along with the pore size distribution (inset) is shown in Figure 3.1 for the Si-MCM-41-P sample. In general, the BET surface area of M-MCM-41-P samples is higher than M-MCM-41-S samples (Table 3.2 and 3.3). The particle size of the samples synthesized in the presence of promoter (M-MCM-41-P) is less than that of those synthesized in its absence (M-MCM-41-S), as confirmed by the scanning electron micrographs of various M-MCM-41-S and M-MCM-41-P samples (Table 3.3). The absence of promoter (e.g. phosphorous) in thoroughly washed Si-MCM-41 samples is

confirmed by carrying out EDX analyses of the central cation of promoter oxyanions. The IR spectra of Si-MCM-41 samples are typical of MCM-41 type mesoporous materials showing bands at 962 cm^{-1} for $\nu(\text{Si-OH})$ vibration, 1090 cm^{-1} for $\nu_{\text{asym.}}(\text{Si-O-Si})$ etc., as shown in Figure 3.2 for Si-MCM-41-P sample.

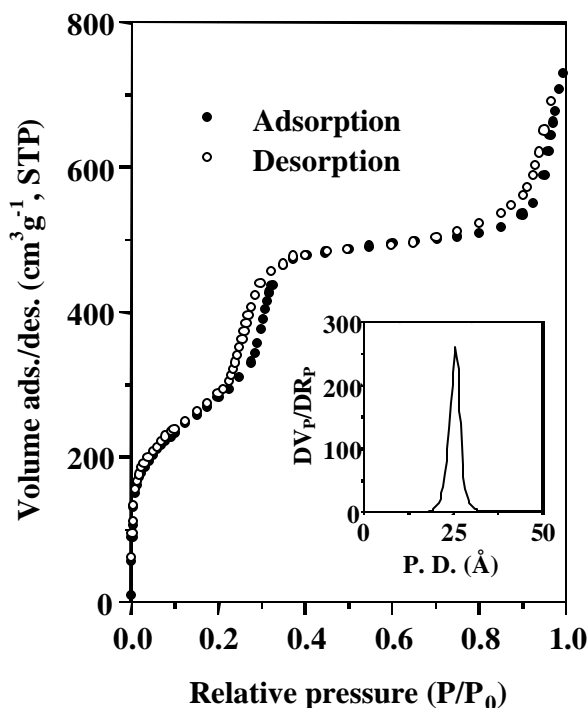


Figure 3.1 Nitrogen adsorption-desorption isotherm and pore size distribution (inset) for Si-MCM-41-P. The pore size distribution is calculated by plotting derivative of pore volume and pore radius (DV_p/DR_p) against pore diameter (P. D.).

By comparison of the ^{13}C CP MAS NMR spectra of as-synthesized M-MCM-41-P (M = Si, Al, Ti and V) samples with that of CTA^+ cation in CDCl_3 solution (Figure 3.3) the presence of intact CTA^+ cation can be inferred. However, the broadness of all the peaks in all the M-MCM-41-P samples compared to that of CTA^+ in CDCl_3 might be attributed to the restricted translational movement of organic molecules in confined void space of MCM-41 samples. ^{31}P MAS NMR spectra of as-synthesized Si-MCM-41-P samples show no signal of

phosphorous (promoter) which further prove the absence of promoter in these samples supporting the EDX data.

Table 3.3
Nitrogen sorption pore diameter, framework wall thickness (FWT), BET surface area and average particle size of M-MCM-41 (M = Si, Al, Ti and V) samples

Sample	Pore diameter (Å) ^a	FWT (Å) ^b	BET surface area (m ² g ⁻¹)	Average particle size (μm) ^c
Si-MCM-41-S ₀	28.0	16.1	1310	2 × 10
Si-MCM-41-S	27.6	16.5	1296	2 × 10
Si-MCM-41-P (50)	27.0	16.8	1480	0.5 × 0.8
Al-MCM-41-S (50)	28.2	15.6	1169	2 × 10
Al-MCM-41-P (50)	27.7	15.6	1245	0.8 × 1.2
Ti-MCM-41-S (50)	30.8	15.0	1242	2 × 10
Ti-MCM-41-P (50)	30.3	15.2	1297	0.4 × 0.6
V-MCM-41-S (50)	29.0	15.3	1194	1.8 × 10
V-MCM-41-P (50)	29.2	15.1	1272	0.4 × 0.8

^aThe pore diameter of the samples was measured by BJH method.

^bFramework wall thickness (FWT) = a_0 - pore diameter.

^cMeasured by scanning electron microscopy.

The SEM photographs of Si-MCM-41-P sample, given in Figure 3.4, are typical of MCM-41 type materials. Two types of particle morphology were obtained. One is worm type may be formed due to stirred synthesis² in contrast to the synthesis in autoclaves under static conditions and the another one is hexagonal type.³ Transmission electron microscopy (TEM)

of Si-MCM-41-P sample, as shown in Figure 3.5a, reveals a clear hexagonal pattern of lattice fringes along the pore direction. Parallel fringes due to the side-on view of the long pores were also observed.

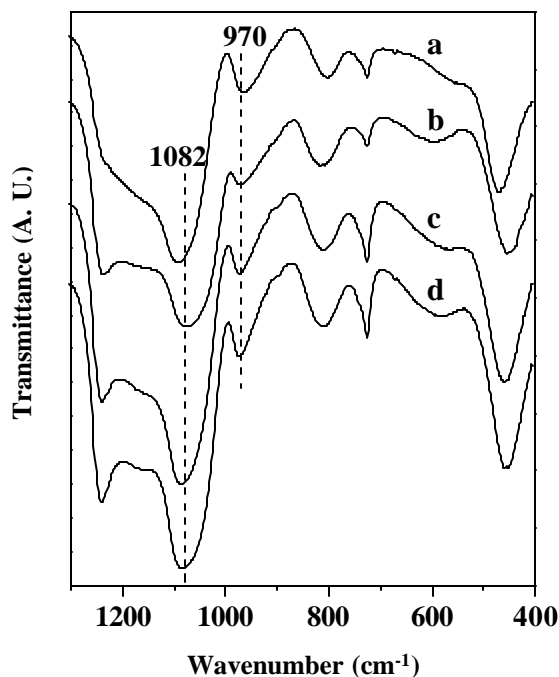


Figure 3.2 Framework IR spectra of calcined Si-MCM-41-P (a), Al-MCM-41-P (50) (b), Ti-MCM-41-P (50) (c) and V-MCM-41-P (50) (d).

3.2.1.2. Al-MCM-41

It is observed that the time taken to obtain ordered Al-MCM-41 material in the presence of promoter P (NaH_2PO_4) was significantly less than that in its absence (Table 3.1). The powder XRD pattern of Al-MCM-41-P sample (Figure 3.6) shows four Bragg peaks corresponding to $hkl = 100, 110, 200$ and 210 . The BET surface area of Al-MCM-41-P sample prepared in the presence of promoter was higher than that of Al-MCM-41-S sample prepared in the absence of any promoter (Table 3.3). The presence of aluminum in Al-MCM-41-S and Al-MCM-41-P as well as the absence of phosphorous (promoter) in Al-MCM-41-P

samples were confirmed by EDX analyses. The Al-MCM-41 samples characterized by SEM, IR (Figure 3.2), and TEM etc. also reveal the formation of hexagonal MCM-41 type materials.

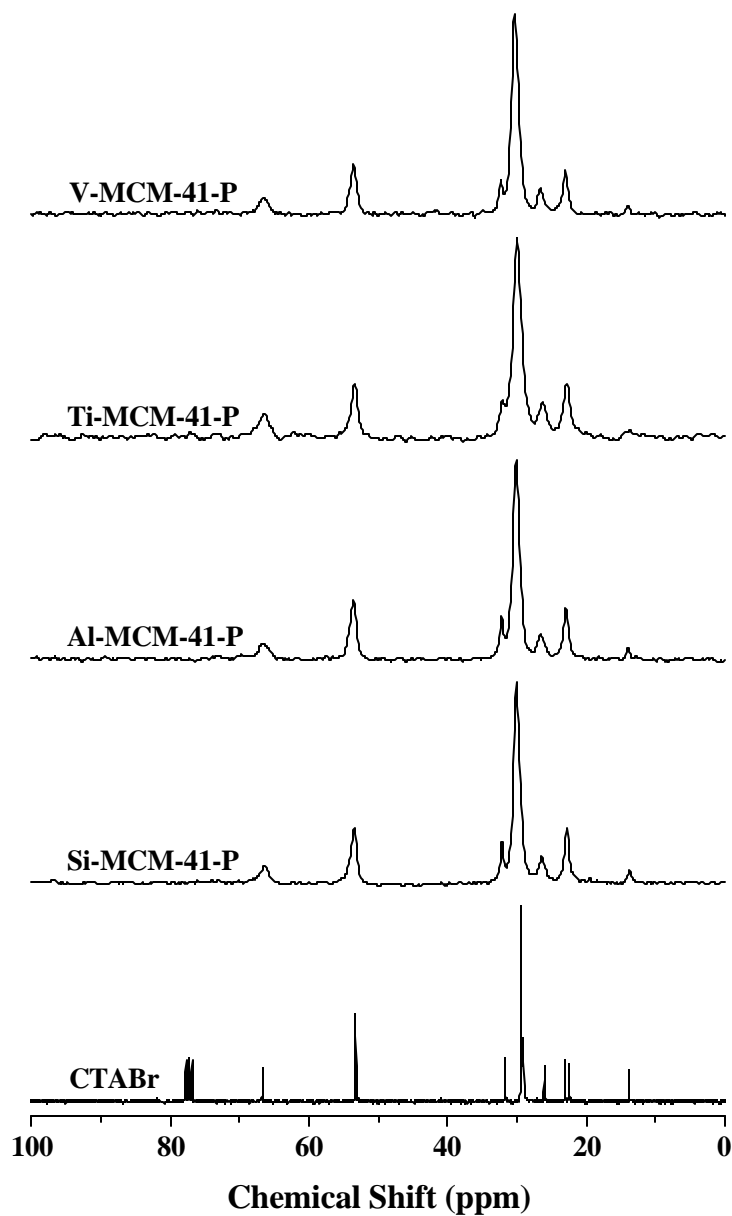


Figure 3.3 ^{13}C CP MAS NMR spectra of CTA^+ ions in solution (CDCl_3) and as-synthesized Si-MCM-41-P, Al-MCM-41-P (50), Ti-MCM-41-P (50) and V-MCM-41-P (50). The triplet observed at *ca.* 77 ppm for CTABr is due to solvent (CDCl_3).

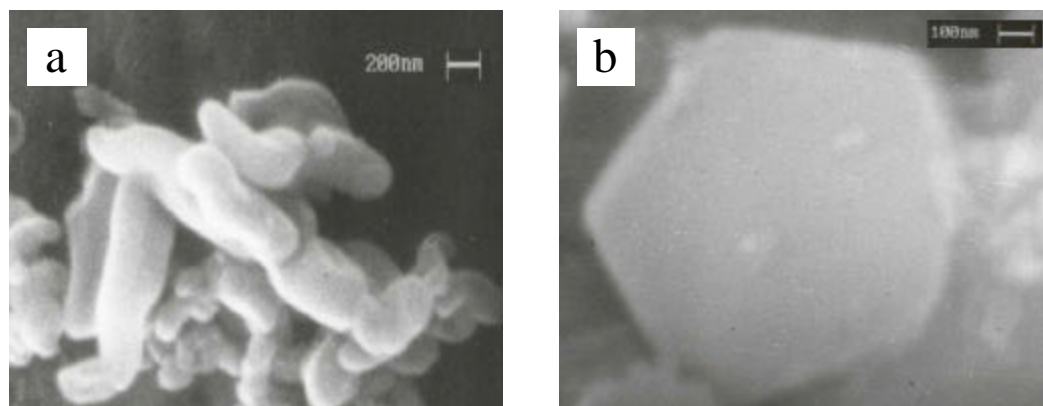


Figure 3.4 Scanning electron micrographs of calcined Si-MCM-41-P having different types of particle morphology : (a) worm type and (b) hexagonal type.

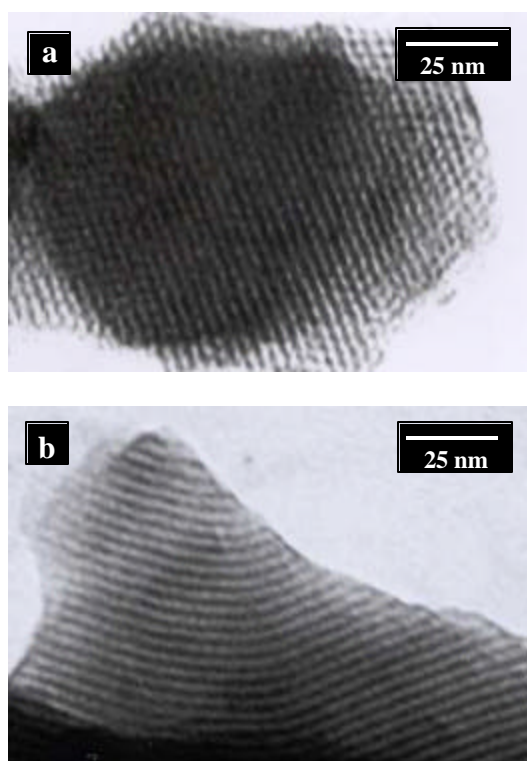


Figure 3.5 Transmission electron micrographs of calcined Si-MCM-41-P (a) and Ti-MCM-41-P (50) (b).

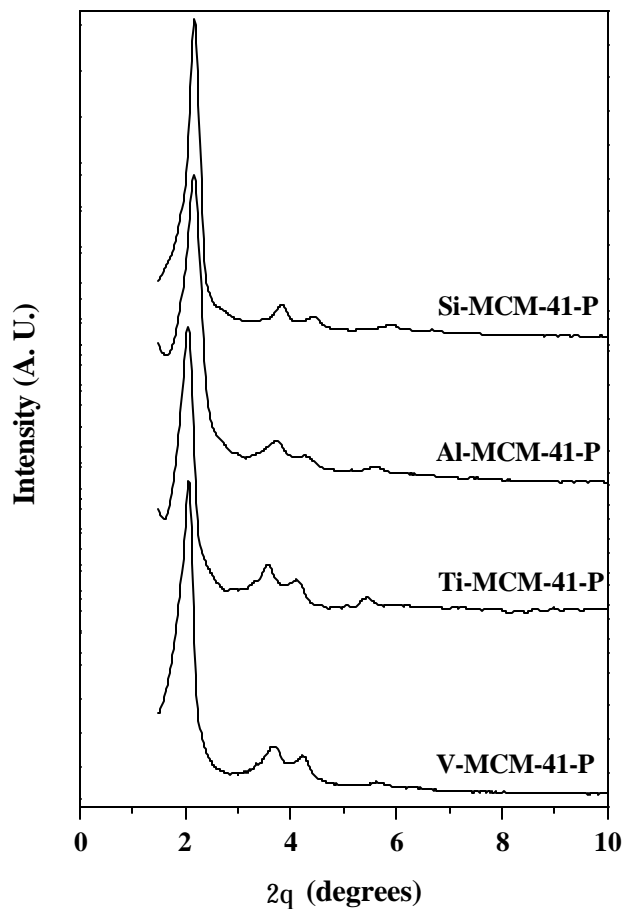


Figure 3.6 X-ray diffraction pattern of as-synthesized Si-MCM-41-P, Al-MCM-41-P (50), Ti-MCM-41-P (50) and V-MCM-41-P (50).

The ^{13}C CP MAS NMR (Figure 3.3) and ^{29}Si MAS NMR spectra of Al-MCM-41-P sample are similar as that of Si-MCM-41 samples. Further, no signal for phosphorous (promoter) monitored by ^{31}P MAS NMR spectra of as-synthesized Al-MCM-41-P sample indicates the absence of phosphate in the sample. ^{27}Al MAS NMR spectra of the two Al-MCM-41 samples prepared in the presence and in the absence of promoter are shown in Figure 3.7. Both the samples show only a single peak ~ 52 ppm, which can be assigned to the tetrahedral coordination of aluminum, suggesting total incorporation of aluminum into the silica network.

3.2.1.2.1. FTIR Spectra of Chemisorbed Pyridine

The FTIR spectra of chemisorbed pyridine in Al-MCM-41-S and Al-MCM-41-P samples are similar and therefore, the peak assignments are also same. Figure 3.8 depicts the FTIR spectra of chemisorbed pyridine in Al-MCM-41-P sample after subtraction from the spectrum

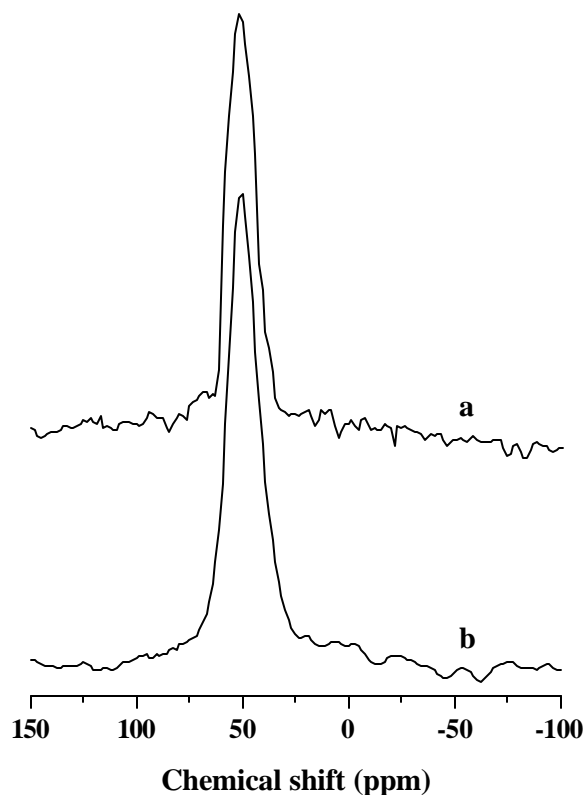


Figure 3.7 ^{27}Al MAS NMR spectra of calcined Al-MCM-41-S (50) (a) and Al-MCM-41-P (50) (b).

of the pure activated sample. It shows Brønsted as well as Lewis acidity. The bands at 1630 and 1550 cm^{-1} are assigned to Brønsted acid sites, whereas the bands at 1610 and 1450 cm^{-1} are assigned to Lewis acid sites. The band at 1490 cm^{-1} is common to both types of site. The band at 1610 cm^{-1} is due to hydrogen-bonded pyridine, which is present in a significant quantity at 373 K. As expected, this band disappears at higher temperatures (473 K and above; Figure 3.8).⁴

The thermal stability of pyridine adsorbed on the acid sites was studied by comparing the bands at 1550 and 1450 cm^{-1} representing Brönsted (B) and Lewis (L) acid sites, respectively. The thermal stability of pyridine adsorbed on Al^{3+} cations in the Al-MCM-41 walls was measured by comparing the B/L ratios as a function of the desorption temperature. On

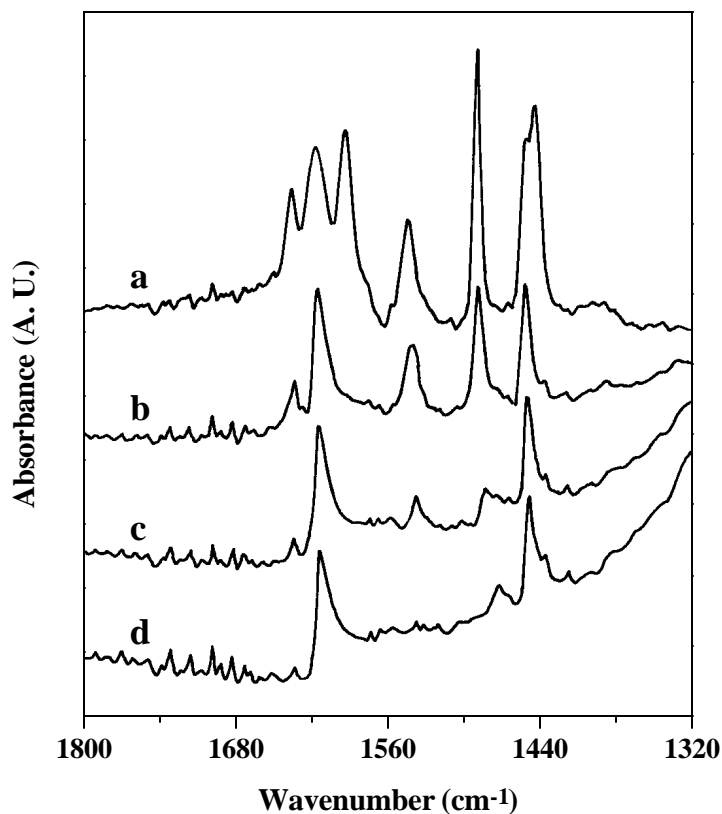


Figure 3.8 FTIR spectra of chemisorbed pyridine on Al-MCM-41-P (50) sample at desorption temperatures of 373 (a), 473 (b), 573 (c) and 673 K (d).

increasing the desorption temperature of from 373 to 673 K, it was observed that the decrease in the Brönsted acidity compared to that in the Lewis acidity was pronounced particularly above 473 K.⁴

3.2.1.3. Ti- and V-MCM-41

A significant decrease in the synthesis time was also observed when phosphoric acid was used as promoter in the synthesis of isomorphously substituted transition metal (Ti and V) containing MCM-41 type mesoporous materials. The materials obtained in the presence of promoter (H_3PO_4) were characterized and compared with that obtained in its absence. The XRD pattern of Ti- and V-MCM-41 samples prepared in the presence and in the absence of promoter shows that well-ordered hexagonal MCM-41 materials, as shown in Figure 3.6 for Ti- and V-MCM-41-P samples, were obtained. The BET surface area values of Ti-MCM-41-P and V-MCM-41-P samples are slightly higher than the corresponding Ti-MCM-41-S and V-MCM-41-S samples (Table 3.3). The metal content of the samples was determined by EDX analysis as given in Table 3.1. The absence of phosphorous (promoter) in the final Ti-MCM-41-P and V-MCM-41-P samples was also confirmed by EDX analysis. The SEM picture shows smaller crystallites are obtained in the presence of promoter than in its absence. Similar observations were made and explained in the case of microporous solids.⁵ The samples also show nice parallel fringes and hexagonal array type TEM photographs. A representative TEM photograph of Ti-MCM-41-P sample is given in Figure 3.5b. Interestingly, unlike V-containing zeolites, as-synthesized V-MCM-41 samples did not exhibit any EPR signals at room temperature (298 K). This may be attributed to the presence of V^{4+} in highly symmetrical lattice positions.⁷

3.2.1.3.1. Diffuse Reflectance UV-Vis Spectroscopy

The diffuse reflectance UV-Vis spectra of Ti and V-MCM-41 samples prepared in the presence and the absence of promoter were carried out as shown in Figure 3.9 for Ti- and V-MCM-41-P samples. Both the calcined Ti-MCM-41 samples exhibit a strong charge transfer band at *ca.* 220 nm and a very weak shoulder at *ca.* 260 nm. The band at *ca.* 220 nm may be attributed to tetra-coordinated titanium in the walls of Ti-MCM-41 samples, whereas the

band at *ca.* 260 nm may be assigned to site-isolated Ti atoms in penta- or octahedral coordination. The presence of penta- or hexa-coordinated Ti sites in Ti-MCM-41 may be associated with the less crystallographic order in the pore walls and much higher accessible surface area.^{2,5,6} However, the absence of any absorption band at *ca.* 330 nm indicates that anatase is not present in the Ti-MCM-41 samples.

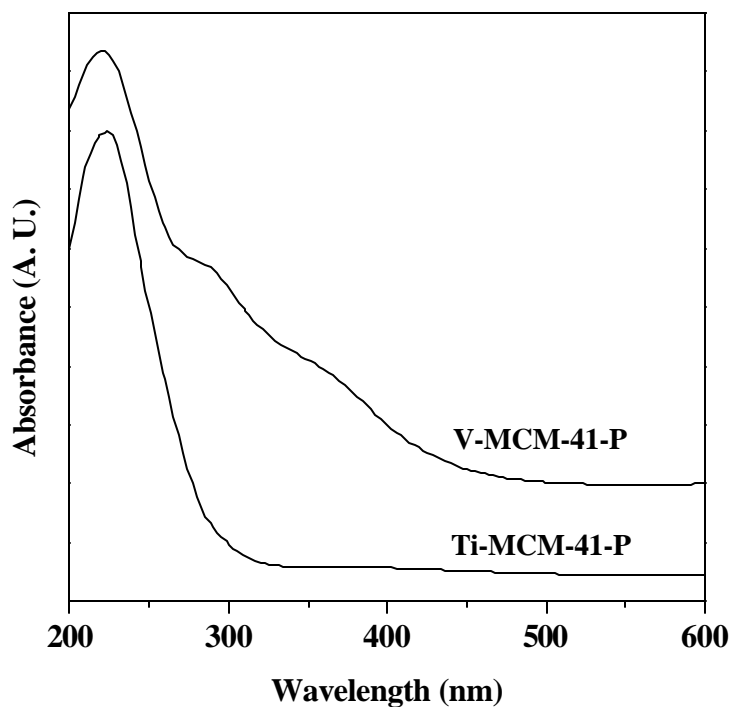


Figure 3.9 Diffuse reflectance UV-Vis spectra of calcined V-MCM-41-P (50) and Ti-MCM-41-P (50).

The diffuse reflectance UV-Vis spectra of V-MCM-41 samples show a strong band at *ca.* 220 nm and weaker bands at *ca.* 290 and 340 nm. A very weak band at *ca.* 400 nm is also observed. The bands at 220, 290 and 340 nm can be attributed to the charge transfer bands of tetra-coordinated vanadium species present in the +5 oxidation state, in the walls of V-MCM-41 samples.^{2,8} However, the weak band at *ca.* 400 nm may be assigned to hexa-coordinated V (V) species, indicating the presence of V as V=O in the defect sites of framework.²

3.2.1.3.2. IR Spectroscopy

The representative IR spectra in the framework region of Ti-MCM-41-P and V-MCM-41-P samples, given in Figure 3.2, show characteristic band at 970 cm^{-1} attributed to $\nu_{\text{asym.}}(\text{Si-O-M})$ vibration, where $M = \text{Ti}$ and V .⁹ However, the band at 962 cm^{-1} for Si-MCM-41 samples is attributed to $\nu(\text{Si-OH})$ vibration.¹⁰ So, 970 cm^{-1} band cannot be taken as proof for the incorporation of Ti and V in the framework of Ti and V-MCM-41 samples. But, the shift of this band ($\sim 8\text{ cm}^{-1}$) to higher wavenumber¹¹ as well as the shift of the $\nu_{\text{asym.}}(\text{Si-O-Si})$ band from 1090 cm^{-1} for Si-MCM-41 to 1082 cm^{-1} for Ti and V-MCM-41 samples,¹² may be taken as an indication for the incorporation of Ti and V in the framework of respective MCM-41 samples.

3.2.1.3.3. ^{51}V MAS NMR

^{51}V MAS NMR spectra of V-MCM-41-S (a) and V-MCM-41-P (b) samples, given in Figure 3.10, also indicate the presence of tetrahedral vanadium in the silica network of MCM-41. In both cases two intense signals, one at -505 and another at -527 ppm were observed. Although, the intensity of these two signals is almost comparable, the signal at -505 ppm is slightly more intense than that at -527 ppm in V-MCM-41-S sample. However, the reverse is true for V-MCM-41-P sample. The isotropic chemical shift (δ) of *ca.* -500 ppm is typical of tetrahedral vanadium (V) and therefore, it may be inferred that the occurrence of two peaks (-505 and -527 ppm) is due to two tetrahedral vanadium (V) species with different local environments.¹³ Moreover, the samples are also free from V_2O_5 impurity, since no NMR signal at *ca.* -300 ppm, characteristic of V_2O_5 , was observed.

3.2.1.3.4. Diffuse Reflectance UV-Vis Spectroscopy of Ti-MCM-41-P (50) : Interaction with aqueous hydrogen peroxide (HP) and urea-hydrogen peroxide (UHP)

The diffuse reflectance UV-Vis spectra of Ti-MCM-41-P interacted with solid urea hydrogen peroxide (UHP), aqueous hydrogen peroxide (HP), water and UHP + acetone are

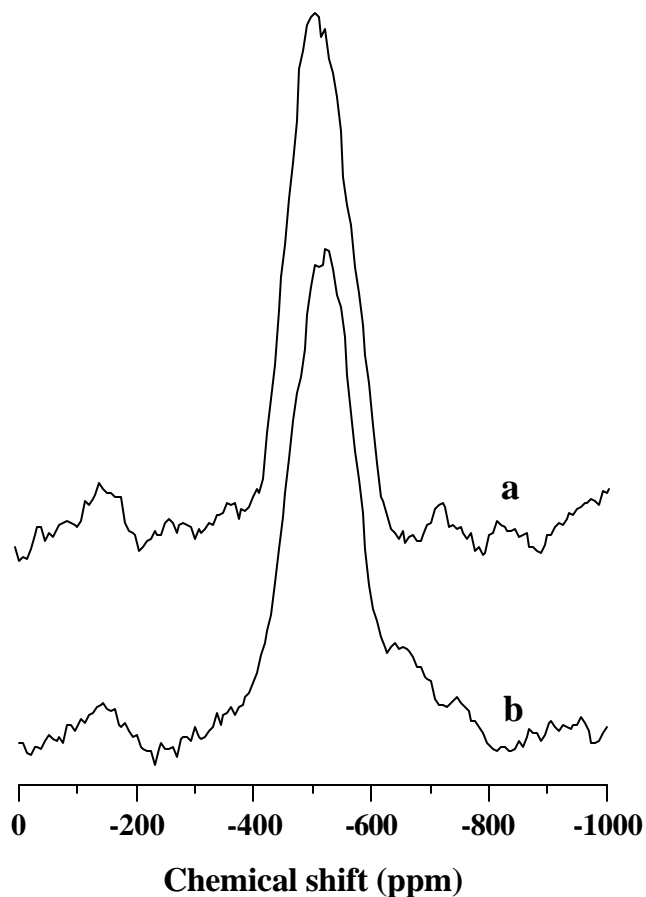


Figure 3.10 ^{51}V MAS NMR spectra of calcined V-MCM-41-S (50) (a) and V-MCM-41-P (50) (b).

compared in Figure 3.11. Curve 'a' (Ti-MCM-41-P) exhibits a sharp absorption at *ca.* 220 nm. When Ti-MCM-41-P sample was physically mixed with UHP (Ti-MCM-41-P/UHP), two absorption bands (curve 'b') were observed. One is a sharp absorption at 220 nm as observed in pure Ti-MCM-41-P and another is a continuous absorption band in the UV-Vis region from 300-500 nm, which is due to the formation of different Ti-superoxo complexes formed by the solid-solid interaction between Ti-MCM-41-P and UHP. The shift of absorption maxima (from 220 to 250 nm) in the hydrated Ti-MCM-41-P sample (curve 'c') may be explained by considering the change in chemical environments of Ti-atoms from tetra-coordination to penta-/hexa-coordination, where one or two water molecules coordinate

with the Ti-atoms. The curves 'd' and 'e', representing Ti-MCM-41-P/UHP/acetone and Ti-MCM-41-P/HP systems, exhibit similar type of absorptions (a strong absorption at 220-225 nm and a continuous absorption in the 300-500 nm) in the UV-Vis region. The absorbance

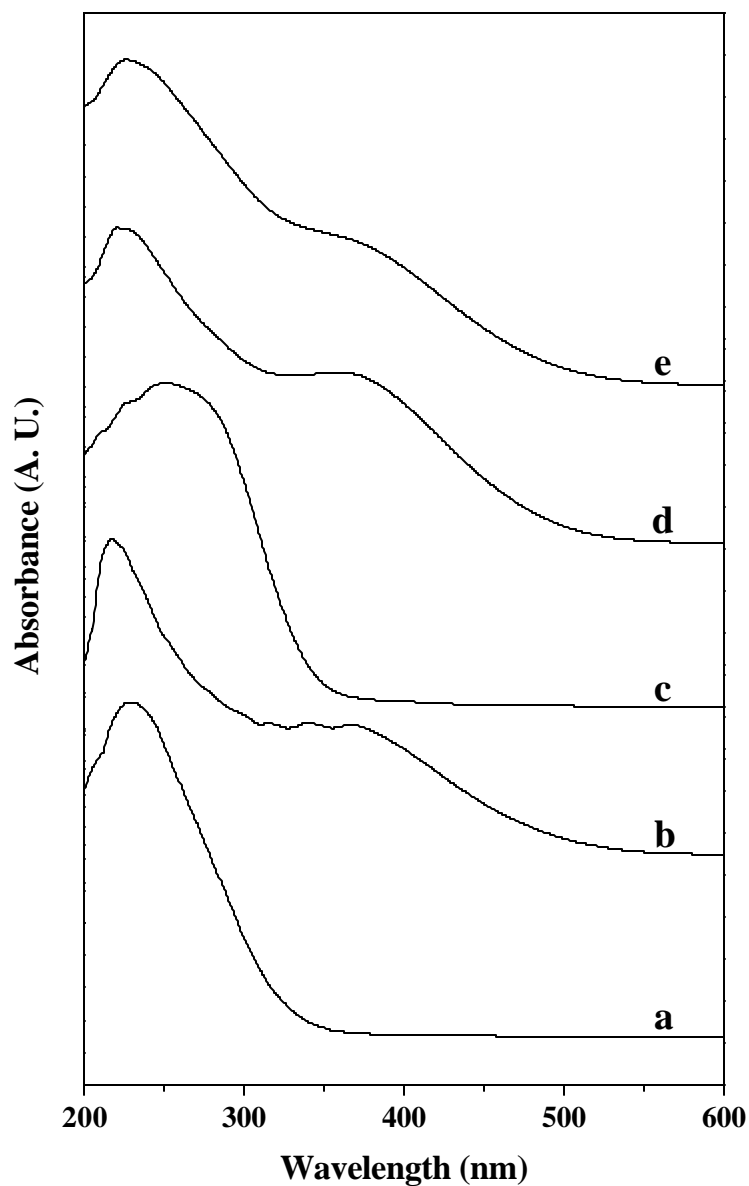


Figure 3.11 Diffuse reflectance UV-Vis spectra of calcined Ti-MCM-41-P (50) (a), Ti-MCM-41-P (50) + UHP (b), Ti-MCM-41-P (50) + H₂O (c), Ti-MCM-41-P (50) + UHP + Acetone (d) and Ti-MCM-41-P (50) + aqueous H₂O₂ (e).

noticed in the range of 250-350 nm (curves 'd' and 'e') can be attributed to coordinated solvents (acetone and water respectively) on Ti-centers.¹⁴ The continuous absorption band (300-500 nm) (curves 'b', 'd' and 'e') and the shift in the peak maxima from 220 to 250 nm for the hydrated Ti-MCM-41 sample (curve 'c') disappear after heating the sample at 523 K for 6 h.

3.2.1.3.5. EPR Spectroscopy of Ti-MCM-41-P (50) : Interaction with HP and UHP

Figure 3.12 depicts the anisotropic EPR spectra of Ti-MCM-41-P with UHP (curve A) and HP (curve B), recorded at 298 and 77 K, respectively. The EPR spectrum of Ti-MCM-41-P/UHP system (curve A) shows two signals for different Ti-superoxo species, a weak one

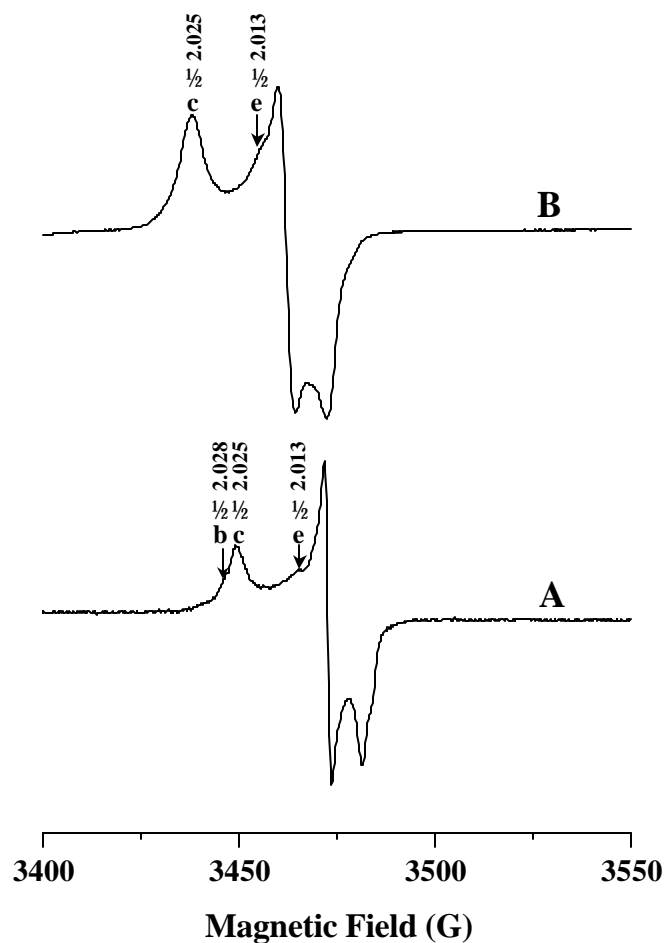


Figure 3.12 EPR spectra of Ti-MCM-41-P (50) + UHP (A) and Ti-MCM-41-P (50) + HP (B).

for species 'b' and a strong one for species 'c'; species 'a' and 'd' are absent (see later; Figure 3.32). A weak signal for superoxo radical attached lattice silicon atoms (species 'e') is also noticed. However, in the case of Ti-MCM-41-P/HP system (curve B), only species 'c' was observed along with a weak shoulder for species 'e'.

3.2.1.4. Ce-MCM-41

3.2.1.4.1. Powder X-ray Diffraction

The powder X-ray diffractograms of as-synthesized Si-MCM-41 and Ce-MCM-41 samples with different Si/Ce ratios along with the Ce-exchanged MCM-41 sample are shown in Figure 3.13. The well-defined XRD patterns may be indexed on the basis of four Bragg peaks, which can be distinguished in hexagonal lattice symmetry, characteristic of MCM-41 structure. A prominent peak for $hkl = 100$ as well as weaker peaks for $hkl = 110, 200$ and 210 were observed in the as-synthesized and in the calcined samples. The d_{100} values of different samples are given in Table 3.4 along with their corresponding unit cell parameter (a_0), calculated from the peak with $hkl = 100$ by the equation $a_0 = 2d_{100}/\sqrt{3}$. A slight increase in the 'd' and 'a₀' values is observed on increasing incorporation of cerium. The increase in unit-cell parameter (a_0) on Ce incorporation is due to the larger size of Ce^{4+} compared to Si^{4+} . Similar observations were also reported by earlier workers with different metal ions incorporated MCM-41.^{15,16} However, a gradual loss of long-range ordering is observed with increasing incorporation of Ce in the Ce-MCM-41 samples. This is probably due to increasing number of defect sites and bond strain in these materials as evidenced by the decreasing intensities of the [100] peak as well as the higher angle peaks. Finally, at very high Ce loading (Si/Ce ≤ 10), amorphous material was obtained. Loss of long-range ordering is also observed for the Ce-exchanged MCM-41 sample.

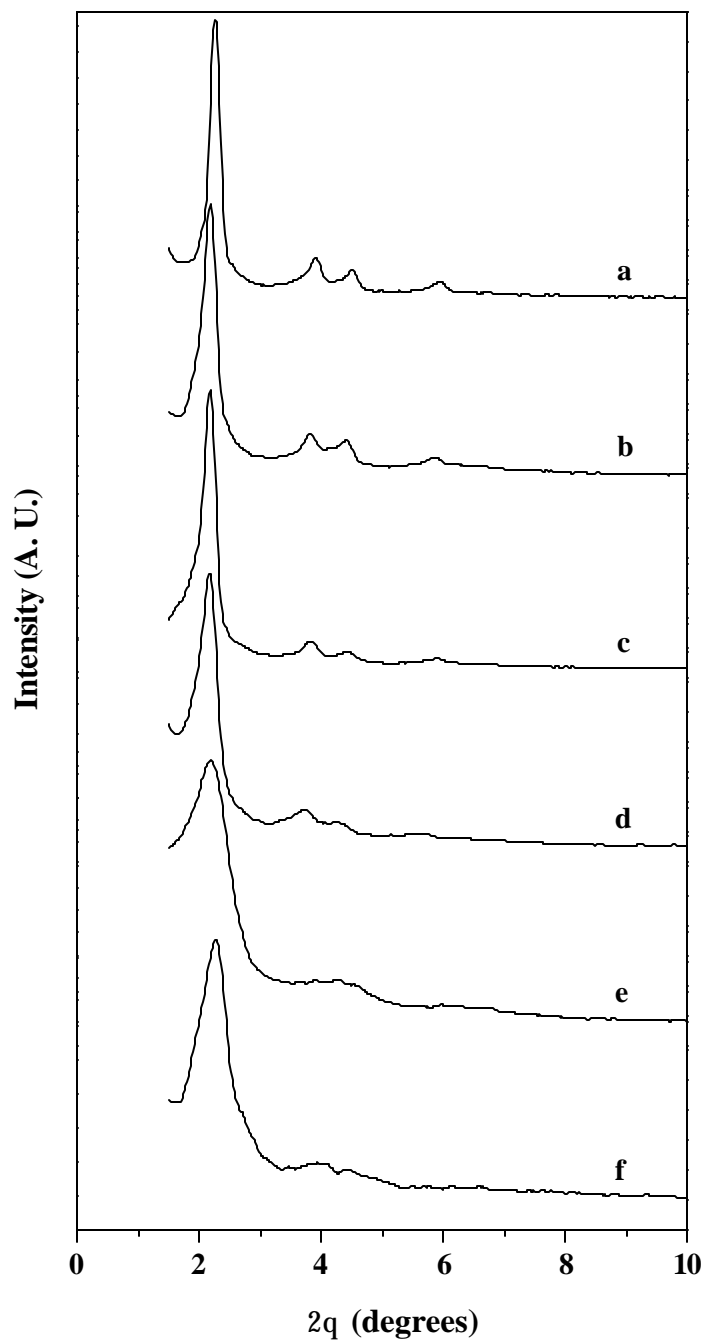


Figure 3.13 X-ray diffraction patterns of as-synthesized (a) Si-MCM-41, (b) Ce-MCM-41-R (160), (c) Ce-MCM-41-R (80), (d) Ce-MCM-41-R (40), (e) Ce-MCM-41-R (20), (f) Ce-exchanged MCM-41.

Table 3.4
Results of elemental analysis, d_{100} spacing and unit cell parameter (a_0) of M-MCM-41
(M = Si and Ce) samples

Sample ^a	(Si/Ce) _{gel}	(Si/Ce) _{solid}	d_{100} (Å)	a_0 (Å)
Si-MCM-41	-	-	38.2	44.1
Ce-MCM-41-R (160) ^b	160	159.6	39.0	44.9
Ce-MCM-41-R (80)	80	80.9	39.4	45.5
Ce-MCM-41-R (40)	40	40.8	40.3	46.5
Ce-MCM-41-A (40)	40	40.6	40.1	46.1
Ce-MCM-41-P (40)	40	40.9	40.2	46.3
Ce-MCM-41-R (20)	20	20.8	40.8	47.1
Ce-Ex-MCM-41 ^c	30	44.1	38.0	43.9
Ce-Im-MCM-41 (20) ^d	20	20.1	38.0	43.9
SiO ₂ -CeO ₂ (20) ^e	20	20.2	-	-

^a R, A and P denote samples synthesized under reflux condition with stirring, in autoclave under static condition and in Parr autoclave with stirring respectively.

^b Si/Ce molar ratio in parentheses.

^c Ce-exchanged MCM-41 sample.

^d Ce-impregnated MCM-41 sample.

^e Mixture of silica and ceric oxide.

3.2.1.4.2. N₂ Adsorption

The porosity of the MCM-41 samples was evaluated by N₂ adsorption isotherms. Figure 3.14 shows the N₂ adsorption-desorption isotherm and the corresponding pore size distribution curve (inset) for the Ce-MCM-41-R (40) sample. All the samples showed similar type IV isotherms having inflection around $P/P_0 = 0.3-0.45$, characteristic of MCM-41 type

ordered mesoporous materials. The samples exhibited two separate well-expressed hysteresis loops. One is in the $P/P_0 = 0.3-0.45$ region indicative of framework confined mesopores and other one is at $P/P_0 \geq 0.8$ corresponds to capillary condensation in the inter-particle pores.¹⁷ The position of inflection in the $P/P_0 = 0.3-0.45$ region, depends on the diameter of the mesopores and its sharpness indicates the uniformity of the narrow pore size distribution.¹ The specific BET surface area, average pore diameters (calculated from N_2 adsorption isotherm using BJH model)¹⁸ and specific pore volume for the MCM-41 samples are presented in Table 3.5.

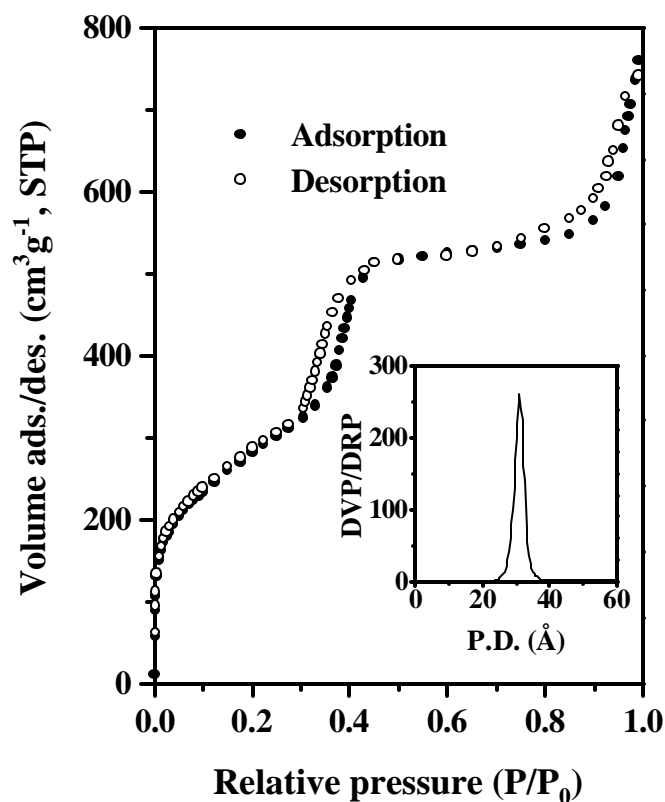


Figure 3.14 Nitrogen adsorption-desorption isotherm and pore size distribution (inset) for Ce-MCM-41-R (40).

Table 3.5
Nitrogen sorption pore diameter, pore volume, FWT and BET surface area of M -MCM-41 (M = Si and Ce) samples

Sample ^a	Pore diameter (Å)	Pore volume (cm ³ g ⁻¹)	FWT ^b (Å)	BET S. A. (m ² g ⁻¹)
Si-MCM-41	28.6	1.08	15.5	1414
Ce-MCM-41-R (160) ^c	29.4	1.02	15.5	1332
Ce-MCM-41-R (80)	30.2	1.15	15.3	1242
Ce-MCM-41-R (40)	31.1	1.14	15.4	1081
Ce-MCM-41-A (40)	30.8	0.98	15.3	998
Ce-MCM-41-P (40)	31.0	1.06	15.3	1062
Ce-MCM-41-R (20)	31.8	0.91	15.3	983
Ce-Ex-MCM-41	27.1	0.98	16.8	1088
Ce-Im-MCM-41 (40)	28.4	0.92	15.5	1041
SiO ₂ -CeO ₂ (40)	-	-	-	-

^a R, A and P denote samples synthesized under reflux condition with stirring, in autoclave under static condition and in Parr autoclave with stirring respectively.

^bFWT: framework thickness = a_0 - pore diameter.

^cSi/Ce molar ratio in parentheses.

It has been observed that the BET surface area gradually decreases with increase in the Ce-content of Ce-MCM-41 samples. However, the average pore diameters slightly increase with increasing Ce content of the samples. It may be inferred that the increase in pore size with Ce incorporation is due to larger size of Ce⁴⁺ compared to Si⁴⁺. A slight decrease in the surface area for the Ce-exchanged MCM-41 sample (Table 3.5) may be attributed to the loss in long-range ordering as clearly evidenced by the XRD pattern (Figure 3.13). In the case of

Ce-exchanged MCM-41 sample, the increase in the wall thickness and decrease in pore size may be due to deposition of cerium species onto the surface of cylindrical channels of MCM-41. However, the data presented in Table 3.5 show that the framework wall thickness (FWT), calculated by subtracting pore diameter by a_0 , of different Ce-containing MCM-41 and purely siliceous MCM-41 samples is comparable and does not change substantially with increasing Ce content. Although, the unit cell parameter (a_0) increases with the increasing incorporation of Ce, like other heterometal ions, which are larger than Si^{4+} ions,^{6,16} the pore diameter was also found to increase slightly leading to comparable FWT of different Ce-MCM-41 as well as Si-MCM-41 samples. Similar observations were made in the case of Sn-MCM-41.¹⁶ The defect site may influence the a_0 or pore diameter or both, depending upon their density and nature.

3.2.1.4.3. Diffuse Reflectance UV-Vis Spectroscopy

The diffuse reflectance UV-Vis spectroscopy is known to be a very sensitive probe for the identification and characterization of metal ion coordination and its existence in the framework and/or in the extra-framework position of metal containing zeolites. The diffuse reflectance UV-Vis spectra of calcined Ce-MCM-41 samples, given in Figure 3.15, show single peak with a maximum at *ca.* 300 nm and also its intensity increases with increase in the Ce content in the samples. However, the diffuse reflectance UV-Vis spectra of the mixture of silica-ceria (Si/Ce = 20) and Ce-exchanged MCM-41 samples show two distinct bands, a weak absorption at *ca.* 300 nm and a strong absorption at *ca.* 400 nm.

The position of ligand to metal charge transfer ($\text{O}^{2-} \rightarrow \text{Ce}^{4+}$) band depends on the ligand field symmetry surrounding the Ce center. The electronic transitions from oxygen to cerium require higher energy for a tetra-coordinated Ce^{4+} than for a hexa-coordinated one. Therefore, it may be inferred that the absorption band centered at 300 nm for Ce-MCM-41 samples is due to the presence of well-dispersed Ce^{4+} species, presumably in tetra-coordinated

environment in the silica network. Whereas, in the case of Ce-exchanged MCM-41 (spectrum 'e') and silica-ceria (spectrum 'f') samples, two distinct absorptions at 300 nm (weak) and 400 nm (strong) corresponding to two different types of Ce^{4+} species were observed. The absorption at higher wavelength (~400 nm) may be assigned to hexa-coordinated Ce^{4+} species.

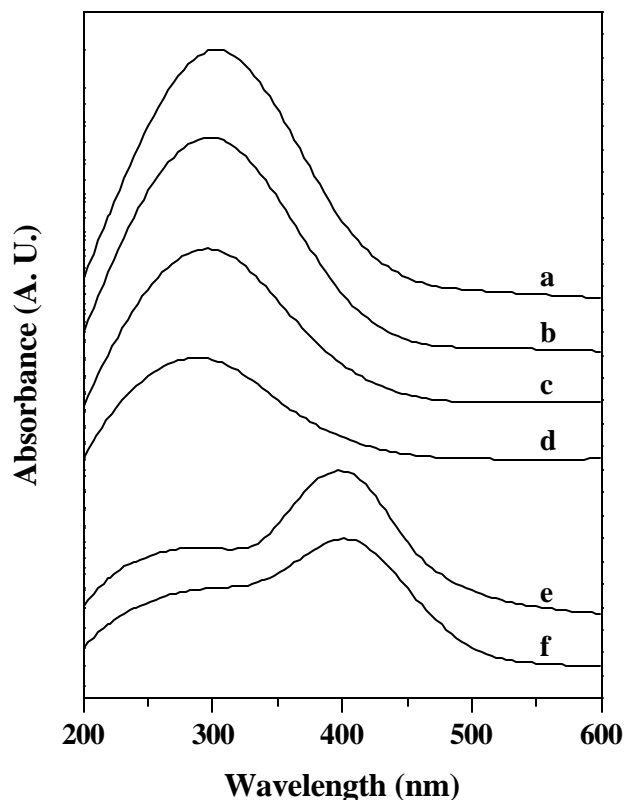


Figure 3.15 Diffuse reflectance UV-Vis spectra of calcined (a) Ce-MCM-41-R (20), (b) Ce-MCM-41-R (40), (c) Ce-MCM-41-R (80), (d) Ce-MCM-41-R (160), (e) Ce-exchanged MCM-41 and (f) $\text{SiO}_2\text{-CeO}_2$ (20).

3.2.1.4.4. FTIR Spectroscopy

The IR spectra in the framework and the hydroxyl region of purely siliceous and different Ce-containing MCM-41 samples show bands characteristic of the MCM-41 type materials as

shown in Figure 3.16. In the framework region ($400\text{-}1300\text{ cm}^{-1}$), the vibration band at *ca.* 1090 cm^{-1} is assigned to $\nu_{\text{asym.}}(\text{Si-O-Si})$ and its wavenumber decreases with increasing incorporation of cerium in the structure. The wavenumber of this band decreases from 1090 cm^{-1} (for Si-MCM-41 sample) to 1082 cm^{-1} (for Ce-MCM-41-R (20) sample). In general, this shift towards the lower wavenumber is considered as an indication for the incorporation of Ce in the silica network of MCM-41. Similarly, the band at *ca.* 970 cm^{-1} , observed for the Ce-MCM-41 samples, can be assigned to $\nu_{\text{asym.}}(\text{Si-O-Ce})$ vibration present in the framework of MCM-41. However, a band at *ca.* 962 cm^{-1} is also observed in the Si-MCM-41 sample. This band has been assigned to the Si-O stretching vibrations of $\text{SiO}^- \text{R}^+$ groups, as $\text{R}^+ = \text{H}^+$ in the calcined state.¹⁹ Therefore, this band cannot be taken as proof for cerium incorporation in the case of MCM-41, because a large number of silanol groups is present even in the calcined Si-MCM-41.²⁰ Nevertheless, it has been observed that the band at *ca.* 962 cm^{-1} (in Si-MCM-41) is shifted towards the higher wavenumber side (970 cm^{-1}) in the case Ce-containing MCM-41 samples. It has also been observed that the $\nu_{\text{asym.}}(\text{Si-O-Ce})$ and/or $\nu(\text{Si-OH})$ band intensity increases with respect to that of the $\nu_{\text{asym.}}(\text{Si-O-Si})$ and/or $\nu(\text{Si-OH})$ band when the Ce content increases. This is generally taken as an indirect proof of the incorporation of metal into the framework of porous metallo-silicates.²¹ It may be demonstrated that the absorption at 970 cm^{-1} is essentially due to the increased degeneracy of the elongation vibration in the tetrahedral structure of SiO_4 induced by the change in the polarity of the Ce-O bond when Si is linked to Ce. The SiOH group formed by the hydrolysis of the Ce-O-Si bonds and the sharing of OH with Ce is then responsible for the absorption at higher wavenumbers compared to ordinary Si-OH groups.¹¹ The lattice band $\nu_{\text{sym.}}(\text{Si-O-Si})$ is also observed at *ca.* 802 and 804 cm^{-1} for (a) Si-MCM-41 (a) and Ce-MCM-41-R (20) (e) samples, respectively. However, the small displacement (2 cm^{-1}) towards the higher wavenumber from sample (a) to

(e) cannot be taken as a proof for Ce incorporation, because this shift is within the spectral resolution of $\pm 2 \text{ cm}^{-1}$.

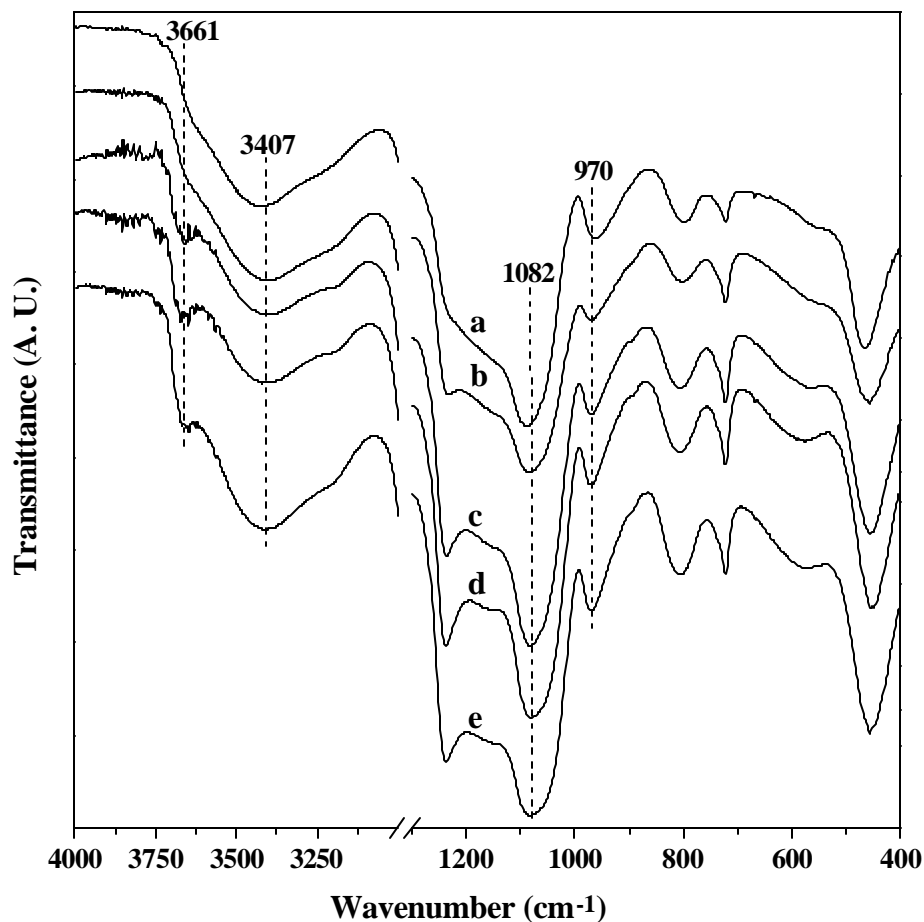


Figure 3.16 IR spectra in the framework and the hydroxyl vibration region of calcined (a) Si-MCM-41, (b) Ce-MCM-41-R (160), (c) Ce-MCM-41-R (80), (d) Ce-MCM-41-R (40) and (e) Ce-MCM-41-R (20).

In the hydroxyl region ($3000\text{--}4000 \text{ cm}^{-1}$), a broad band centered at 3422 cm^{-1} is observed for Si-MCM-41. However, in Ce-MCM-41 this band is shifted towards the lower wavenumber (15 cm^{-1}) and is observed at 3407 cm^{-1} for all the Ce-MCM-41 samples. A weak band at *ca.* 3661 cm^{-1} is also observed for all the Ce-MCM-41 samples. However, this band is not observed in the Si-MCM-41 sample. Both the bands were assigned to silanol group

vibrations situated inside the channels of MCM-41. The bands at 3422 and 3407 cm^{-1} results from silanol groups interacting via hydrogen bonding, whereas the other band at 3661 cm^{-1} is due to isolated silanol groups not interacting with each other via hydrogen bonding. The band shift from 3422 to 3407 cm^{-1} for Ce-MCM-41 samples compared to Si-MCM-41 may be assumed to have more hydrogen bonding in Ce-MCM-41 samples due to presence of more defect sites (SiOH groups). The band assignments for the IR spectra of Si-MCM-41 and Ce-MCM-41-R (20) are given in Table 3.6.

Table 3.6
Band assignments in the IR spectra of Si-MCM-41 and Ce-MCM-41-R (20)

Wavenumber (cm^{-1})	Bond assignment for Si-MCM-41	Wavenumber (cm^{-1})	Bond assignment for Ce-MCM-41-R (20)
3422	$\nu_{\text{OH}}(\text{Si-O-H})$	3661, 3407	$\nu_{\text{OH}}(\text{Si-O-H})$
1633	$\delta_{\text{OH}}(\text{H}_2\text{O})$	1626	$\delta_{\text{OH}}(\text{H}_2\text{O})$
1090	$\nu_{\text{asym}}(\text{Si-O-Si})$	1082, 1234	$\nu_{\text{asym}}(\text{Si-O-Si})$
962	$\nu_{\text{asym}}(\text{Si-O-Si})$ and/or $\nu(\text{Si-OH})$	970	$\nu_{\text{asym}}(\text{Si-O-Ce})$ and/or $\nu(\text{Si-OH})$
802, 721	$\nu_{\text{sym}}(\text{Si-O-Si})$	804, 721	$\nu_{\text{sym}}(\text{Si-O-Si})$
464	$\delta(\text{Si-O-Si})$	457	$\delta(\text{Si-O-Si})$

3.2.1.4.5. FTIR Spectra of Chemisorbed Pyridine

Figure 3.17 depicts the FTIR spectra of chemisorbed pyridine in Ce-MCM-41-R (40) sample after subtraction from the spectrum of the pure activated sample. As expected, the sample does not show any absorption characteristic for Brønsted acid sites. However, it shows considerable Lewis acidity. The pyridine coordinated to Lewis acid centers exhibits

signals around 1595, 1576 and 1444 cm^{-1} .²² The thermal stability of pyridine chemisorbed on the Lewis acid sites was measured by increasing the desorption temperature from 373 to 523 K (Figure 3.17). It is observed that pyridine is completely desorbed at 523 K.

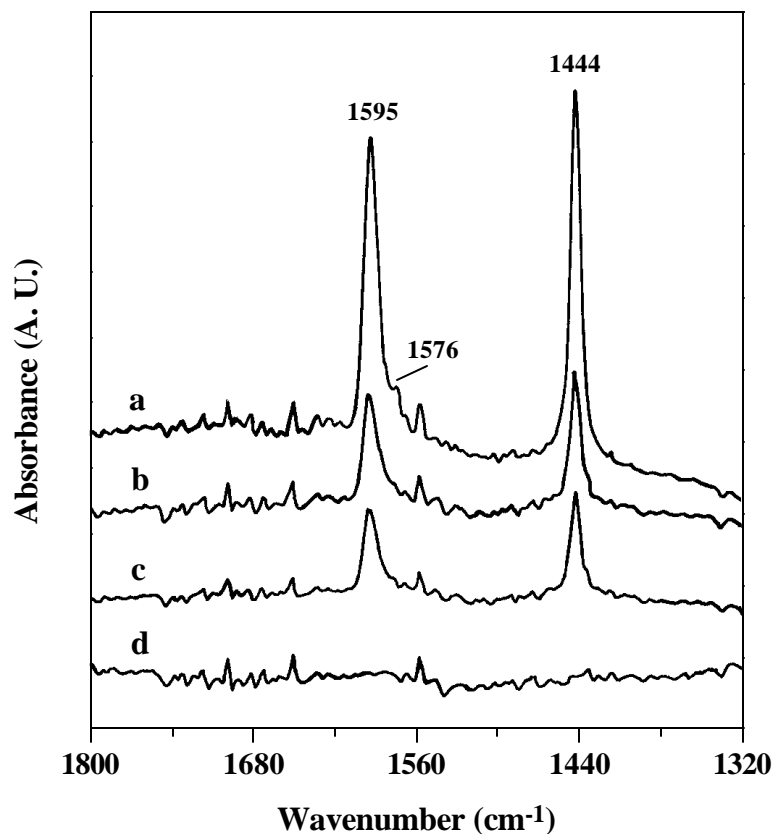


Figure 3.17 FTIR spectra of chemisorbed pyridine on Ce-MCM-41-R (40) at desorption temperatures of 373 (a), 423 (b), 473 (c) and 523 K (d).

3.2.1.4.6. FTIR Spectra of Chemisorbed Ammonia

The FTIR spectra of chemisorbed ammonia on Ce-MCM-41-R (40) sample in the range of 1800-1300 cm^{-1} are shown in Figure 3.18 after subtraction from the spectrum of the pure activated sample. Curve 'a' shows a strong characteristic absorption signal for ammonia coordinated to Lewis acid centers around 1625 cm^{-1} along with very weak signals of

chemisorbed NH_3 on Brönsted acid sites (probably due to the presence of $\equiv\text{Ce}-\text{OH}$ moieties) around 1440, 1480 and 1693 cm^{-1} after the sample being exposed to gaseous NH_3 for 30 min.²³ Upon purging N_2 and increasing the desorption temperature signals for chemisorbed ammonia were decreased steadily as shown in Figure 3.18.

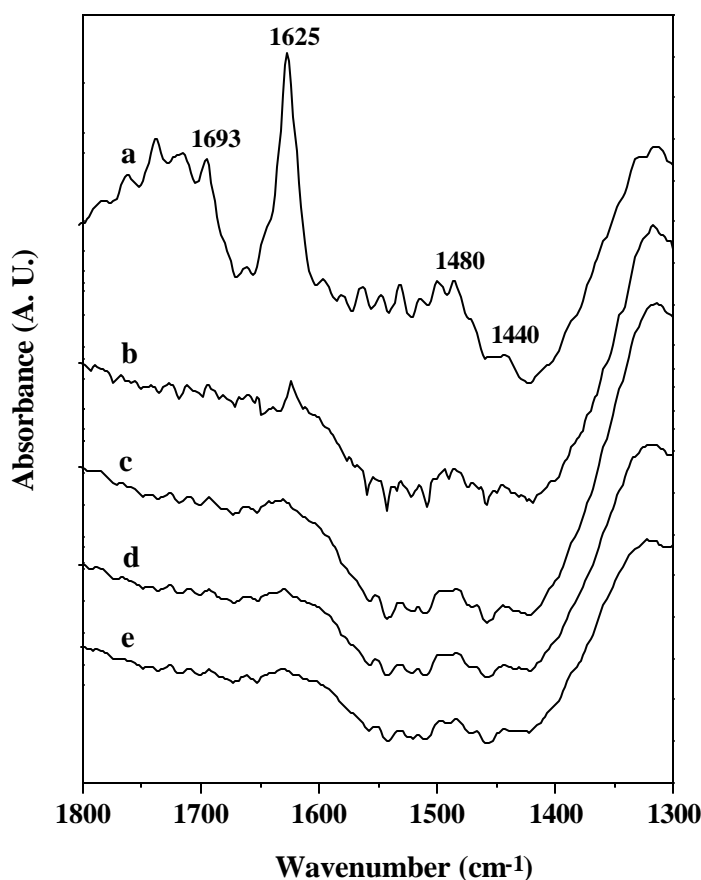


Figure 3.18 FTIR spectra of Ce-MCM-41-R (40) in the 1800-1300 cm^{-1} region after being exposed to gaseous NH_3 for 30 min (a) and at desorption temperatures of 373 (b), 423 (c), 473 (d) and 523 K (e).

In the region of 3700-3500 cm^{-1} , the characteristic narrow bands for free silanol groups disappeared on chemisorption of ammonia. However, in the region of 3500-2700 cm^{-1} , as shown in Figure 3.19, characteristic absorptions at 3410 and 3396 cm^{-1} were developed due

to interaction of ammonia with silanol groups and Ce (IV) centers, respectively. Further, signals at 3333 and 3319 indicate interaction of ammonia with two different types silanol groups as discussed earlier (Section 3.2.1.4.4, p.). Assignment for various signals observed due to chemisorbed ammonia on Ce-MCM-41-R (40) is given in Table 3.7.

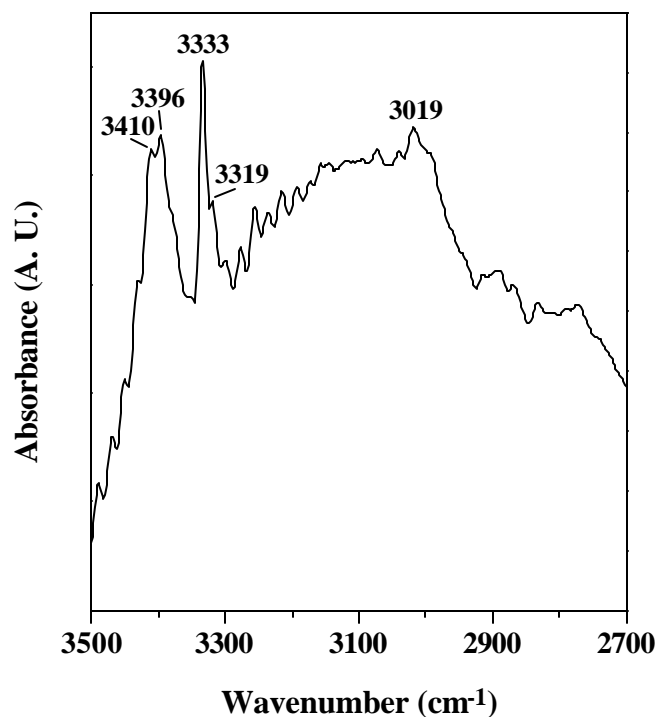


Figure 3.19 FTIR spectra of Ce-MCM-41-R (40) in the 3500-2700 cm^{-1} region after being exposed to gaseous NH_3 for 30 min.

3.2.1.4.7. ^{13}C CP MAS NMR

The solid state ^{13}C CP MAS NMR spectra of as-synthesized Ce-MCM-41-R (40), Si-MCM-41 and CTA^+ ions in solution (CDCl_3) are shown in Figure 3.20. A comparison of the three spectra shows the presence of intact CTA^+ ions inside the pores of the MCM-41 channels. All the three ^{13}C NMR spectra are similar and therefore, the peak assignments are also same. The peaks at *ca.* 66 ppm in the spectra can be assigned to the CH_2 group of the

cetyl chain neighboring the nitrogen atom. The peaks at *ca.* 53 ppm can be assigned to the three CH₃ groups bonded to nitrogen atom, whereas the resonances between 32 and 22 ppm are due to different CH₂ carbon atoms of the cetyl chain. The peaks observed at *ca.* 14 ppm can be attributed to the terminal CH₃ group of the cetyl chain. The peaks (triplet) at *ca.* 77 ppm for CTA⁺ in solution are due to solvent (CDCl₃).

Table 3.7
IR spectroscopic assignments of vibrational modes and wavenumbers for bands formed upon chemisorption of NH₃ on Ce-MCM-41-R (40)

Bands	Vibrational mode	Wavenumber (cm ⁻¹)
OH...NH ₃	v asym	3410
Ce...NH ₃	v asym	3396
OH...NH ₃	v sym	3319
v (SiO-H...NH ₃)		3019
NH ₄ ⁺	δ sym	1693
OH...NH ₃	δ asym	1625
NH ₄ ⁺	δ asym	1480
NH ₄ ⁺	δ asym	1440

A peak broadening is observed in ¹³C CP MAS NMR spectra of both the Ce-MCM-41 (curve 'a') and Si-MCM-41 (curve 'b') in comparison with that in the case of CTABr dissolved in CDCl₃ solution (curve 'c'). The broadening of these peaks is generally attributed to the restricted translation movement of the organic molecules in the confined space.

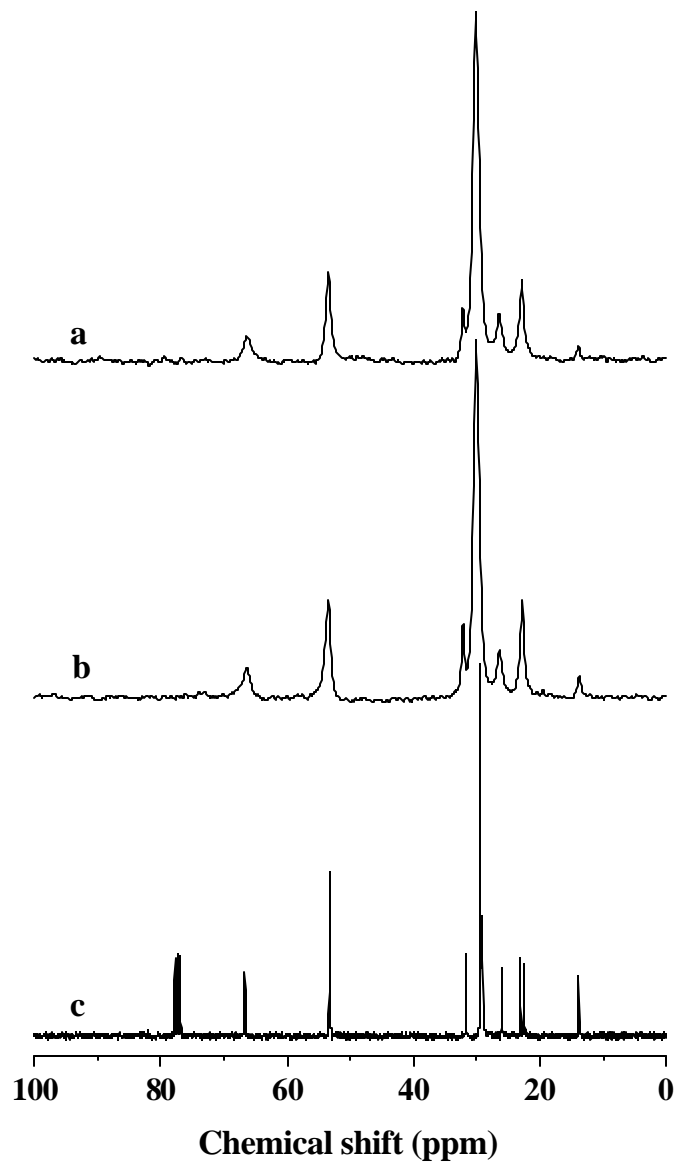


Figure 3.20 ^{13}C CP MAS NMR spectra of as-synthesized (a) Ce-MCM-41-R (40), (b) Si-MCM-41 and (c) CTMA^+ ions in solution (CDCl_3).

3.2.1.4.8. ^{29}Si MAS NMR

Although, the ^{29}Si MAS NMR spectroscopy is a very sensitive probe for the characterization and identification of crystalline microporous zeolites and metallo-silicates, in MCM-41, which is an ordered array of amorphous material, the observed peaks are broad due to the flexibility and broad range of T-O-T angles in the pore walls. The ^{29}Si MAS NMR

spectrum of calcined Ce-MCM-41-R (40) sample (curve 'a'; Figure 3.21a) shows characteristic peaks at around -91, -102 and -110 ppm, which are usually assigned to Q₂, Q₃ and Q₄ species, respectively. However, the peaks for Q₂ and Q₃ species are not observed distinctly for the calcined Si-MCM-41 sample (curve 'b'; Figure 3.21b). Instead, a broad peak centered at -108.5 ppm (Q₄ species) is observed. It can be assumed that the presence of defect sites (Q₂ and Q₃ species) in the Ce-MCM-41 samples, may provide mild acidic sites along with the $\equiv\text{Ce}-\text{OH}$ groups.

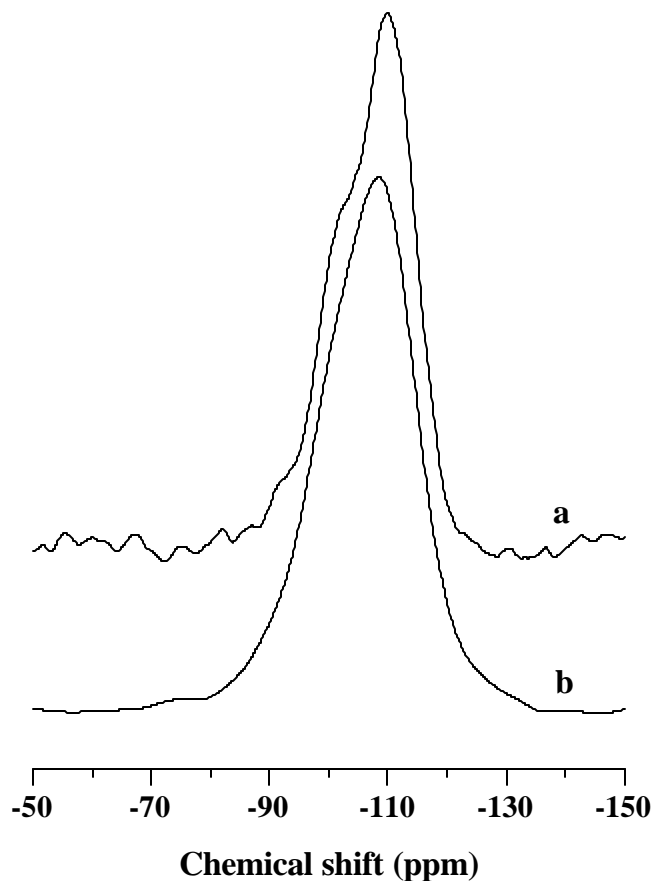


Figure 3.21 ²⁹Si MAS NMR spectra of calcined (a) Ce-MCM-41-R (40) and (b) Si-MCM-41.

3.2.1.4.9. SEM and EDX

The particle size and morphology of Si-MCM-41 and different Ce-MCM-41 samples were determined by scanning electron microscopy. The SEM micrographs of Ce-MCM-41-R (40) sample, as shown in Figure 3.22, are typical of MCM-41 type materials exhibiting two different kinds of particle morphology. One is winding worm type (Figure 3.22a)² and other one is hexagonal (Figure 3.22b).³ The hexagonal particles are of two types (i) well-formed relatively bigger particles of *ca.* 2 μm and (ii) smaller particles of *ca.* 0.5 μm size. The unique hexagonal rod type particle was also observed for the first time as shown in Figure 3.22, indicative of long-range ordering of Ce-MCM-41 samples. The worm type particles may be formed due to the stirred synthesis, in contrast to the conventional static autoclaves.

The energy dispersive X-ray analysis (EDX) for Si and Ce of the Ce-MCM-41 samples is given in Table 3.4. The Si/Ce ratios of the gels and the calcined Ce-MCM-41 samples do not differ significantly, which indicate quite high efficiency for the incorporation of well-dispersed cerium into the framework and/or walls of silica matrix of MCM-41.

3.2.1.4.10. TEM

Transmission electron microscopy (TEM) reveals parallel fringes corresponding to the side-on view of the long pores as well as a hexagonal system of lattice fringes along the pore direction as shown in Figure 3.23a and 3.23b, respectively. The equidistant parallel fringes of Ce-MCM-41-R (80) sample (Figure 3.23a) show unique feature of separate layers and the addition of such layers, one after one, resulting to the formation of a bunch of layers. Therefore, it supports that the formation of MCM-41 begins with the deposition of two to three monolayers of silicate precursor onto isolated surfactant micellar rods. Subsequently, these silicate-encapsulated composite species spontaneously form the long-range order characteristic of MCM-41.^{3,24} The pore size, d_{100} value and framework thickness of each hexagonal array, shown in Figure 3.23b for Ce-MCM-41-R (80) sample, were measured and

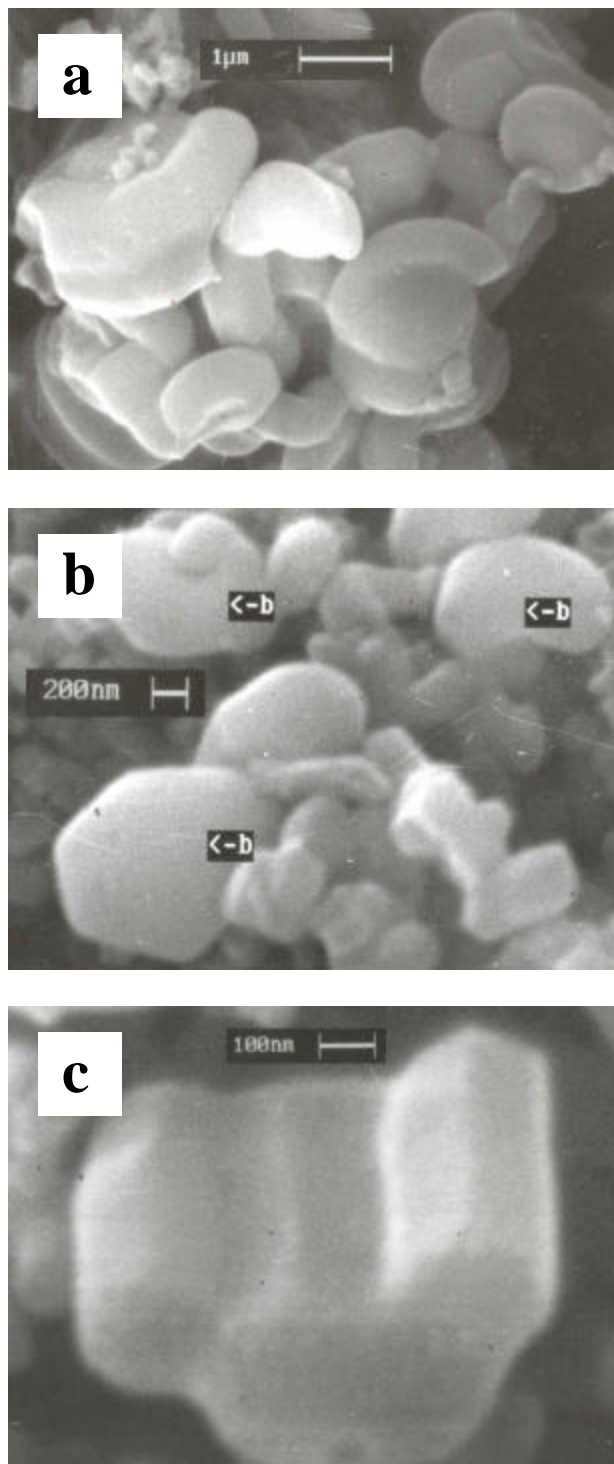


Figure 3.22 Scanning electron micrographs of calcined Ce-MCM-41-R (40) sample having different types of particle morphology : (a) winding worm type, (b) hexagonal type and (c) unique hexagonal rod type.

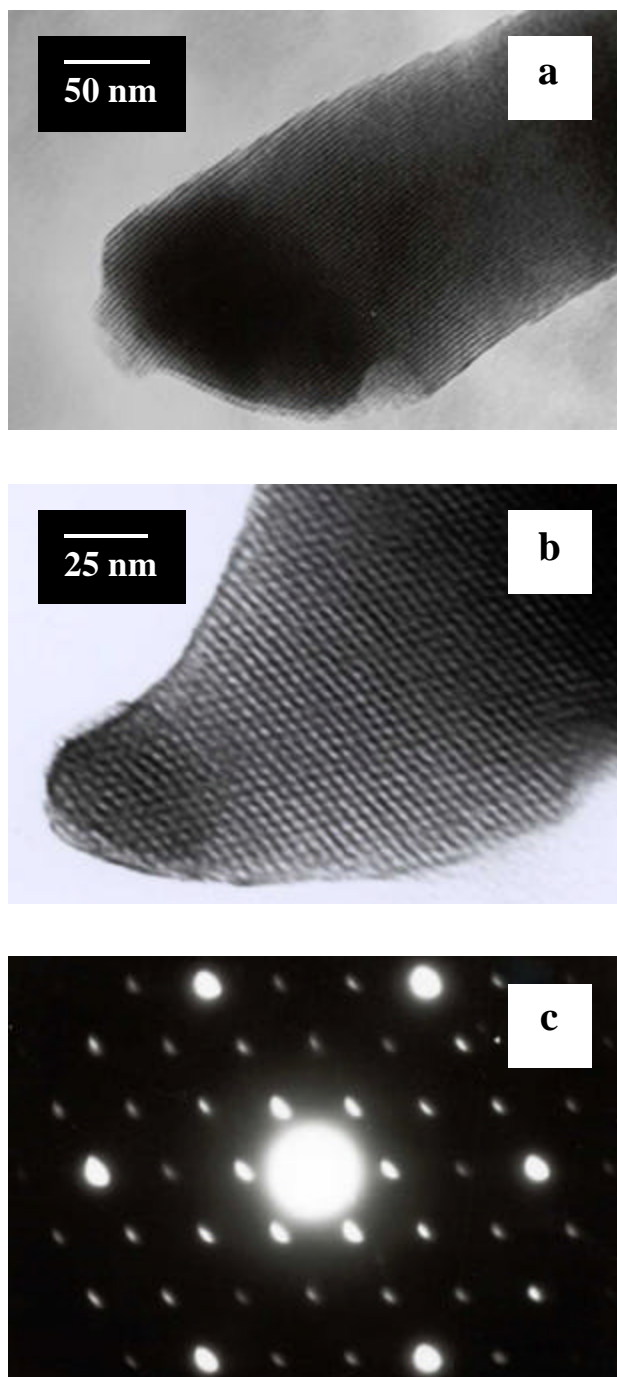


Figure 3.23 Transmission electron micrographs of calcined Ce-MCM-41-R (80) sample : (a) parallel fringes (side-on view), (b) hexagonal array (viewed along the pore direction) and (c) selected area electron diffraction pattern of (b).

found to be ≈ 30 , ≈ 40 and ≈ 7 Å, respectively. Therefore, the values of parameters obtained from the TEM measurements are approximately equal to those presented in Table 3.4 and 3.5. A representative selected area electron diffraction pattern, shown in Figure 3.23c, also exhibits well-defined hexagonal maxima and confirms the periodicity of the structure.

3.2.1.4.11. TG-DTA

Thermogravimetry (TG) and differential thermal analyses (DTA) of Si-MCM-41 and Ce-MCM-41 samples, carried out under same experimental conditions, were quite similar. The total weight losses were 38 and 41 wt.% for Si-MCM-41 (curve 'a') and Ce-MCM-41-R (40) (curve 'b'), respectively, as shown in Figure 3.24. The TG-DTA curves of the two samples

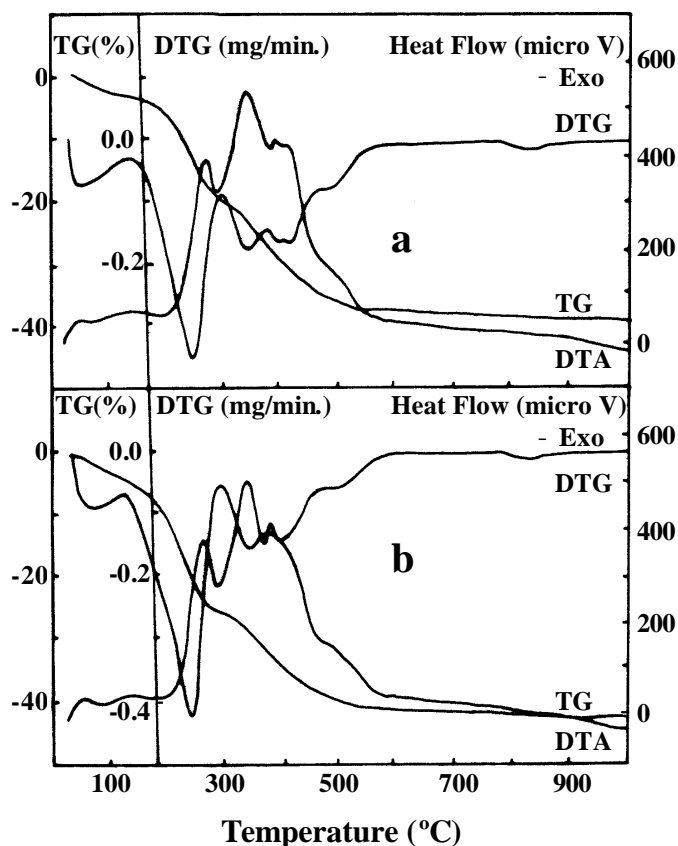


Figure 3.24 TGA-DTA curves of as-synthesized (a) Si-MCM-41 and (b) Ce-MCM-41-R (40).

reveal that nearly all the template including the water formed due to condensation of silanol groups is lost from the pore system at a temperature of ~ 600 °C. The TGA curves of the two samples show five steps of weight loss. The steps can be distinguished as 35-130 °C, 130-300 °C, 300-380 °C, 380-480 °C and 480-600 °C. The weight loss for both the samples is ~ 4.0% in the first step due to desorption of physisorbed water held in the pores. The weight losses in the 2nd (~ 20.0%) and 3rd (~ 7.0%) steps are mainly associated with oxidative decomposition of templates. In the 4th step, the weight loss (~ 7.0%) is probably due to removal of coke formed in the previous steps by the decomposition of templates. Whereas, in the last step, the weight loss (~ 2.0%) is mainly due to water loss formed by the condensation of silanol groups. It can be noticed that the weight losses of both Si-MCM-41 and Ce-MCM-41-R (40) samples are similar indicative of similar pore filling of Ce-MCM-41 vis-à-vis Si-MCM-41 samples. Higher amount of weight loss for Ce-MCM-41-R (40) (41 wt.%) than Si-MCM-41 (38 wt.%) may be due to slightly bigger pore size of the Ce-MCM-41-R (40) sample.

3.2.1.5. *Organo-functionalized MCM-41*

3.2.1.5.1. Powder X-ray Diffraction

The powder X-ray diffractograms of all as-synthesized samples are shown in Figure 3.25. All organo-functionalized MCM-41 samples exhibited characteristic strong (100) and weak (110, 200 and 210) reflections. This indicates that the samples have high degree of hexagonal ordering.

3.2.1.5.2. C, H, N and S analysis

The Table 3.8 contains the theoretical and as well as the observed C, H, N and S values of all samples. The theoretical C, H, N and S values were calculated according to the initial gel composition of the samples. The chemical analysis of the respective samples, after extraction

of the surfactant, confirms the presence of respective organic functionalities in the respective organo-functionalized MCM-41 mesoporous materials.

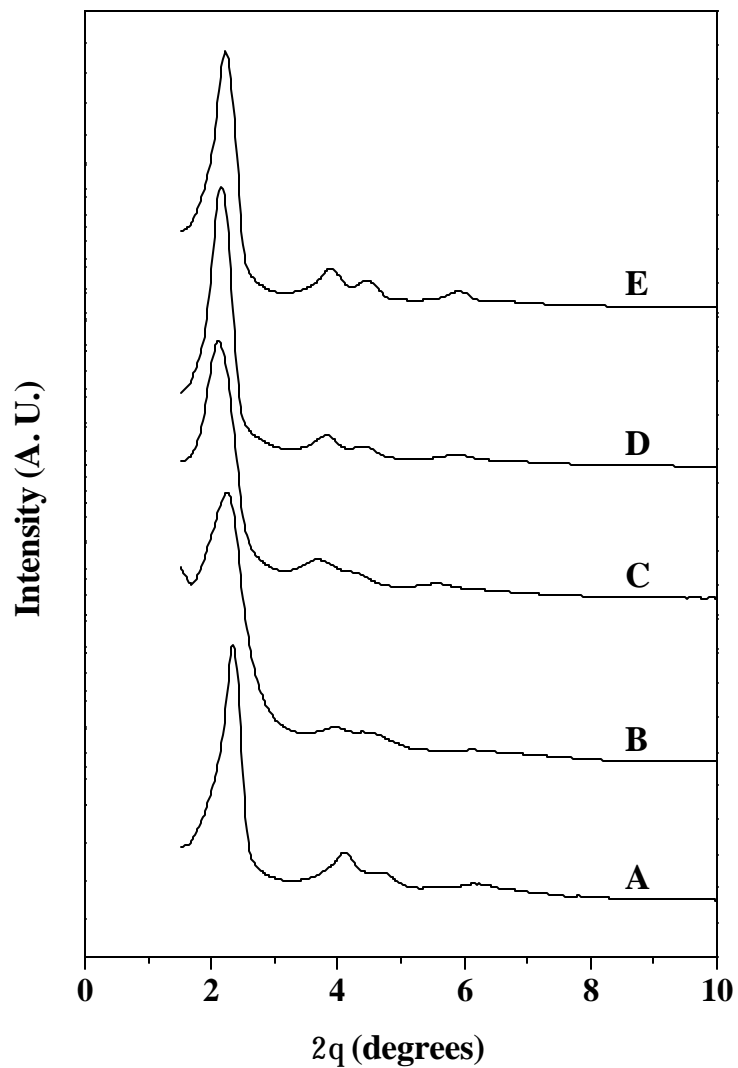


Figure 3.25 X-ray diffraction patterns of as-synthesized HS-MCM-41 (A), H₂N-MCM-41 (B), HS-H₂N-MCM-41 (C), HS-AI-MCM-41 (D) and Vinyl-MCM-41 (E).

3.2.1.5.3. N₂ adsorption

The surface area and the pore size distribution of organo-functionalized MCM-41 samples are given in Table 3.9. The samples have surface area in the range 500 - 900 m²g⁻¹.

Table 3.8
Theoretical and observed organic composition of the organo-functionalized MCM-41 samples

Samples ^a	Theoretical (wt.%)				Experimental (wt.%)			
	C	H	N	S	C	H	N	S
A : HS-MCM-41	12.63	2.46	-	11.23	11.55	2.25	-	10.27
B : H ₂ N-MCM-41	13.43	2.98	5.22	-	11.63	2.61	4.53	-
C : HS-H ₂ N-MCM-41	9.82	2.05	1.90	4.36	7.85	1.65	1.53	3.52
D : HS-Al-MCM-41	4.73	0.92	-	4.21	4.05	0.80	-	3.61
E : Vinyl-MCM-41	3.49	0.44	-	-	3.06	0.41	-	-

^aHS : 3-mercaptopropyl; H₂N : 3-aminopropyl.

Table 3.9
BET surface area and pore size distribution of organo-functionalized MCM-41 samples

Samples	Pore Size (Å)	BET Surface Area (m ² g ⁻¹)
A : HS-MCM-41	40.0	840
B : H ₂ N-MCM-41	24.0	550
C : HS-H ₂ N-MCM-41	35.0	510
D : HS-Al-MCM-41	38.0	673
E : Vinyl-MCM-41	35.0	775

The highest surface area was observed in the case of the sample A (HS-MCM-41, 840 m²g⁻¹) and lowest was obtained in the case of sample C (HS-H₂N-MCM-41, 510 m²g⁻¹) with all other sample having their surface area in the intermediate range. The pore size distribution shows that they have pore diameter in the range of 2-4 nm.

3.2.1.5.4. Diffuse Reflectance IR Spectroscopy

The diffuse reflectance IR spectra of H₂N-MCM-41 and HS-MCM-41 samples, given in Figure 3.26, shows spectroscopic evidence for the presence of intact aminopropyl and mercaptopropyl groups. The IR spectrum of H₂N-MCM-41 showed the presence of two bands at 2936 and 2880 cm⁻¹ assigned to the asymmetrical and symmetrical vibrations of the CH₂ groups of the propyl chains, respectively. It also showed two bands at 3365 and 3300 cm⁻¹ characteristic of NH₂ groups.²⁵ Similarly, in the case of HS-MCM-41, two bands at 2933 and 2881 cm⁻¹ assigned to asymmetrical and symmetrical vibrations of the CH₂ groups of the propyl chains and the most important band at 2565 cm⁻¹ characteristic of ν_{S-H} vibration are observed.²⁶

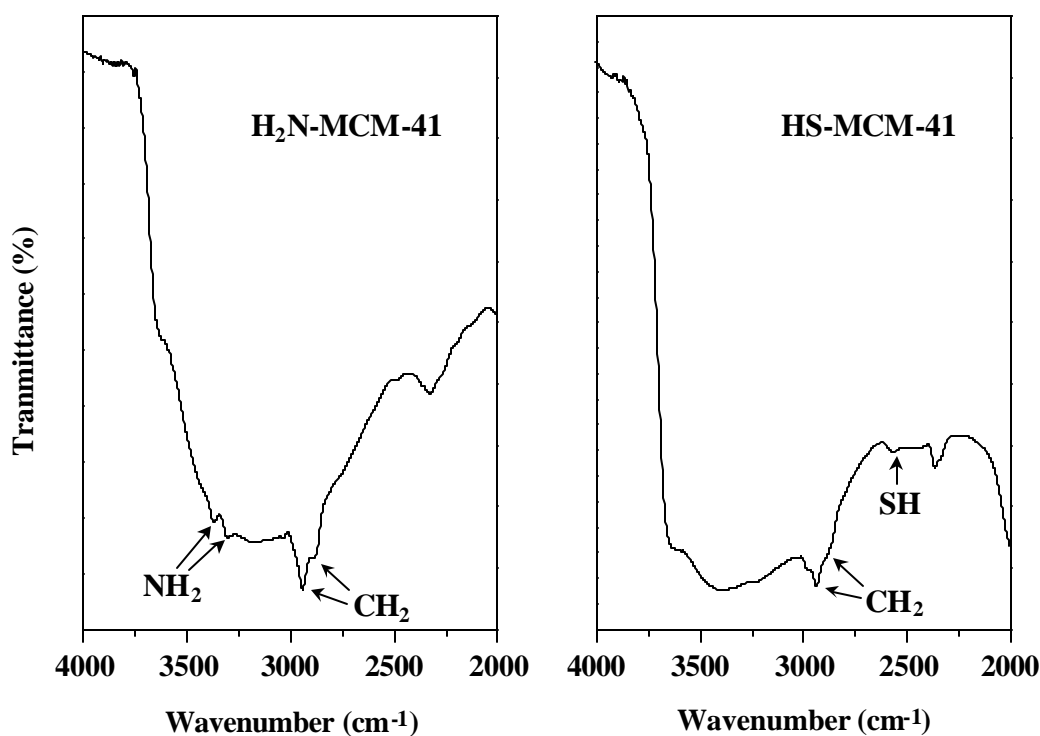


Figure 3.26 IR spectra of H₂N-MCM-41 and HS-MCM-41 after removal of the template (surfactant) by acid-solvent extraction.

3.2.1.5.5. ^{13}C CP MAS NMR

The ^{13}C CP MAS spectrum of the sample A (Figure 3.27) shows the presence of most prominent peak at 27.2 ppm for C_1 (adjacent to the SH group) and C_2 carbons of the 3-mercaptopropyl group. The peak at 11.0 ppm arises from the C_3 carbon attached to 3-mercaptopropyl group. Some additional minor resonance at 22.3 ppm is assigned to C_1 and C_2 carbon atoms of dipropyl disulfide. The presence of dipropyl disulfide in the sample A may be due to the oxidation or dehydrogenation of two adjacent thiol groups leading to the formation of disulfide (S-S) group. The C_3 carbon of the disulfide produces an unresolved shoulder slightly downfield to the C_3 carbon of the thiol. Two additional weak resonances observed at 50.3 and 36.6 are assigned to methanol used in the extraction and additional oxidation products (such as sulfinate groups), respectively.^{27,28}

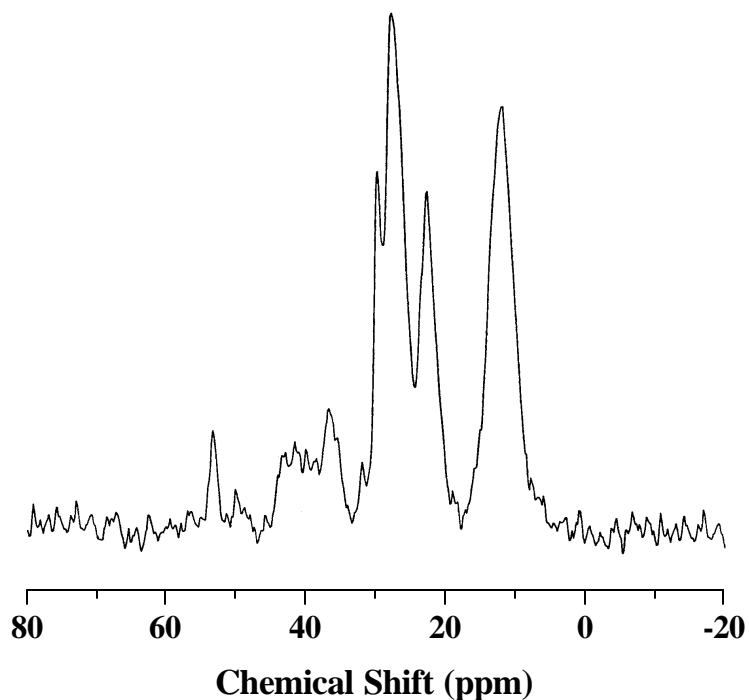


Figure 3.27 ^{13}C CP MAS NMR spectrum of template free HS-MCM-41.

The ^{13}C CP MAS NMR spectrum of the sample B (Figure 3.28) shows three peaks of almost equal intensity. The three peaks observed at 9.9, 20.8 and 42.6 ppm can be attributed to the three different carbons of the 3-aminopropyl group, C_3 , C_2 , and C_1 , respectively.²⁹

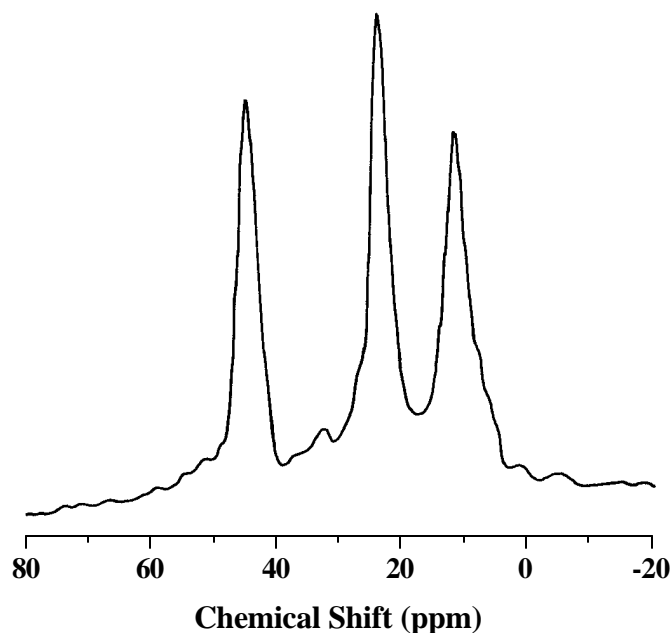


Figure 3.28 ^{13}C CP MAS NMR spectrum of template free H_2N -MCM-41.

3.2.1.5.6. ^{29}Si CP MAS NMR

The ^{29}Si CP MAS NMR spectrum of HS-MCM-41 (Figure 3.29) shows evidence for the close-packed conformation of carbon chains in the functionalized material. The peaks at about -101 and -109 ppm are attributed to Q_3 and Q_4 species present in Si-MCM-41, respectively. Three additional peaks observed at *ca.* -49, -57 and -66, corresponding to three different environments for the siloxane groups in the functionalized monolayers, are due to the presence of isolated (not bound to any siloxane), terminal (bound to one neighboring siloxane) and cross-linked (bound to two neighboring siloxane) groups as shown schematically in Figure 3.29.³⁰ Among the three, the most dominant peak comes from the

terminal group. However, the quantification of these groups on the basis of ^{29}Si CP MAS NMR will not be authentic because of differences in relaxation behavior.

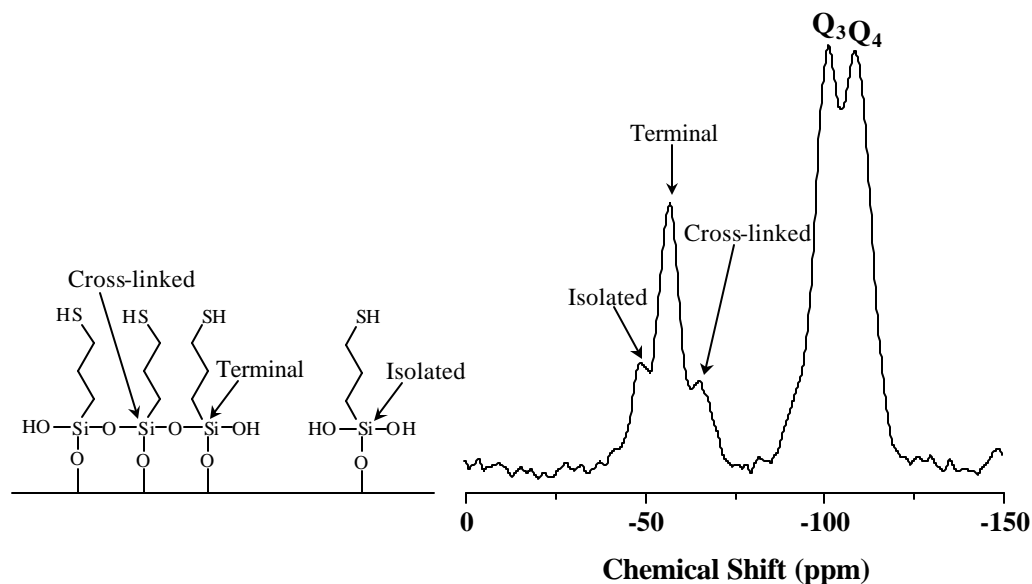


Figure 3.29 ^{29}Si CP MAS NMR spectrum of template free HS-MCM-41.

In Figure 3.30, the presence of close-packed conformation of aminopropyl carbon chains is also evident from the ^{29}Si CP MAS NMR spectrum of H_2N -MCM-41 sample. While the two peaks at about -101 and -111 ppm are attributed to Q_3 and Q_4 species for Si-MCM-41, the three peaks at about -50, -60 and -67 ppm are assigned to isolated, terminal and cross-linked siloxane groups attached with hanging aminopropyl groups.²⁹ The schematic representation of different siloxane groups as shown in Figure 3.29 for thiol functionalized MCM-41 is very much similar for amine functionalized MCM-41. In the case of H_2N -MCM-41, however, the peak intensities of different siloxane groups are in the order : isolated < terminal < cross-linked.

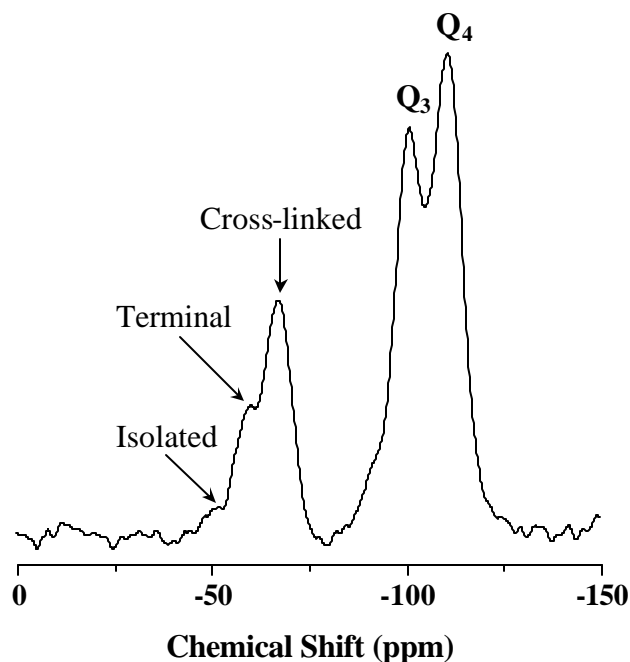


Figure 3.30 ^{29}Si CP MAS NMR spectrum of template free $\text{H}_2\text{N-MCM-41}$.

3.2.2. TS-1 and TS-2

The TS-1 and TS-2 samples were mainly characterized by the powder X-ray diffraction (XRD), diffuse reflectance UV-Vis spectroscopy, FTIR spectroscopy, energy dispersive X-ray analysis (EDX), scanning electron microscopy (SEM) and electron paramagnetic resonance (EPR) spectroscopy.

The XRD patterns of the calcined samples are characteristic of MFI and MEL topologies for TS-1 and TS-2 respectively. The absorption maxima at *ca.* 210 nm in the diffuse reflectance UV-Vis spectra and characteristic band at *ca.* 960 cm^{-1} in the IR spectra clearly indicate that Ti is incorporated in the framework of TS-1 and TS-2. The absence of any bands at *ca.* 260 and 330 nm in the UV-Vis spectra indicate that hexa-coordinated Ti in the extra-framework position and anatase form of TiO_2 are not present in the TS-1 and TS-2 samples. The average particle size of the crystallites determined by scanning electron microscopy is in

the range between 100-200 nm. The Si/Ti molar ratios in the solids were 32 and 33 as determined by chemical analysis (EDX) for the TS-1 and TS-2 samples, respectively.

3.2.2.1. Diffuse Reflectance UV-Vis Spectroscopy : Interaction with HP and UHP

Figure 3.31 depicts the diffuse reflectance UV-Vis spectra of TS-1 (Figure 3.31A) and TS-2 (Figure 3.31B) samples in the presence of water, aqueous hydrogen peroxide (HP) and solid urea-hydrogen peroxide (UHP). Intense absorption bands at 210 nm (curves 'a' and 'f' in Figure 3.31) are obtained in the spectra for calcined TS-1 and TS-2 samples. However, the mixtures of TS-1/TS-2 and urea-hydrogen peroxide (UHP) show two absorption bands (curves 'b' and 'g'), a sharp absorption band at 210 nm as well as a continuous absorption band in the region of 300-500 nm. The presence of continuous absorption band (300-500 nm) indicates the formation of different Ti-superoxo complexes by the solid-solid interaction between catalyst and UHP. The hydrated TS-1 and TS-2 samples in the presence of adsorbed water show a shift in the absorption maxima from 210 to 230 nm and some absorption in the region of 250-350 nm (curves 'c' and 'h') due to ligand-to-metal charge transfer involving isolated penta-/hexa-coordinated Ti atoms, where one or two water molecules form part of the metal coordination sphere. The curves 'd' and 'e', representing TS-1/UHP/acetone and TS-1/HP (Figure 3.31A), as well as curves 'i' and 'j', representing TS-2/UHP/acetone and TS-2/HP samples (Figure 3.31B), exhibit similar type of absorptions (a strong absorption at 210-215 nm and a continuous absorption in the 300-500 nm) in the UV-Vis region. Interestingly, curves 'd' and 'i' also show some absorbance in the 250-350 nm region, assigned to solvent molecules coordinated to Ti-centers, which has not been observed in the solvent free systems i.e. in the absence of water and acetone (curves 'b' and 'g').^{31,32}

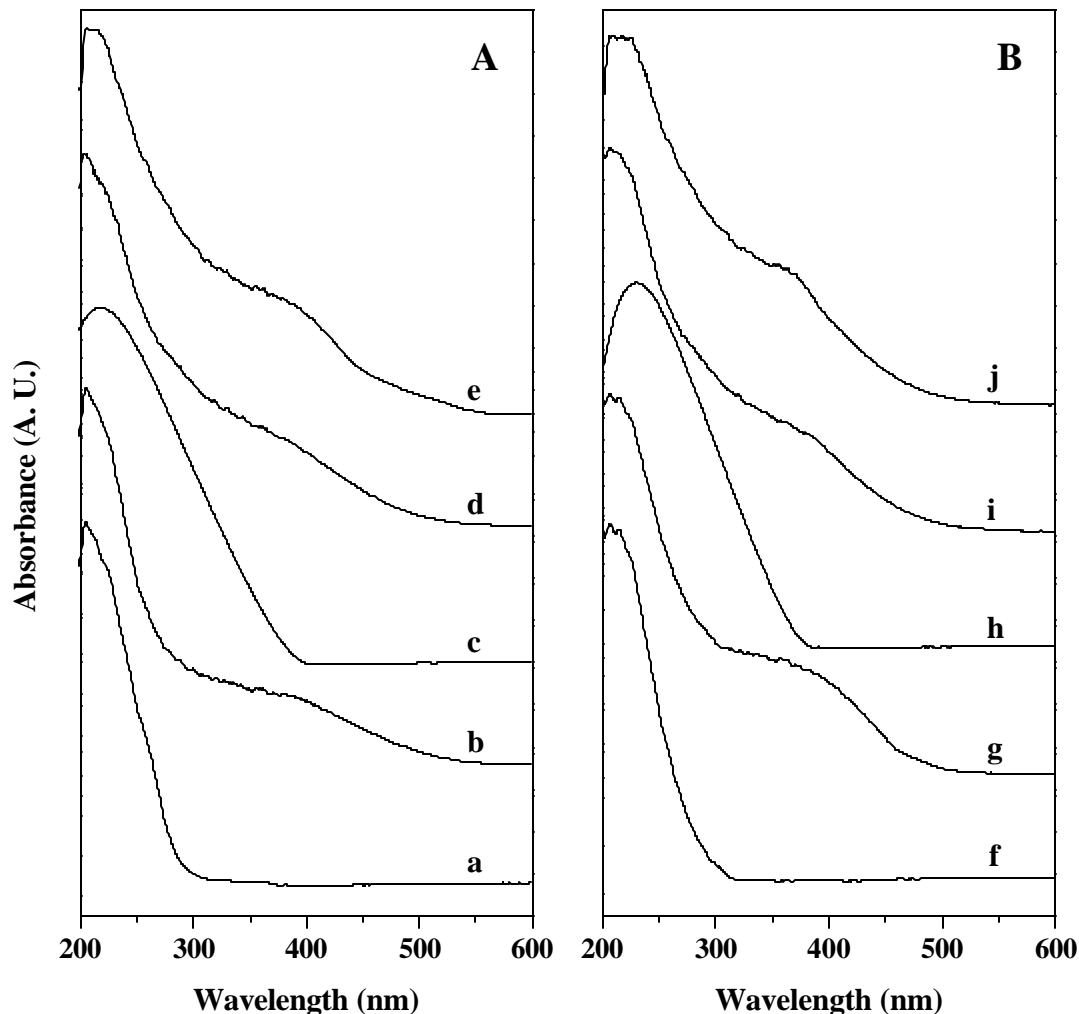


Figure 3.31 Comparison of diffuse reflectance UV-Vis spectra of different TS-1 (Figure 1A) and TS-2 (Figure 1B) samples: calcined TS-1 and TS-2 (curves ‘a’ and ‘f’), TS-1/TS-2 + UHP (curves ‘b’ and ‘g’), TS-1/TS-2 + H₂O (curves ‘c’ and ‘h’), TS-1/TS-2 + UHP + Acetone (curves ‘d’ and ‘i’) and TS-1/TS-2 + aqueous H₂O₂ (curves ‘e’ and ‘j’).

3.2.2.2. EPR Spectroscopy : Interaction with HP and UHP

Figure 3.32 compares the anisotropic EPR spectra of TS-1 and TS-2 samples in the presence of HP and UHP. The EPR spectra of TS-1/UHP and TS-2/UHP systems, recorded at 298 K, provide direct spectroscopic evidence for the existence of different Ti-superoxo

species in TS-1 and TS-2. The presence of four non-equivalent Ti-superoxo species (a, b, c and d) in curve 'A' indicates the existence of different Ti^{4+} sites in original TS-1 and TS-2³³ and/or generated due to solid-solid interaction between TS-1 and UHP, whereas free superoxo radical weakly attached to lattice silicon represents species 'e'. The EPR spectrum of TS-2/UHP system (curve C) is similar to that of TS-1/UHP system (curve A). Expectedly,

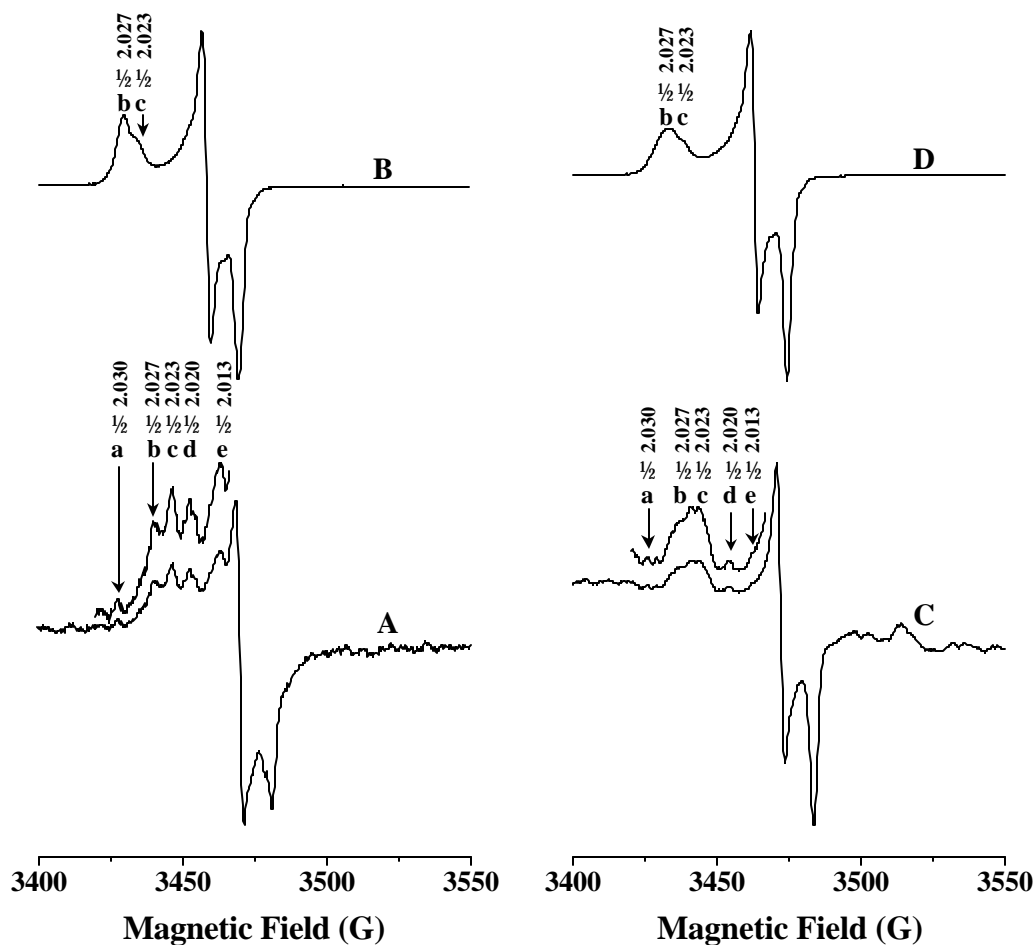


Figure 3.32 Comparison of EPR spectra of different TS-1 + UHP (A), TS-1 + aqueous H_2O_2 (B), TS-2 + UHP (C) and TS-2 + aqueous H_2O_2 (D).

in the case of TS-1/HP and TS-2/HP systems, recorded at 77 K, where aqueous H_2O_2 (instead of anhydrous H_2O_2 (UHP) as in the case of TS-1/UHP and TS-2/UHP systems) is used, the

different EPR signals originating from non-equivalent Ti-environments seem to lose their inequality leading to the observation of two broad signals (curves B and D). In both the curves B and D, the dominant Ti-superoxo species is 'b' which represents that other coordination sites of Ti are occupied by water molecules. However, solvent (water) molecules cannot fill vacant coordination sites of Ti in case of TS-1/UHP and TS-2/UHP systems.^{31,32} The 'g' values of four curves are in good agreement with those reported in the literature for the superoxide radical ion stabilized on Ti (IV) centers of both supported and bulk titanium dioxide.³⁴

3.3. REFERENCES

1. Luan, Z., He, H., Zhou, W., Cheng, C. F., and Klinowski, J., *J. Chem. Soc., Faraday Trans.* **91**, 2955 (1995).
2. Carvalho, W. A., Varaldo, P. B., Wallau, M., and Schuchardt, U., *Zeolites* **18**, 408 (1997).
3. Beck, J. S., Vartulli, J. C., Roth, W. J., Leonowicz, M. E., Kresge, C. T., Schmitt, K. D., Chu, C. T.-W., Olson, D. H., Sheppard, E. W., McCullen, S. B., Higgins, J. B., and Schlenker, J. L., *J. Am. Chem. Soc.* **114**, 10834 (1992).
4. Sasidharan, M., Hegde, S. G., and Kumar, R., *Microporous Mesoporous Mater.* **24**, 59 (1998).
5. Kumar, R., Bhaumik, A., Ahedi, R. K., and Ganapathy, S., *Nature* **381**, 298 (1996).
6. Zhang, W., Fröba, M., Wang, J., Tanev, P. T., Wong, J., and Pinnavaia, T. J., *J. Am. Chem. Soc.* **118**, 9164 (1996).
7. Sayari, A., *Chem. Mater.* **8**, 1840 (1996).
8. Sen, T., Rajmohan, P. R., Ganapathy, S., and Sivasanker, S., *J. Catal.* **163**, 354 (1996).
9. Tuel, A., and Taârit, Y. B., *Appl. Catal. A* **102**, 201 (1994).
10. Cambor, M. A., Corma, A., and Pariente, J. P., *J. Chem. Soc., Chem. Commun.* 557 (1993).
11. Alba, M. D., Luan, Z., and Klinowski, J., *J. Phys. Chem.* **100**, 2178 (1996).
12. Sohn, J. R., *Zeolites* **6**, 225 (1986).
13. Reddy, K. M., Moudrakovski, I., and Sayari, A., *J. Chem. Soc. Chem. Commun.* 1059 (1994).
14. Bengoa, J. F., Gallegos, N. G., Marchetti, S. G., Alvarez, A. M., Cagnoli, M. V., and Yeramian, A. A., *Microporous and Mesoporous Mater.* **24**, 163 (1998).
15. Ho, D., Cheng, C.-H., He, H., and Klinowski, J., *J. Mater. Chem.* **7**, 159 (1997).

16. Chaudhari, K., Das, T. K., Rajmohanam, P. R., Lazar, K., Sivasanker, S., and Chandwadkar, A. J., *J. Catal.* **183**, 281 (1999).
17. Chen, X., Huang, L., and Li, Q., *J. Phys. Chem. B* **101**, 8460 (1997).
18. Barret, E. P., Joyner, L. G., and Halenda, P. P., *J. Am. Chem. Soc.* **73**, 373 (1951).
19. Decottiguies, M., Phalippou, J., and Zarzycki, J., *J. Mater. Sci.* **13**, 2605 (1978).
20. Kolodziejewski, W., Corma, A., Navarro, M. T., and Pariente, J. P., *Solid State Nucl. Magn. Reson.* **2**, 253 (1993).
21. Boccuti, M. R., Rao, K. M., Zecchina, A., Leofanti, G., and Petrini, G., *Stud. Surf. Sci. Catal.* **48**, 133 (1989).
22. Keshavaraja, A., Hegde, V. R., Pandey, B., Ramaswamy, A. V., Kumar, P., and Ravindranathan, T., *Angew. Chem. Int. Ed. Engl.* **34**, 2143 (1995).
23. Coluccia, S., Marchese, L., and Martra, G., *Microporous Mesoporous Mater.*, **30**, 43 (1999).
24. Chen, C.-Y., Burkett, S. L., Li, H.-X., and Davis, M. E., *Microporous Mater.* **2**, 27 (1993).
25. Brunel, D., Fajula, F., Nagy, J. B., Deroide, B., Verhoef, M. J., Veum, L., Peters, J. A., and van Bekkum, H., *Appl. Catal.* **213**, 73 (2001).
26. Rhijn, W. M. V., Vos, D. E. D., Sels, B. F., Bossaert, W.D., and Jacobs, P. A., *Chem. Commun.* 317 (1998).
27. Lim, M. H., Blanford, C. F., and Stein, A., *J. Am. Chem. Soc.* **119**, 4090 (1997).
28. Lim, M. H., Blanford, C. F., and Stein, A., *Chem. Mater.* **10**, 467 (1998).
29. Carvalho, W. A., Wallau, M., and Schuchardt, U., *J. Mol. Catal. A* **144**, 91 (1999).
30. Feng, X., Fryxell, G. E., Wang, L.-Q., Kim, A. Y., Liu, J., and Kemner, K. M., *Science* **276**, 923 (1997).
31. Laha, S. C., and Kumar, R., *J. Catal.* **204**, 64 (2001).

32. Laha, S. C., and Kumar, R., *J. Catal.* (in press).
33. Tuel, A., Taârit, Y. B., *Appl. Catal. A: General* **110**, 137 (1994).
34. Che, M., and Tench, A. J., *Adv. Catal.* **32**, 1 (1983).

CHAPTER 4

CATALYTIC PROPERTIES

4. CATALYTIC PROPERTIES

Section 4.1 of this present chapter deals with the selective **acid catalyzed reactions** such as :

1. Isopropylation of naphthalene over Al-MCM-41 samples.
2. Dehydration of cyclohexanol over Ce-MCM-41 samples.
3. Chemoselective acylation of alcohols, amines, phenols and thiols over Ce-MCM-41 samples.

Section 4.2 of this chapter deals with the selective **oxidation catalysis** :

1. Hydroxylation of 1-naphthol over Ti-, V- and Ce-MCM-41 samples.
2. Epoxidation of cyclohexene over Ti-MCM-41 and V-MCM-41.
3. Epoxidation of a variety of olefinic compounds over TS-1 and TS-2.

The details of the methods of preparation and the results of physico-chemical characterization of the above-mentioned materials have been presented in Chapter 2 and Chapter 3, respectively.

4.1. ACID CATALYZED REACTIONS

4.1.1. Experimental

4.1.1.1. Isopropylation of Naphthalene

The isopropylation of naphthalene was carried out using different Al-MCM-41 samples as solid acid catalysts. The mixture of naphthalene dissolved in cyclohexane (cyclohexane/naphthalene (wt./wt.) = 4) and isopropanol (naphthalene/isopropanol (mol./mol.) = 4) was added to the catalyst (10 wt.% of naphthalene) taken in Parr type autoclave. The reaction mixture was then heated for 6 h at 448 K under autogeneous pressure and mechanical stirring (300 rpm). After the reaction, the product mixture was cooled to room temperature and the organic layer was separated and then analyzed by HP 6890 series GC system (DB-5, 50 m ×

0.20 mm \times 0.33 μ m film thickness) using FID detector. Selected samples were also analyzed by GCMS (Shimadzu, GCMS-QP 2000A).

4.1.1.2. Dehydration of Cyclohexanol

The catalytic reaction of dehydration of cyclohexanol was carried out in a fixed bed down flow reactor. The Ce-MCM-41 samples were pretreated at 673 K for 1 h in a flow of N₂ gas. Cyclohexanol was fed into the catalyst bed at 473 K using air as the carrier gas. After 1 h, the product was collected and analyzed by Shimadzu 17A series gas chromatograph (HP 101, methyl silicone fluid, 50 m \times 0.2 mm \times 0.2 μ m film thickness) using FID detector.

4.1.1.3. Acylation of Alcohols, Amines, Thiols and Phenols

In a typical procedure for the chemoselective acylation of different substrates (alcohol/amine/phenol/thiol; 10 mmol) were added to 11 mmol of acylating agent (mostly acetic anhydride) and the mixture was refluxed under stirring in acetonitrile (5 ml) in the presence of Ce-MCM-41 catalyst (20 wt.%, w/w with respect to the substrate) for stipulated period of time for the completion of the reaction (monitored by TLC). After completion of the reaction, the catalyst was separated by centrifugation/filtration and then the filtrate was concentrated, treated with water (15 ml) and extracted with CH₂Cl₂ (3 \times 15 ml). The organic layer was separated, washed with 10% aqueous NaHCO₃, brine, water, and dried over Na₂SO₄. The solvent was removed to produce crude product, which was then purified by column chromatography over silica gel (3% EtOAc in light petroleum ether) to furnish pure product. The structure was confirmed by ¹H NMR, FTIR, mass spectrometry, and also by comparison with authentic sample. Some of the samples were also analyzed using Agilent 6890 series GC system (HP chiral, 20% permethylated β -cyclodextrin, 30 m \times 0.32 mm \times 0.25 μ m film thickness), GCIR (Perkin Elmer, GC-IR 2000) and GCMS (Shimadzu, GCMS-

QP 2000A). The catalyst recovered from the reaction mixture was reactivated by calcining it at 813 K for 8 h in the presence of air and was reused again for acylation reactions.

4.1.2. Results and Discussion

4.1.2.1. Isopropylation of Naphthalene over Al-MCM-41

The isopropylation of naphthalene was carried out as a test reaction to compare the catalytic activity and selectivity of Al-MCM-41-S and Al-MCM-41-P samples under same reaction conditions (Figure 4.1). The conversion (*ca.* 36.4 and 36.7 mol% for Al-MCM-41-S and Al-MCM-41-P samples respectively) was comparable. In both the cases the ratio of 2-isopropylnaphthalene/1-isopropylnaphthalene (2-IPN/1-IPN) was also comparable (≈ 2.6).

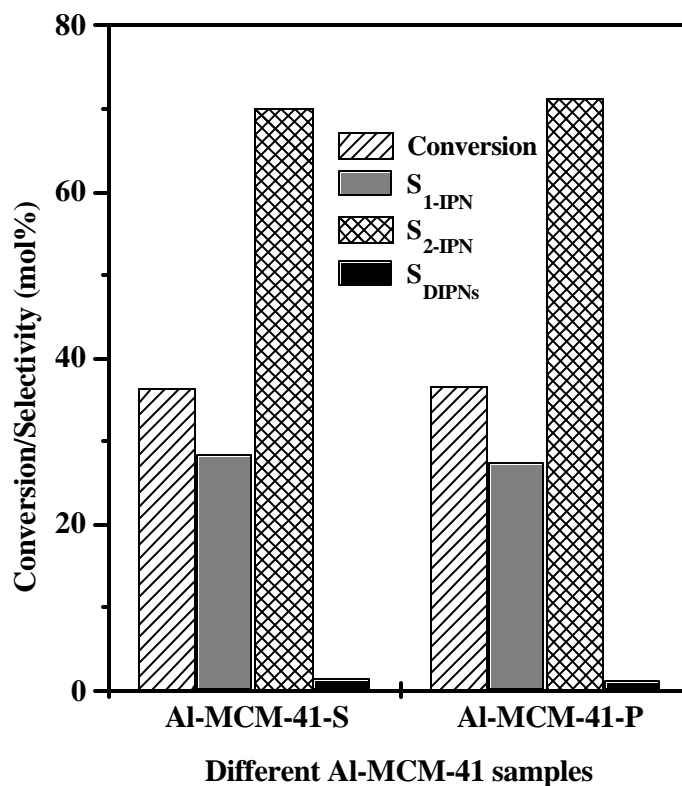


Figure 4.1 Comparison of catalytic activity and selectivity of Al-MCM-41-S and Al-MCM-41-P samples. S_{1-IPN} = Selectivity of 1-isopropylnaphthalene; S_{2-IPN} = Selectivity of 2-isopropylnaphthalene; S_{DIPNs} = Selectivity of diisopropylnaphthalenes.

Further, the formation of small amount of diisopropylnaphthalenes (DIPNs; 1.2-1.5 mol%) was also noticed in both cases. So, it can be inferred that the active Al-sites responsible for the isopropylation of naphthalene are also similar in nature for Al-MCM-41-S and Al-MCM-41-P samples.

4.1.2.2. Dehydration of Cyclohexanol over Ce-MCM-41

The dehydration of cyclohexanol was carried out using different Ce-MCM-41 samples, as shown in Figure 4.2. Ce-exchanged MCM-41, Ce-impregnated MCM-41 and silica-ceria catalysts were also used simultaneously to compare the catalytic results. It is observed that

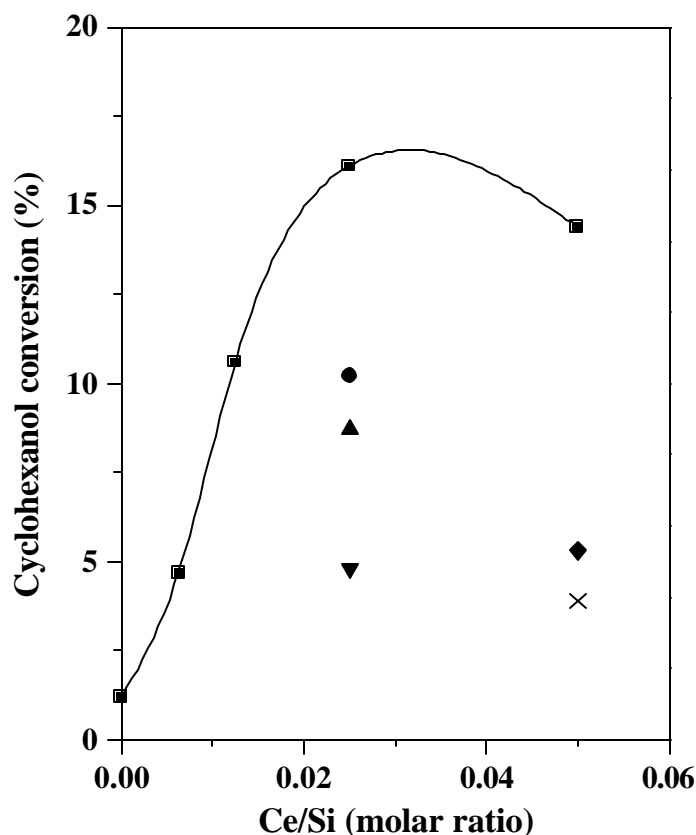


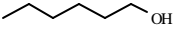
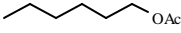
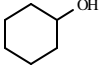
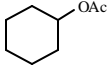
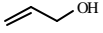

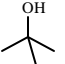
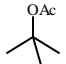
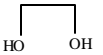
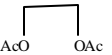
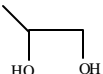
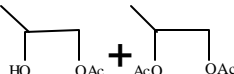
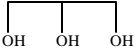
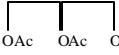
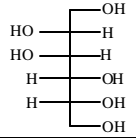
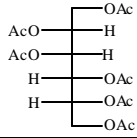
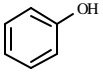
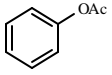
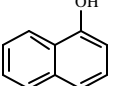
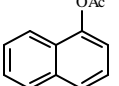
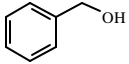
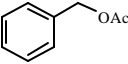
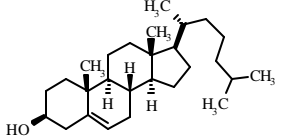
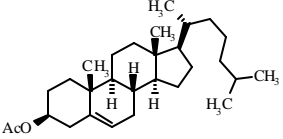
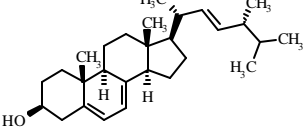
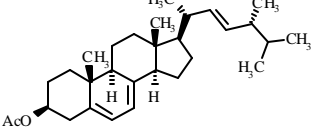
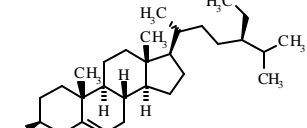
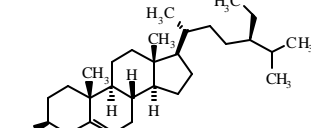
Figure 4.2 Activity of Ce-MCM-41 samples in the dehydration of cyclohexanol to cyclohexene. (□) Ce-MCM-41-R, (●) Ce-MCM-41-P (40), (▲) Ce-MCM-41-A (40), (▼) Ce-Ex-MCM-41, (◆) Ce-Im-MCM-41 (20) and (×) SiO₂-CeO₂ (20).

the cyclohexanol conversion is reduced considerably when Ce-Ex-MCM-41, Ce-Im-MCM-41 and silica-ceria were used as catalysts compared to that over Ce-MCM-41 samples with same Si/Ce ratio. It has also been observed that as the Ce content increases in the Ce-MCM-41 samples, cyclohexanol conversion increases and reaches a maximum of ~16 % conversion for Ce-MCM-41-R (40) sample. However, further increase in the Ce content of Ce-MCM-41 samples does not increase the conversion, instead it decreases a little bit. A comparison of Ce-MCM-41 (40) samples prepared by three different methods (R, A and P) (see Table 3.4), also show that the Ce-MCM-41-R (40) sample is most active, whereas Ce-MCM-41-A (40) is the least active. While, the quite low activity for Ce-Ex-MCM-41, Ce-Im-MCM-41 and silica-ceria is expected (due to poor Ce dispersion), the lower conversion of Ce-MCM-41-P (40) and Ce-MCM-41-A (40) compared to Ce-MCM-41-R (40) needs attention. It may be possible that higher conversion of cyclohexanol in the case of Ce-MCM-41-R (40) sample synthesized at atmospheric pressure under magnetic stirring (~1000 rpm) is due to the presence of highly dispersed Ce. However, an unambiguous explanation needs further work.

4.1.2.3. Acylation of Alcohols, Amines, Phenols and Thiols over Ce-MCM-41

The acylation or simple esterification of a wide range of structurally varied alcohols, amines, phenols and thiols (primary, secondary, tertiary, allylic, benzylic, cyclic and heterocyclic etc.) is one of the most important and frequently used organic transformations.^{1,2} It provides not only an efficient and inexpensive route for protecting hydroxy, amino, phenolic and thiol groups but also produces important organic ester intermediates in multistep synthetic processes which are widely employed in the synthesis of fine chemicals, pharmaceuticals, perfumes, plasticizers, cosmetics, chemical auxiliaries etc. The results of acylation of different alcohols using stoichiometric amount of acetic anhydride in the presence of Ce-MCM-41-R (40) sample are given in Table 4.1.

Table 4.1
Acylation of alcohols and polyols with acetic anhydride as acylating agent over cerium containing MCM-41

Entry	Substrate	Reaction time (h)	Product ^a	Yield ^b (mol%)
1		03		90
2		06		90
3		04		70
4		12		70
5		06		90
6		24 ^c		90 (4 : 1)
7		08		90
8		10		90
9		16		90
10		24		90
11		06		90
12		24		75
13		24		70
14		24		70

^a Products were characterized by usual spectral analyses.

^b Isolated yield.

^c Reaction was performed at 338 K.

In general, the reactions are moderately fast and also the isolated yields of the acylated products are very good to excellent. In the case of different types of alcohols, it was observed that although the acylation of acyclic 1-hexanol (Table 4.1, entry 1) is fast (~3 h) its cyclic analogue cyclohexanol (Table 4.1, entry 2) takes longer time for completion of the reaction (~6 h), which may be explained on the basis of steric factor. Since, the reactions were carried out under mild conditions, the probability of induced isomerization is expected to be almost nil. This was observed experimentally in the case of allyl alcohol (Table 4.1, entry 3). In the case of *tertiary*-butanol (Table 4.1, entry 4), the yield of the acylated product (~70%) is low in comparison with the other substrates mainly due to the formation of side products.

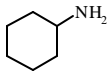
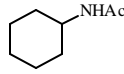
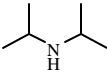
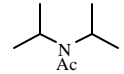
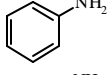
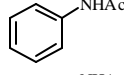
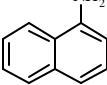
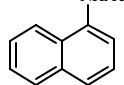
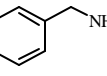
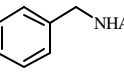
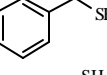
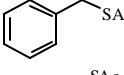
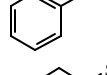
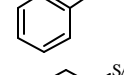
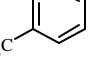
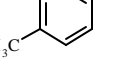
It is noteworthy that the acylation of ethanediol, 1,2-propanediol, propanetriol and polyols (D-mannitol) (Table 4.1, entries 5, 6, 7 and 8) also takes place smoothly over Ce-MCM-41 to afford corresponding mono and poly-acylated product depending upon the reaction conditions. It demonstrates the practical utility of this method particularly in sugar chemistry. In the case of 1,2-propanediol, primary alcoholic group was acylated preferentially over the secondary one. However, the ratio of mono-acylated to di-acylated product was *ca.* 4 : 1.

Although in general, the acylation of aliphatic alcohols is moderately fast in the presence of Ce-MCM-41, acylation of aromatic alcohols (Table 4.1, entries 9, 10 and 11) is rather sluggish (Table 4.1) mainly because of less nucleophilicity and therefore, longer time is required to complete the reaction. However, the yield of the products is comparable with other alcohols. The acylation of benzyl alcohol, where the phenyl group is not attached directly to the OH group, is relatively fast.

Most importantly, the acylation of cholesterol, ergosterol and β -sitosterol (Table 4.1, entries 12, 13, and 14) carried out in heterogeneous system using Ce-MCM-41, although takes longer time as compared to homogeneous system, is of great importance from the industrial, pharmaceutical and environmental point of view.

In order to explore the generality and expand the scope of the Ce-MCM-41-based Lewis acid catalyzed acylation reactions, a variety of other substrates such as different types of amines and thiols were also acylated with acetic anhydride. The results, given in Table 4.2, demonstrate that the amines and thiols are also acylated very selectively with excellent yields of the products. It was observed that the reaction is very fast with amines as compared to thiols. Cyclohexylamine takes only one hour (~1 h) for the completion of the reaction, whereas diisopropylamine takes little longer time (~1.5 h) for the same. In general, the aromatic amines take longer time for the completion of the reaction as compared to benzyl

Table 4.2
Acylation of amines and thiols with acetic anhydride as acylating agent over cerium containing MCM-41

Entry	Substrate	Reaction time (h)	Product ^a	Yield ^b (mol%)
1		1		90
2		1.5		90
3		2		90
4		2		95
5		1.5		90
6		6		90
7		8		90
8		8		90



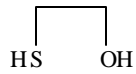
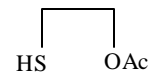
^a Products were characterized by usual spectral analyses.

^b Isolated yield.

amine. The same trend is also observed in the case of thiophenols. Benzylthiol takes ~6 h for the completion of the reaction whereas the same for thiophenol and *p*-thiocresol is ~8 h in both cases.

The chemoselective acylation of bifunctional amino ethanol and 2-mercapto ethanol, given in Table 4.3, shows very good chemoselectivity provided the reactions are carried out at lower temperatures. It is observed that the acylation of amino ethanol carried out at room temperature selectively produced the corresponding *N*-acetate only, in excellent yield, and the hydroxyl group remained untouched. The high chemoselectivity observed may be because of the greater nucleophilicity of the amine group vis-à-vis alcohol. Similarly, 2-mercapto ethanol reacted preferentially with the hydroxyl group over the thiol and accordingly afforded the corresponding *O*-acetate in high yield.

Table 4.3
Chemoselective acylation of amino alcohol and mercapto alcohol with acetic anhydride as acylating agent over cerium containing MCM-41

Entry	Substrate	Reaction time (h)	Product ^a	Yield ^b (mol%)
1		4 ^c		90
2		6 ^d		90

^a Products were characterized by usual spectral analyses.

^b Isolated yield.

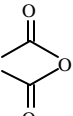
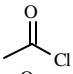
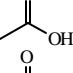
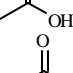
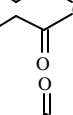
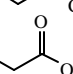
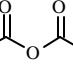
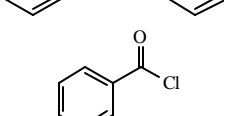
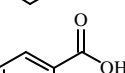
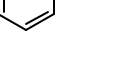
^c Reaction was performed at room temperature (298 K).

^d Reaction was carried out at 358 K.

Apart from acetylation, propionylation and benzylation of 1-hexanol were also carried out using different acylating agents over Ce-MCM-41. The results (Table 4.4) show that Ce-

MCM-41 is also a good catalyst for acylation with different acylating agents. Compared to acetic anhydride and acetyl chloride, acetic acid is a better choice as the acylating agent because it produces only water as the co-product, which is environmentally friendly. However, the reactivity of acetic acid is rather poor compared to that of acetic anhydride or

Table 4.4
Acylation of 1-hexanol with different acylating agents over cerium containing MCM-41

Entry	Acylating agents	Reaction time (h)	Product ^a	Yield ^b (mol%)
1		3	Hexyl acetate	90
2		3	Do	90
3		24	Do	90
4		10 ^c	Do	90
5		10	Hexyl propionate	85
6		6	Do	90
7		24	Do	85
8		15	Hexyl benzoate	85
9		5	Do	90
10		24	Do	85

^a Products were characterized by usual spectral analyses.

^b Isolated yield.

^c 10 Equivalents of acid was used.

acetyl chloride. Nevertheless, when the reaction was carried out using excess acetic acid (10 equivalent with respect to 1-hexanol), to fulfill the purposes of both acylating agent as well as solvent at ~ 383 K, a considerable decrease in reaction time was observed with comparable yield of the acylated product (Table 4.4, entries 3 and 4). It is also important to note that the same trend is observed for propionylation and benzylation (Table 4.4).

The effect of Ce content on the acylation of 1-hexanol is demonstrated in Table 4.5 using various Ce-MCM-41 samples with different Si/Ce ratios (∞ , 80, 40 and 20). It is observed that the yield of hexyl acetate increases with increasing Ce loading in the Ce-MCM-41 samples (up to *ca.* Si/Ce = 40) and therefore, it may be inferred that highly dispersed Ce present in the silica network in MCM-41 walls is the only active sites in the acylation reaction. The turn over frequency (TOF, h^{-1}), however, decreases with increasing Ce content (Table 4.5). This may be due to the reason that increasing Ce content in Ce-MCM-41 samples may lead to increased presence of Ce inside the walls of MCM-41 and therefore not available for catalytic reaction. However, higher activity of Ce-MCM-41 samples compared to CeO_2 observed for acylation of 1-hexanol under same reaction condition indicate that high surface area (working as a good dispersive support for Ce) and mesoporosity of Ce-MCM-41 samples also play an important role in these reactions.

Table 4.6 compares the catalytic activity and selectivity of Ce-MCM-41 with that of Ti-MCM-41 and Zr-MCM-41 in the acylation of 1-hexanol under same reaction conditions and at comparable Si/M ratio (M = Ti, Zr and Ce). It is clear that the activity of Ti- and Zr-MCM-41 towards acylation is substantially low as compared to that of Ce-MCM-41. This is probably due to the reason that Ce acts as a better electron pair acceptor (Lewis acidity) and able to expand its coordination number easily.

To verify the leaching of Ce as well as recyclability and reusability of Ce-MCM-41 catalysts, the used Ce-MCM-41-R (40) was recycled twice and used for the acylation of 1-

hexanol. The yield of hexyl acetate obtained with recycled Ce-MCM-41-R (40) samples was comparable (80 and 85 mol% for first and second recycle, respectively vs. 90 mol% for fresh catalyst). The Ce-MCM-41 catalysts can be reused for these reactions without substantial loss in its intrinsic activity, at least for three cycles.

Table 4.5
Activity of different cerium containing MCM-41 samples in the acylation of 1-hexanol with acetic anhydride

Sample ^a	(Si/Ce) _{solid}	Reaction time	Conversion ^b	Yield ^c	TOF ^d (h ⁻¹)
		(h)	(mol%)	(mol%)	
Si-MCM-41	∞	3	5	-	-
		6	7	-	-
		9	8	-	-
Ce-MCM-41 (80)	80.9	3	48	-	39.4
		6	94	90	38.5
Ce-MCM-41 (40)	40.8	3	>99	90	42.3
Ce-MCM-41 (20)	20.8	3	>99	90	22.9
CeO ₂	-	3	18	-	0.5
		6	28	-	0.4
		9	38	30	0.4

^a Si/Ce molar ratio in parentheses.

^b Conversion was calculated by GC analyses.

^c Isolated yield.

^d Turnover frequency (TOF) = Moles of 1Hexanol converted for producing 1-Hexyl acetate per mole of Ce per hour.

Table 4.6
Activity of Different Metal Containing MCM-41 Samples (Ce, Ti and Zr) in the
Acylation of *n*-Hexanol with Acetic Anhydride

Sample ^a	(Si/M) _{solid}	Reaction time (h)	Conversion ^b (%)	Yield ^c (%)	TOF ^d (h ⁻¹)
Ce-MCM-41 (40)	40.8	3	> 99	90	42.3
Ti-MCM-41 (50)	52	3	24	-	12.5
		6	41	-	10.7
		9	54	50	9.4
Zr-MCM-41 (50)	54	3	28	-	15.4
		6	40	-	11.0
		9	51	45	9.3

^a Si/Ce molar ratio in parentheses.

^b Conversion was calculated by GC analyses.

^c Isolated yield.

^d Turnover frequency (TOF) = Moles of 1-Hexanol converted for producing 1-Hexyl acetate per mole of Ce per hour.

4.2. OXIDATION REACTIONS

4.2.1. Experimental

4.2.1.1. Hydroxylation of 1-Naphthol

The hydroxylation of 1-naphthol was carried out using 45 wt.% aqueous H₂O₂ and 70 wt.% aqueous TBHP as oxidants in the presence of V-, Ti- and Ce-MCM-41 samples as solid catalysts. The mixture of 1-naphthol, oxidant and acetonitrile as solvent (1-naphthol/H₂O₂ or TBHP (mol./mol.) = 4; acetonitrile/1-naphthol (wt./wt.) = 5) was added to the catalyst (20

wt.% of 1-naphthol) and the reaction mixture was heated for 12 h at a constant temperature of 353 K under stirring. After the reaction, the reaction mixtures were cooled to room temperature, the organic layer was separated by centrifugation and/or by extraction with dichloromethane and then analyzed by Shimadzu 17A series gas chromatograph using a capillary column (HP 101, methyl silicone fluid, 50 m × 0.2 mm × 0.2 μm film thickness) using FID detector. Selected samples were also analyzed by GCIR (Perkin Elmer, GC-IR 2000) and GCMS (Shimadzu, GCMS-QP 2000A) to identify the products.

4.2.1.2. Epoxidation Reactions

The epoxidation of different olefins were carried out in a glass batch reactor (50 mL capacity). In a typical reaction, a solution of 20 mmol olefinic substrate in solvent was added slowly to the mixture of catalyst (20 wt.% of the substrate) and 5 mmol urea-hydrogen peroxide (UHP) or aqueous hydrogen peroxide (HP, 45 wt.%) or aqueous *tert*-butyl hydroperoxide (TBHP, 70 wt.%). The reaction mixture was heated in the temperature range 313-323 K under stirring. After the completion of the reaction, the organic layer was collected by centrifugation and analyzed using Shimadzu 17A series gas chromatograph (HP 101, methyl silicone fluid, 50 m × 0.2 mm × 0.2 μm film thickness) and/or Agilent 6890 series GC system (HP chiral, 20% permethylated β-cyclodextrin, 30 m × 0.32 mm × 0.25 μm film thickness) using flame ionization detector. Selected samples were also analyzed by GCIR (Perkin Elmer, GC-IR 2000) and GCMS (Shimadzu, GCMS-QP 2000A).

4.1.3. Results and Discussion

4.1.3.1. Hydroxylation of 1-Naphthol over V-, Ti- and Ce-MCM-41

The hydroxylation of 1-naphthol was carried out using both aqueous H₂O₂ and TBHP as oxidants and V-MCM-41-S, V-MCM-41-P and Ti-MCM-41-P as catalysts. The results obtained over these three catalyst systems were compared as shown in Table 4.7. It can be

noted that the activity and selectivity of two V-MCM-41 samples are similar and from this it can be inferred that the nature of V-sites/species present in the V-MCM-41 samples are also similar. However, the major product in the hydroxylation of 1-naphthol is 1,4-naphthoquinone. This may result from the subsequent oxidation of primarily formed 1,4-dihydroxynaphthalene to the corresponding quinone derivative. When Ti-MCM-41-P sample was used for the hydroxylation of 1-naphthol, the observed selectivity of dihydroxynaphthalene derivatives was higher than that obtained with V-MCM-41-P sample under same reaction conditions.

The hydroxylation of 1-naphthol using Ce-MCM-41 samples as catalysts in the presence of aqueous H_2O_2 and TBHP is given in Table 4.8 and 4.9. For comparison, the reactions were also carried out over Si-MCM-41, Ce-exchanged MCM-41, Ce-impregnated MCM-41 and $\text{SiO}_2\text{-CeO}_2$ samples. The results show that Si-MCM-41 is inactive, whereas Ce-Ex-MCM-41, Ce-Im-MCM-41 and $\text{SiO}_2\text{-CeO}_2$ are less active than the corresponding Ce-MCM-41 samples. The inactivity of Si-MCM-41 sample suggests that Ce^{4+} ions are responsible for the activity. This is also confirmed by an increasing trend on the conversion of 1-naphthol with increase in Ce content of the Ce-MCM-41 samples (Table 4.8 and 4.9). However, the higher activity of Ce-MCM-41 than the corresponding Ce-Ex-MCM-41, Ce-Im-MCM-41 and $\text{SiO}_2\text{-CeO}_2$ samples may be attributed to considering the presence of highly dispersed tetra-coordinated Ce^{4+} ions in the ordered silica network of Ce-MCM-41 compared to Ce-Ex-MCM-41, Ce-Im-MCM-41 and $\text{SiO}_2\text{-CeO}_2$ samples. It has been observed that 1-naphthol conversion as well as the peroxide selectivity is slightly higher for TBHP than H_2O_2 . The major product in the hydroxylation of 1-naphthol, using both H_2O_2 and TBHP, is 1,4-naphthoquinone.

Table 4.7
Comparison of the catalytic activity and selectivity of V-MCM-41-S, V-MCM-41-P and Ti-MCM-41-P samples
in the hydroxylation of 1-naphthol^f

Sample	Oxidant	1-Naphthol conversion (mol.%)	Peroxide selectivity (mol.%)	TOF (h ⁻¹) ^b	Product distribution (mol.%) ^c			
					1,2-DHN	1,4-DHN	1,2-NQ	1,4-NQ
V-MCM-41-S (50)	H ₂ O ₂	7.1	52.7	1.6	2.9	11.6	3.1	82.4
	TBHP	9.5	68.1	2.0	3.4	17.4	2.1	77.1
V-MCM-41-P (50)	H ₂ O ₂	7.2	53.1	1.5	2.8	12.8	3.1	81.3
	TBHP	9.6	69.4	2.0	3.6	15.7	2.2	78.5
Ti-MCM-41-P (50)	H ₂ O ₂	4.1	27.7	0.6	7.6	23.6	3.1	65.7
	TBHP	7.7	52.7	1.2	7.2	21.8	2.7	68.3

^a Reaction conditions: 1-naphthol = 1.44 g; 1-naphthol/H₂O₂ or TBHP (mol/mol) = 4; catalyst = 20 wt% of the substrate (1-naphthol); solvent (acetonitrile)/1-naphthol (wt/wt) = 5; temperature = 353 K; reaction time = 12 h.

^b Turn over frequency (TOF) = moles of peroxide (H₂O₂ or TBHP) converted for producing products per mole of V or Ti per hour.

^c 1,2-DHN = 1,2-Dihydroxynaphthalene, 1,4-DHN = 1,4-dihydroxynaphthalene, 1,2-NQ = 1,2-naphthoquinone and 1,4-NQ = 1,4-naphthoquinone.

Table 4.8
Activity of the Ce-MCM-41 samples in the hydroxylation of 1-naphthol with H₂O₂^a

Sample	1-Naphthol conversion (mol.%)	H ₂ O ₂ selectivity (mol.%)	TOF (h ⁻¹) ^b	Product distribution (mol.%) ^c			
				1,2-DHN	1,4-DHN	1,2-NQ	1,4-NQ
Si-MCM-41							
Ce-MCM-41-R (160)	5.2	9.7	0.68	3.7	9.6	1.7	85.0
Ce-MCM-41-R (80)	6.6	12.2	0.44	4.3	11.5	1.4	82.8
Ce-MCM-41-R (40)	8.9	16.3	0.31	4.5	12.7	1.2	81.6
Ce-MCM-41-A (40)	7.2	13.1	0.25	4.5	12.9	1.0	81.6
Ce-MCM-41-P (40)	7.5	13.7	0.26	4.6	12.7	1.3	81.4
Ce-MCM-41-R (20)	9.0	16.3	0.17	4.7	13.7	0.9	80.7
Ce-Ex-MCM-41	1.4	2.2	0.03	14.4	25.3	0.8	59.5
Ce-Im-MCM-41 (20)	1.1	1.7	0.02	15.1	26.7	0.5	57.7
SiO ₂ -CeO ₂ (20)	1.0	1.6	0.02	16.2	28.5	0.4	54.9

^a Reaction conditions: 1-naphthol = 1.44 g; 1-naphthol/H₂O₂ (mol/mol) = 4; catalyst = 20 wt% of the substrate (1-naphthol); solvent (acetonitrile)/1-naphthol (wt/wt) = 5; temperature = 353 K; reaction time = 12 h.

^b Turn over frequency (TOF) = moles of H₂O₂ converted for producing products per mole of Ce per hour.

^c 1,2-DHN = 1,2-Dihydroxynaphthalene, 1,4-DHN = 1,4-dihydroxynaphthalene, 1,2-NQ = 1,2-naphthoquinone and 1,4-NQ = 1,4-naphthoquinone.

Table 4.9
Activity of the Ce-MCM-41 samples in the hydroxylation of 1-naphthol with *tert*-butyl hydroperoxide (TBHP)^a

Sample	1-Naphthol conversion (mol.%)	TBHP selectivity (mol%)	TOF (h ⁻¹) ^b	Product distribution (mol.%) ^f			
				1,2-DHN	1,4-DHN	1,2-NQ	1,4-NQ
Si-MCM-41		No detectable activity					
Ce-MCM-41-R (160)	5.5	10.1	0.71	3.8	12.9	1.6	81.7
Ce-MCM-41-R (80)	7.1	12.9	0.47	4.2	14.5	1.3	80.0
Ce-MCM-41-R (40)	9.7	17.4	0.33	4.7	15.8	1.1	78.4
Ce-MCM-41-A (40)	8.2	14.8	0.28	4.6	15.5	1.2	78.7
Ce-MCM-41-P (40)	8.6	15.4	0.29	4.8	15.9	1.0	78.3
Ce-MCM-41-R (20)	9.8	17.5	0.18	5.2	16.7	0.9	77.2
Ce-Ex-MCM-41	2.1	3.3	0.04	14.6	25.6	0.6	59.2
Ce-Im-MCM-41 (20)	1.8	2.8	0.03	15.4	27.0	0.5	57.1
SiO ₂ -CeO ₂ (20)	1.4	2.2	0.03	16.1	26.8	0.4	56.7

^a Reaction conditions: 1-naphthol = 1.44 g; 1-naphthol/TBHP (mol/mol) = 4; catalyst = 20 wt% of the substrate (1-naphthol); solvent (acetonitrile)/1-naphthol (wt/wt) = 5; temperature = 353 K; reaction time = 12 h.

^b Turn over frequency (TOF) = moles of H₂O₂ converted for producing products per mole of Ce per hour.

^c 1,2-DHN = 1,2-Dihydroxynaphthalene, 1,4-DHN = 1,4-dihydroxynaphthalene, 1,2-NQ = 1,2-naphthoquinone and 1,4-NQ = 1,4-naphthoquinone.

4.1.3.2. Epoxidation Reactions

4.1.3.2.1. Epoxidation of Cyclohexene over Ti-MCM-41 and V-MCM-41

The epoxidation of cyclohexene was carried out using Ti-MCM-41 and V-MCM-41 samples and the results were compared as shown in Table 4.10. The catalytic activity and selectivity of two Ti-MCM-41 samples prepared with and without using promoter, are very much similar which also indicate that the Ti species must be quite similar on these two catalysts. Comparable conversion was obtained over V-MCM-41-P sample also. Cyclohexene oxide was the dominating product when *tert*-butyl hydroperoxide (TBHP) was used as oxidant. The hydrolyzed (diol) and allylic oxidation products (cyclohexenol + cyclohexenone) were the major products when aqueous H₂O₂ was used. In the presence of urea-hydrogen peroxide (UHP), the formation of secondary product (cyclohexane diol) was suppressed. However, allylic oxidation was still quite high. In the presence of aqueous H₂O₂, the selectivity of cyclohexene oxide was significantly low mainly due to its hydrolysis to produce cyclohexanediol. Similar trend was also obtained when V-MCM-41-P sample was used for the epoxidation of cyclohexene with aqueous H₂O₂, UHP and TBHP. However, over V-MCM-41 (*vis-à-vis* Ti-MCM-41) higher selectivity for allylic oxidation products was observed.

After finding out significant difference in the cyclohexene oxide selectivity in the case of Ti-MCM-41 when UHP was used as oxidizing agent compared to aqueous H₂O₂, it was considered to be interesting to compare the epoxidation behavior of TS-1 and TS-2 with different sources of hydrogen peroxide (HP, U+HP, and UHP) as oxidants. TS-1 and TS-2 were chosen for the detailed study of the effect of different sources of H₂O₂ mainly because these are well-studied catalysts in oxidation in general, and in epoxidation in particular, using aqueous H₂O₂.³⁻⁵ Further, the nature of active sites in TS-1 and TS-2 are relatively better understood. Since H₂O has a strong affinity to coordinate with the tetra-coordinated Ti

species and generate acid centers particularly in the presence of hydrogen peroxide, it is of great importance from the catalytic point of view to carry out the reaction using anhydrous oxidants (e.g. UHP) to reduce isomerization and hydrolysis of the desired epoxide in the epoxidation reactions.⁶⁻⁸

Table 4.10
Comparison of the catalytic activity and selectivity of Ti-MCM-41-S, Ti-MCM-41-P and V-MCM-P samples in the epoxidation of cyclohexene^a

Sample	Oxidant ^b	CX conv. (mol.%) ^f	TOF (h ⁻¹) ^d	Product distribution (mol.%) ^e		
				CO	C-OL	Others ^f
Ti-MCM-41-S (50)	H ₂ O ₂	12.4	0.5	9	38	53
	UHP	26.8	1.1	46	14	40
	TBHP	58.0	2.3	91	4	5
Ti-MCM-41-P (50)	H ₂ O ₂	13.6	0.6	11	41	48
	UHP	26.0	1.0	51	12	37
	TBHP	58.8	2.4	88	6	6
V-MCM-41-P (50)	H ₂ O ₂	10.4	0.5	8	38	54
	UHP	26.4	1.3	38	15	47
	TBHP	42.4	2.1	61	12	27

^a Reaction conditions: cyclohexene = 0.82 g; cyclohexene/H₂O₂, UHP or TBHP (mol/mol) = 4; catalyst = 20 wt% of the substrate (cyclohexene); solvent (acetone)/cyclohexene (wt/wt) = 5; temperature = 323 K; reaction time = 12 h.

^b In the case of UHP, the reaction was carried out at 313 K.

^c (Cyclohexene(CX) conversion/theoretically possible cyclohexene conversion) × 100.

^d Turn over frequency (TOF) = moles of peroxide (H₂O₂, UHP or TBHP) converted for producing products per mole of Ti per hour.

^e CO = cyclohexene oxide and C-OL = cyclohexanediol

^f Includes cyclohexenol, cyclohexenone and high boiling compounds.

4.1.3.2.2. Epoxidation of Styrene and Allylbenzene over TS-1 and TS-2

The effect of different sources of the oxidizing agent (H_2O_2) on the styrene conversion (mol.%) and product selectivity (mol.%) using TS-1 and TS-2 as catalysts is given in Table 4.11, for comparative purpose. It is observed that for both catalysts, TS-1 and TS-2, the styrene conversion as well as the selectivity for the desired epoxide increases when instead of aqueous hydrogen peroxide (HP), the anhydrous solid urea-hydrogen peroxide adduct (UHP) is used as the oxidant. In the case of U+HP system, where urea and aqueous hydrogen peroxide solution (45 wt.%) were added separately, both the conversion and the selectivity of the desired epoxide was found to be slightly lower compared to solid UHP system and significantly higher in comparison to aqueous hydrogen peroxide system. Probably, the urea not only acts as a dehydrating agent but also as a buffer for the system, which prevents further isomerization and hydrolysis of the desired epoxide. It has been noticed that considerable amount of benzaldehyde (29 mol.%) is also produced during styrene epoxidation using aqueous H_2O_2 as the oxidizing agent and TS-1/TS-2 as the redox catalysts.^{9,10} Probably, the cleavage of highly reactive benzylic C=C double bond in styrene is capable of producing benzaldehyde via a radical type of transformation. In the case of U+HP (where urea-hydrogen peroxide adduct is prepared *in situ*) and UHP systems, *anhydrous* H_2O_2 is released into the solution in a controlled manner and therefore excess oxidizing agent is not present in the reaction system, which in turn minimizes the formation of benzaldehyde.

If this is so, one could expect to control the formation of benzaldehyde by adding aqueous H_2O_2 very slowly over the period of time (8 h) through a mechanical syringe pump. Indeed, the result obtained in the case of TS-1/HP system shows a considerable decrease in the formation of benzaldehyde (15 mol.% versus 30 mol%). However, the selectivity of styrene oxide (8 mol.%) is merely increased because of its isomerization into phenylacetaldehyde (57 mol.%) in the presence of highly polar water. Although statistically, acetophenone is also

expected to be produced due to isomerization of styrene oxide, very high regioselectivity towards the formation of phenylacetaldehyde may be explained on the basis of stabilization of benzylic carbinium ion formed during rearrangement.

Table 4.11
Effect of different oxidants on epoxidation of styrene and allylbenzene over TS-1 and TS-2^a

Substrate	Catalyst	Oxidant	Conversion (mol %) ^b	TOF (h ⁻¹) ^c	Product distribution (mol%) ^d			
					EP	PAD	BD	DIOLS
Styrene	TS-1	HP	56	1.1	5	44	29	22
		U+HP	65	1.3	81	8	7	4
		UHP	71	1.4	87	5	7	1
	TS-2	HP	57	1.2	7	42	28	23
		U+HP	62	1.3	80	8	8	4
		UHP	67	1.4	85	6	7	2
Allylbenzene	TS-1	HP	60	1.1	58	-	-	42
		U+HP	68	1.2	95	-	-	5
		UHP	70	1.2	98	-	-	2

^a *Reaction conditions*: Substrate : Oxidant (mol/mol) = 4.0; Solvent = Acetone; Substrate : Acetone (wt/wt) = 1.0; Reaction time (h) = 12; Catalyst wt. = 20 wt% of the substrate; T = 313 K; ^b (Styrene or allylbenzene conversion/theoretically possible maximum conversion) × 100. ^c Turn over frequency (TOF) = moles of H₂O₂ converted for producing epoxides + secondary products per mole of Ti per h.; ^d EP = Epoxy allylbenzene and styrene oxide, PAD = phenylacetaldehyde, BD = benzaldehyde and DIOLS = 3-Phenyl-1,2-propanediol and styrene diol including some high boiling products.

Very high epoxide selectivity for allylbenzene (having an allylic C=C double bond) in comparison with styrene (having a benzylic C=C double bond) is obtained using UHP. These results (Table 4.11) also corroborate the above explanation in view of the results obtained for different epoxidation reactions.

The graphic profile of temperature dependence on styrene epoxidation over TS-1 (Figure 4.3) shows that in the case of both U+HP and UHP systems, the styrene conversion first increases (273-313 K), reaches a maximum level at 313 K and then decreases with increase in temperature (313-353 K). In the case of HP system, although initially the reaction was slow, the maximum conversion was higher compared to that in the case of U+HP and UHP systems at higher temperature (>313 K) without any decrease in the conversion. At higher temperature (>313 K), the stability of solid urea-hydrogen peroxide adduct decreases and therefore, the decomposition of hydrogen peroxide becomes more competitive than the desired epoxidation. However, in the case of HP system, in which aqueous hydrogen peroxide is stabilized by hydrogen bonding, the decomposition of hydrogen peroxide is rather low particularly at higher temperature (>313 K). In that case, the styrene conversion increases with increasing temperature. The selectivity of styrene oxide and benzaldehyde + phenylacetaldehyde is plotted in Figure 4.3B, for all the three systems. In all the cases, upon increasing the temperature from 273 K to 353 K, the selectivity of undesired secondary/side products increases at the expense of styrene oxide. However, at all reaction temperatures, the styrene oxide selectivity was quite high in the case of UHP and U+HP (70-90%), while in the case of HP system, the same was very low (5-10%).

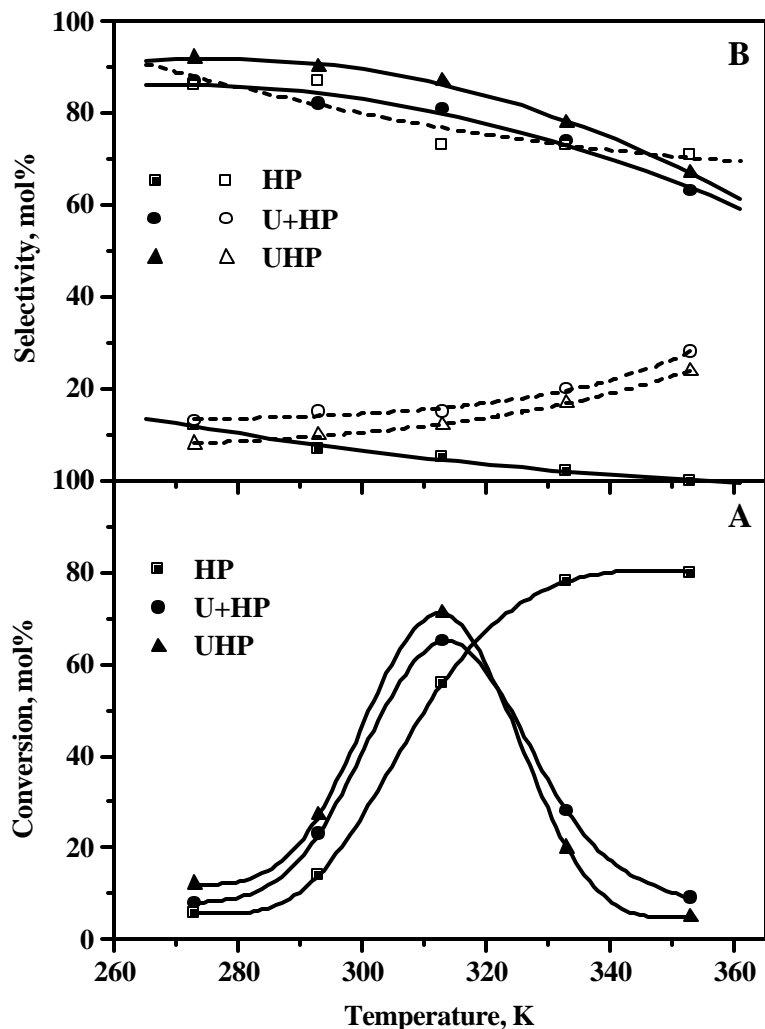


Figure 4.3 Effect of reaction temperature on the epoxidation of styrene. Reaction conditions: Catalyst TS-1 (20 wt% with respect to styrene); styrene : H₂O₂ (mol/mol) = 4.0; styrene : acetone (wt/wt) = 1.0; reaction time = 12 h. (A) Comparison of styrene conversion with different H₂O₂ sources: (■) HP, (●) U+HP, and (▲) UHP. (B) Comparison of selectivities for styrene oxide (solid symbol) and benzaldehyde + phenylacetaldehyde (open symbol) with different H₂O₂ sources: (□) HP, (○) U+HP, and (△) UHP.

In the Figure 4.4, styrene conversion is plotted as a function of reaction time over TS-1 at 313 K. In the three systems, HP, U+HP and UHP, the reaction proceeds in a similar fashion with time in the order : UHP>U+HP>HP. The reaction is fast at the beginning, since the total

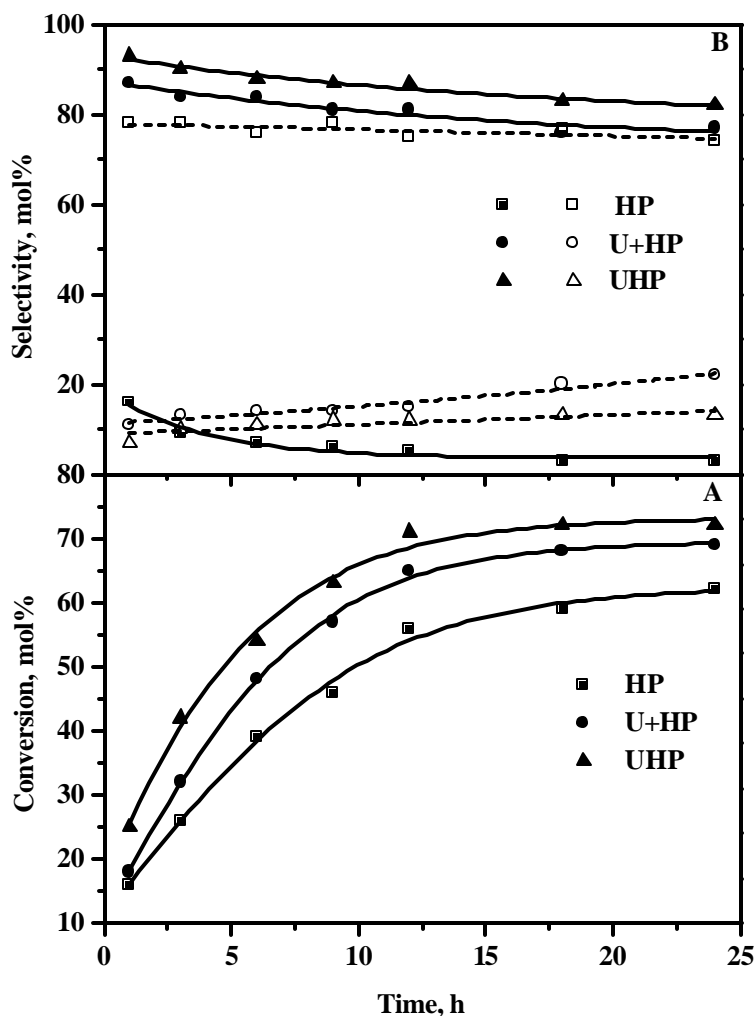


Figure 4.4 Effect of reaction time on the epoxidation of styrene. Reaction conditions: Temperature = 313 K; catalyst TS-1 (20 wt% with respect to styrene); styrene : H₂O₂ (mol/mol) = 4.0; styrene : acetone (wt/wt) = 1.0. (A) Comparison of styrene conversion with different H₂O₂ sources: (□) HP, (●) U+HP, and (▲) UHP. (B) Comparison of selectivities for styrene oxide (solid symbol) and benzaldehyde + phenylacetaldehyde (open symbol) with different H₂O₂ sources: (□) HP, (●) U+HP, and (▲) UHP.

amount of oxidant was added in one lot at the beginning of the reaction. The conversion for the reaction reaches a maximum level at *ca.* 12 h. However, as the hydrogen peroxide added becomes more and more anhydrous in nature (HP < U+HP < UHP), the conversion level

increases. Figure 4.4B depicts the selectivities of styrene oxide and benzaldehyde + phenylacetaldehyde plotted against reaction time for the three different systems over TS-1.

The effect of styrene/UHP mole ratio on the styrene conversion and the product selectivity over TS-1 is shown in Figure 4.5. The styrene conversion increases with the increase in styrene/UHP mole ratio mainly due to increased H_2O_2 utilization for styrene oxidation. However, the selectivity of styrene oxide increases very slowly over the range. It is also observed that the concentrations of phenylacetaldehyde + benzaldehyde are remaining unchanged with the increase of styrene/UHP molar ratio.

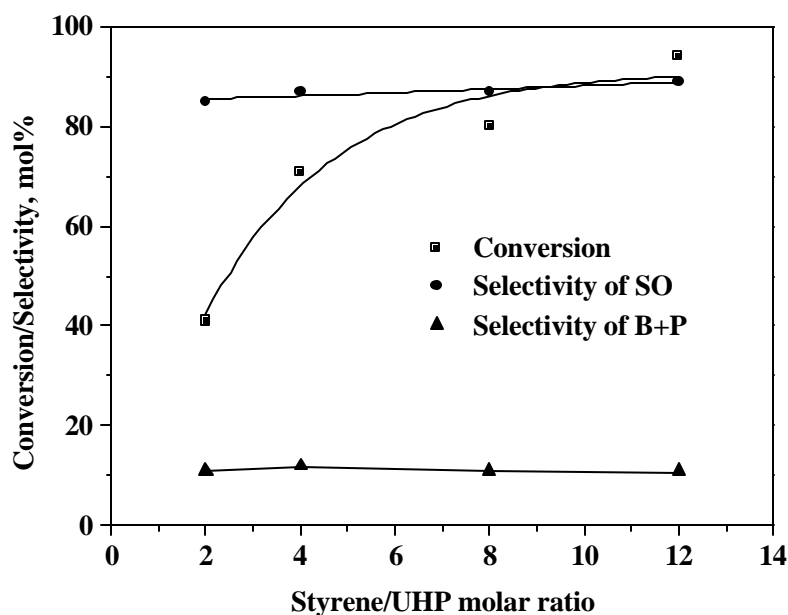


Figure 4.5 Effect of styrene to H_2O_2 molar ratios on the epoxidation of styrene. Reaction conditions: Temperature = 313 K; catalyst TS-1 (20 wt% with respect to styrene); styrene : acetone (wt/wt) = 1.0; reaction time = 12 h. (□) Styrene conversion, (●) styrene oxide (SO) selectivity and (▲) benzaldehyde + phenylacetaldehyde (B + P) selectivity.

Table 4.12 discusses the effect of solvent on styrene epoxidation over TS-1/UHP system. As expected, in aprotic solvents like acetone and acetonitrile, the product selectivity is higher

than in protic solvent like methanol. In methanol, the concentrations of secondary products (phenylacetaldehyde, benzaldehyde and styrene diol) are higher compared to acetone and acetonitrile. Still, the selectivity of the desired styrene oxide (~ 72%) is quite high in methanol due to anhydrous reaction conditions.

Table 4.12
Effect of solvent on epoxidation of styrene with UHP over TS-1^{a, b}

Solvent	Styrene conv. (mol %)	TOF (h ⁻¹)	Product distribution (mol%)			
			Styrene oxide	Ph-CH ₂ -CHO	Ph-CHO	Others
Acetone	71	1.4	87	5	7	1
Acetonitrile	51	1.0	82	7	6	5
Methanol	54	1.1	72	11	9	8

^a *Reaction conditions*: Catalyst wt = 0.416 g; T = 313 K; Styrene: UHP (mol/mol) = 4.0; Styrene: solvent (wt/wt) = 1.0; Reaction time = 12 h. ^b Also see Table 4.11.

Figure 4.6 illustrates the effect of solvent (acetone) concentration on styrene conversion and styrene oxide selectivity over TS-1. Upon increasing the acetone/styrene wt. ratio, the selectivity of styrene oxide increases, at the expense of secondary products indicating that in concentrated reaction mixture, the secondary reactions are facilitated. However, styrene conversion decreases with increase in acetone/styrene wt. ratio. Here, it will be pertinent to mention that although the substrate to catalyst ratio was the same in these experiments, catalyst concentrations with respect to total reaction volume was changed considerably.

Figure 4.7 depicts the effect of catalyst concentration on styrene epoxidation over TS-1. It is observed that increase in the catalyst concentration (with respect to styrene) resulted in an increase in the styrene conversion initially before leveling off at *ca.* 70 ± 5 mol.%. Styrene

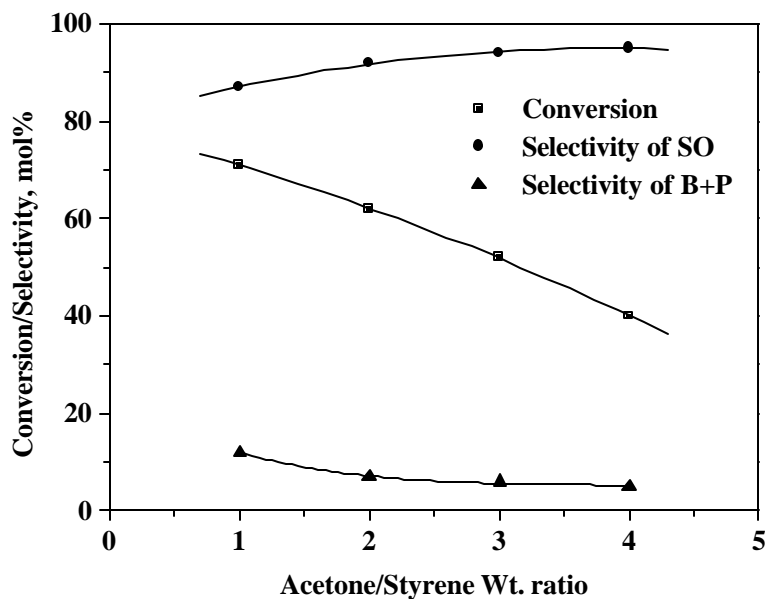


Figure 4.6 Effect of acetone to styrene weight ratios on the epoxidation of styrene. Reaction conditions: Temperature = 313 K; catalyst TS-1 (20 wt% with respect to styrene); styrene : H_2O_2 (mol/mol) = 4.0; reaction time = 12 h. (□) Styrene conversion, (●) styrene oxide (SO) selectivity and (▲) benzaldehyde + phenylacetaldehyde (B + P) selectivity.

oxide selectivity also increases with increase in catalyst concentration before reaching a limiting value of 85 ± 5 mol.%. As expected, at low catalyst concentration, the concentration of Ti-superoxo complex is low and therefore, secondary reactions are facilitated. With the increase in the catalyst concentration, the concentration of Ti-superoxo complex also increases which facilitates the formation of desired styrene oxide inside the zeolitic pore.

The addition of urea has significant effect on the selectivity of the epoxide. This motivated us to carry out epoxidation of styrene over TS-1 with aqueous H_2O_2 in the presence of varying amount of urea separately added to the reaction mixture. The results obtained are plotted as a function of urea/hydrogen peroxide mole ratio in Figure 4.8. The styrene conversion first increases steadily, and then it reaches a limiting value of 65 ± 2

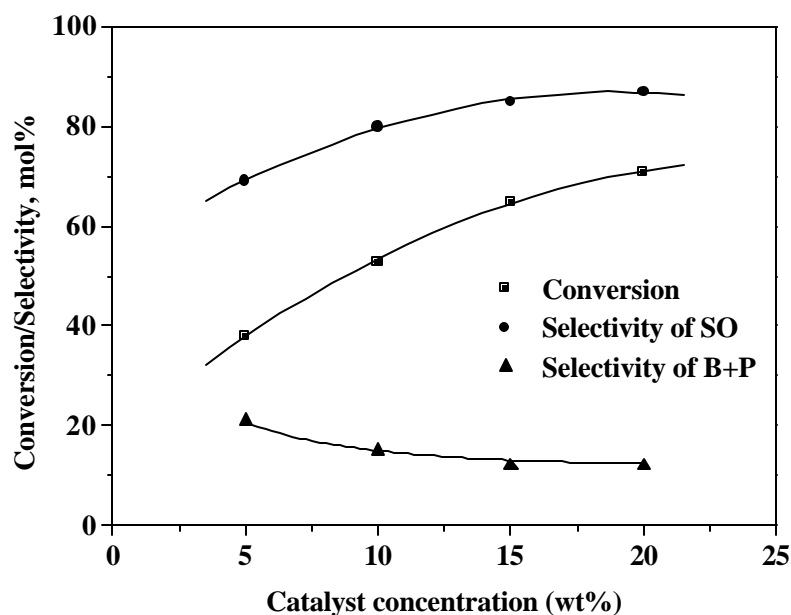


Figure 4.7 Effect of catalyst concentration on the epoxidation of styrene. Reaction conditions: Temperature = 313 K; styrene : H_2O_2 (mol/mol) = 4.0; styrene : acetone (wt/wt) = 1.0; reaction time = 12 h. (□) Styrene conversion, (●) styrene oxide (SO) selectivity and (▲) benzaldehyde + phenylacetaldehyde (B + P) selectivity.

mol.%, when urea/hydrogen peroxide molar ratio becomes ≥ 1 . The selectivity of styrene oxide increases considerably from 5 (urea/ H_2O_2 = 0.0) to 61 mol.% (urea/ H_2O_2 = 0.25) by the addition of little amount of urea which indicates the importance of its presence in the reaction mixture. Further increase in the urea/ H_2O_2 molar ratio, also increases the styrene oxide selectivity before leveling off at *ca.* 82 ± 3 mol.%. On the contrary, the selectivity of benzaldehyde + phenylacetaldehyde decreases drastically by the addition of little amount of urea and reaches a limiting value of 15 ± 3 mol.%, when urea/hydrogen peroxide molar ratio becomes ≥ 1 .

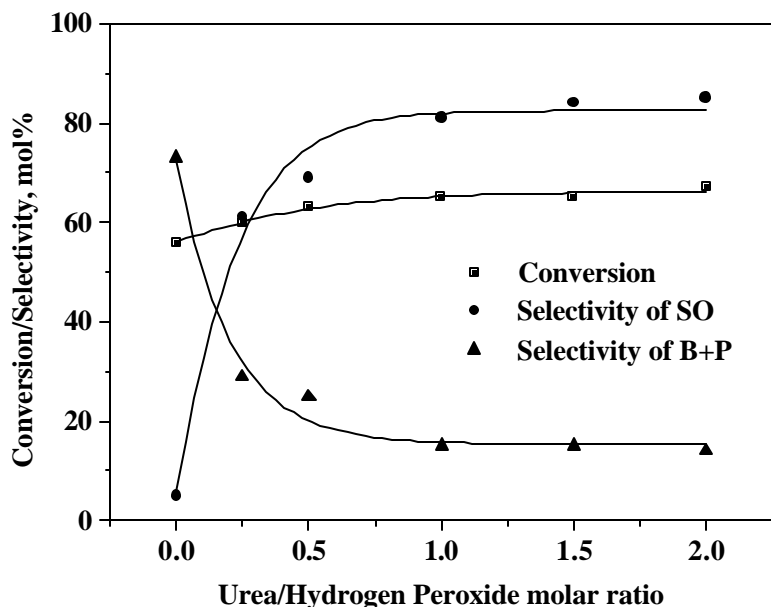


Figure 4.8 Effect of urea to H_2O_2 molar ratios on the epoxidation of styrene. Reaction conditions: Temperature = 313 K; catalyst TS-1 (20 wt% with respect to styrene); styrene : H_2O_2 (mol/mol) = 4.0; styrene : acetone (wt/wt) = 1.0; reaction time = 12 h. (□) Styrene conversion, (●) styrene oxide (SO) selectivity and (▲) benzaldehyde + phenylacetaldehyde (B + P) selectivity.

4.1.3.2.3. Epoxidation of Allyl alcohol, Allyl chloride, Allyl bromide and Methylallyl chloride over TS-1

Table 4.13 shows the effect on the activity and selectivity for the epoxidation of different allylic compounds using TS-1 as solid redox catalyst and different H_2O_2 sources as oxidants. The results (Table 4.13) clearly show that the epoxide selectivity exhibited by three oxidants decreases in the order : UHP > U+HP > HP. It is observed that the conversion as well as the selectivity for the three allylic substrates increases in the order : allyl alcohol < allyl chloride < allyl bromide. This is mainly due to the decrease in the electronegative character of the three electron withdrawing groups (OH > Cl > Br) present in the three allylic substrates¹¹ and

Table 4.13
Effect of different oxidants on epoxidation of allyl alcohol, allyl chloride, allyl bromide and methylallyl chloride over TS-1^a

Substrate	Oxidant ^b	Conversion (mol %) ^c	TOF (h ⁻¹) ^d	Product distribution (mol.%)	
				Epoxide	Diof ^e
Allyl alcohol	HP	66	4.7	84	11 ^f
	U+HP	72	5.2	90	10
	UHP	74	5.3	98	2
Allyl chloride	HP	95	5.2	87	13
	U+HP	95	5.2	92	8
	UHP	96	5.2	97	3
Allyl bromide	HP	94	3.2	87	14
	U+HP	95	3.3	94	7
	UHP	97	3.3	98	2
Methylallyl chloride	HP	64	2.9	76	24
	U+HP	71	3.3	92	8
	UHP	74	3.4	94	6

^a *Reaction conditions*: Substrate : Oxidant (mol/mol) = 2.0; Solvent = Methanol; Substrate : Methanol (wt/wt) = 3.0; Reaction time (h) = 8; Catalyst wt. = 20 wt.% of the substrate; T = 313 K; ^b HP = Hydrogen peroxide (45 wt.%); U+HP = Urea and hydrogen peroxide mixture (1: 1, mole ratio); UHP = Urea-hydrogen peroxide adduct. ^c (Conversion/theoretically possible conversion) × 100. ^d Turn over number (TON) = moles of H₂O₂ converted for producing epoxide + secondary products per mole of Ti. ^e Mostly the corresponding diols including some high boiling products. ^f Remaining 5 mol.% is acrolein.

therefore, the C=C double bond becomes much more localized (electron rich) and also accessible for the epoxidation which accounts for the increasing trend in the conversion. Similarly, the increase in the selectivity stands for the increased hydrophobic character of the allylic molecules. However, higher activity of allyl chloride vis-à-vis methylallyl chloride, also observed earlier using aqueous H₂O₂, in contrast to the homogeneous systems,^{11,12} is probably a manifestation of the reactant shape selectivity exhibited by TS-1 in retarding the diffusion of bulkier methylallyl chloride vis-à-vis allyl chloride to the active Ti centers located inside the channel system.

4.1.3.2.4. Epoxidation of 1-Hexene and Cyclohexene over TS-1 and TS-2

Effect of different oxidants (HP, U+HP and UHP) on the epoxidation of 1-hexene and cyclohexene is demonstrated in Table 4.14. In the case of TS-1 and TS-2 molecular sieves used as catalyst for the cyclohexene epoxidation (Table 4.14), it is clear that if one takes into account the pore diameters and hydrophobic character of the TS-1 and TS-2 catalysts, one should expect some what similar intrinsic activity and selectivity for the epoxide in both the cases, as it is observed experimentally. It is observed that the selectivity of both 1,2-epoxyhexane and cyclohexene oxide are very low in aqueous hydrogen peroxide in comparison with the allylic substrates (Table 4.13 and 4.14). This difference may be attributed to increasing diffusional constraints for relatively bulky molecules (e.g. 1-hexene vs. cyclohexene). Further, slower diffusion of bulkier epoxides than that of substrates from the Ti-sites of TS-1 and TS-2 may result in consecutive hydrolysis of epoxides to the corresponding diols due to increased residence time of the former on the active sites. In the case of smaller allylic substrates, such diffusional limitation is expected to be very low and therefore, the desorption of the product (epoxide) from the active Ti-sites will be faster and hence, the cleavage of oxirane ring is very low leading to high epoxide selectivity even in the case of HP. The low conversion for both the substrates may also be attributed to diffusional

restriction of comparatively bulky molecules,⁵ which may face increased diffusional resistance through the pores of MFI and MEL structures.

Table 4.14
Effect of different oxidants on epoxidation of 1-hexene and cyclohexene over TS-1 and TS-2^{a, b}

Substrate	Catalyst	Oxidant	Conversion (mol %)	TOF (h ⁻¹)	Product distribution (mol.%) ^c			
					EP	OL	ONE	DIOLS
1-Hexene	TS-1	HP	35	0.87	29	-	-	71
		U+HP	42	1.04	94	-	-	6
		UHP	47	1.17	98	-	-	2
Cyclohexene	TS-1	HP	38	0.97	21	2	8	69
		U+HP	41	1.04	96	-	-	4
		UHP	45	1.14	99	-	-	1
	TS-2	HP	40	1.01	26	2	10	62
		U+HP	42	1.06	94	-	-	6
		UHP	44	1.11	98	-	-	2

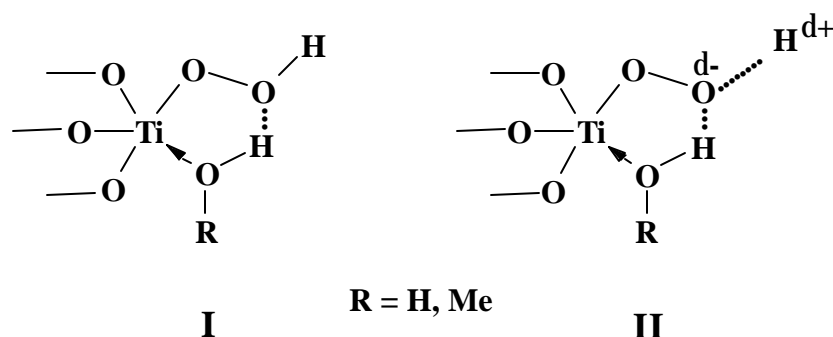
^a *Reaction conditions*: Substrate : Oxidant (mol/mol) = 4.0; Solvent = Methanol; Substrate : Methanol (wt/wt) = 1.0; Reaction time (h) = 12; Catalyst wt. = 20 wt.% of the substrate; T = 313 K; ^b See also Table 4.3; ^c EP = 1,2-Epoxyhexane and cyclohexene oxide; OL = Cyclohexeneol; ONE = Cyclohexenone; DIOLS = 1,2-Hexanediol and mixture of *cis/trans*-1,2-cyclohexanediols.

In the presence of aqueous H₂O₂, allylic oxidation of cyclohexene (~10 mol%) occurs at the α -carbon of the C=C double bond to produce undesired cyclohexenol which then further oxidized to more stable cyclohexenone via radical type mechanism. However, in U+HP and

UHP systems, neither cyclohexenol nor cyclohexenone were produced in detectable quantity, mainly due to the anhydrous nature of the oxidizing agents. As expected, it is observed that the 1-hexene and cyclohexene conversion as well as the selectivity for epoxides increases as the hydrogen peroxide becomes more and more anhydrous in nature (HP <U+HP <UHP).

4.1.3.2.5. Explanation for high epoxide selectivity over titano-silicates/U+HP or UHP systems

It has been reported that the presence of protic solvents with high degree of polarity (e.g. water, alcohols etc.) generates acidity on active Ti-centers in titanium-silicate molecular sieves leading to the formation of corresponding isomerized and hydrolyzed secondary products particularly for epoxidation reactions. These types of phenomena are not only observed for TS-1 and TS-2,¹³ but also for other silica based Ti containing catalysts e.g. Ti β ,¹⁴ Ti-MCM-41¹⁵ etc. The Ti-OOH species formed by the interaction between framework Ti atom and H₂O₂ molecule, is able to form a stable five membered cyclic structure with a donor hydroxyl moiety coordinated on titanium (species I) as shown in Scheme 4.1. The enhanced acid strength may be generated in charge-separated species (species II) due to greater hydrogen bonding. The acid centers (species I and II) are able to catalyze the epoxide ring opening. When aqueous H₂O₂ is used as oxidant for epoxidation reaction, the selectivity of



Scheme 4.1 Different cyclic Ti-species active for epoxidation reactions.

the desired epoxide was poor mainly because of its isomerization and hydrolysis to form hydrolyzed and cleaved products, catalyzed by the acid centers generated on Ti-containing molecular sieves. However, in the case of U+HP system, the selectivity of epoxide increases considerably. This is mainly due to the presence of urea, which acts as a dehydrating agent as well as buffer for the system and thereby reduces the acid catalyzed isomerization and cleavage of the desired epoxide. Expectedly, maximum selectivity of epoxide is achieved in case of UHP system because of the absence of water in the reaction mixture. Still, the formation of water molecules in the vicinity of active Ti-centers due to consumption of H_2O_2 during epoxidation reaction causes some epoxide ring opening leads to isomerized product. In methanol, the selectivity of styrene oxide over TS-1 is less compared to that in other solvents (acetone and acetonitrile) also because of the same acid catalyzed isomerization of the epoxide.^{7,8}

4.3. REFERENCES

1. Greene, T. W., and Wuts, P. G. M., *Protective Groups in Organic Synthesis*, 2nd Edition, Wiley, New York, 1991.
2. Choudary, B. M., Bhaskar, V., Kantam, M. L., Rao, K. K., and Raghavan, K. V., *Green Chem.*, **67** (2000).
3. Notari, B., *Stud. Surf. Sci. Catal.* **37**, 413 (1987).
4. Kumar, P., Kumar, R., and Pandey, B., *Synlett* 289 (1995).
5. Arends, I. W. C. E., Sheldon, R. A., Wallau, M., and Schuchardt, U., *Angew. Chem. Int. Ed. Engl.* **36**, 1144 (1997).
6. Adam, W., Kumar, R., Reddy, T. I., and Renz, M., *Angew. Chem. Int. Ed. Engl.* **35**, 880 (1996).
7. Laha, S. C., and Kumar, R., *J. Catal.* **204**, 64 (2001).
8. Laha, S. C., and Kumar, R., *J. Catal.* (in press).
9. Neri, C., and Buonomo, F., *Eur. Pat* 0 102 097 (1984).
10. Kumar, S. B., Mirajkar, S. P., Pais, G. C. G., Kumar P., and Kumar, R., *J. Catal.* **156**, 163 (1995).
11. Bhaumik, A., Kumar, R., and Ratnasamy, P., *Stud. Surf. Sci. Catal.* **84**, 1883 (1994).
12. Mimoum, H., Saussine, L., Daire, E., Postel, M., Fishcher, R., and Weiss, R., *J. Am. Chem. Soc.* **105**, 3101 (1983).
13. Bellussi, G., Carati, A., Clerici, M. G., Maddinelli, G., and Millini, R., *J. Catal.* **133**, 220 (1992).
14. Cambor, M. A., Costantini, M., Corma, A., Gilbert, L., Esteve, P., Martinez, A., and Valencia, S., *Chem. Commun.*, 1339 (1996).
15. Blasco, T., Corma, A., Navarro, M. T., and Pariente, J. P., *J. Catal.* **156**, 65 (1995).

CHAPTER 5
SUMMARY
AND
CONCLUSIONS

The present thesis gives an account of synthesis, characterization and catalytic applications of mesoporous metallo-silicate and organo-silicate molecular sieve materials. Microporous titano-silicates (TS-1 and TS-2) are also included for comparative purpose.

The *chapter one* provides general introduction to the salient features of microporous and mesoporous molecular sieves with particular emphasis on different synthesis routes and mechanisms proposed for the formation of mesoporous materials. The modified (metallo-silicate and organo-silicate) MCM-41, their synthesis and different physico-chemical characterization along with potential catalytic applications are briefly discussed. The scope and objectives of the present thesis is also briefly mentioned at the end of the chapter.

The *chapter two* gives the detailed description for synthesis of mesoporous silicate, metallo-silicate, and organo-silicate materials obtained in the presence and/or the absence of promoters. It also includes a brief description for the synthesis of TS-1 and TS-2.

The *Chapter three* presents a brief compilation of various spectroscopic (XRD, EDX, diffuse reflectance UV-Vis, FTIR, solid state MAS NMR and EPR), microscopic (SEM and TEM), volumetric (adsorption and surface area analysis), and thermogravimetric (TG-DTA) methods used to characterize the materials synthesized in the present study. The results of different physico-chemical characterization of various mesoporous and microporous materials are discussed in detail in this chapter.

The *chapter four* (Section 4.1.) describes the selective acid catalysis (isopropylation of naphthalene, dehydration of cyclohexanol and acylation of alcohols, phenols, amines and thiols) over AlMCM-41 and Ce-MCM-41 molecular sieves. Section 4.2. of this chapter deals with the selective oxidation catalysis (hydroxylation of 1-naphthol and epoxidation of different olefinic compounds) using Ti-MCM-41, V-MCM-41 and Ce-MCM-41 as well as TS-1 and TS-2 molecular sieves.

Conclusions :

Synthesis and Characterization

- The presence of catalytic amount of promoter oxyanions of group VA, VIA and VIIA, either in their acid or salt form, in the synthesis mixture of MCM-41 type mesoporous materials, reduces the synthesis time considerably. The results show that the effect is quite general and is applicable not only to Si-MCM-41 but also to Al-MCM-41, Ti-MCM-41 and V-MCM-41 materials. Promoters having higher polarizing ability ($Z/r, \text{\AA}^{-1}$) are more effective for the faster synthesis of MCM-41 materials. The materials characterized by different techniques show that the quality of materials obtained in the presence of promoter(s) were comparable with, if not better than, that of corresponding materials obtained in its absence.
- All the Ce-MCM-41 samples synthesized hydrothermally by different procedures are having very high surface area ($\geq 1000 \text{ m}^2\text{g}^{-1}$) with pore size of $\sim 3.0 \text{ nm}$. Evidences for the presence of Ce in the framework and/or walls of silica matrix were obtained from different spectroscopic, microscopic, volumetric and thermogravimetric characterization techniques. The absence of significant broadening of the ^{13}C signal of the CH_3 and CH_2 groups attached to N of the surfactant reveals the absence of a charged framework, suggesting the incorporation of Ce in its +4 oxidation state. Further, all the Ce-MCM-41 samples are EPR inactive, indicating the incorporation of Ce as Ce^{4+} ions and not as Ce^{3+} ions. Although, the FTIR spectra of chemisorbed pyridine shows only Lewis acid sites in Ce-MCM-41 samples, the same for chemisorbed ammonia shows the presence of very weak Brönsted acid sites also along with strong Lewis acid sites.
- The organo-functionalized MCM-41 materials synthesized by *in situ* as well as post synthesis method and characterized by spectroscopic (XRD, IR and MAS NMR), volumetric (surface area and pore size measurements) and chemical (Al, C, H, N and S)

methods suggest that well-ordered MCM-41 materials with intact organic functional groups anchored to the silica matrix of MCM-41 were prepared.

- Direct spectroscopic evidences for the formation of different Ti-superoxo complexes by the solid-solid interaction between Ti-MCM-41/TS-1/TS-2 and urea-hydrogen peroxide adduct were obtained from the characteristic continuous absorption band in the UV-Vis region (300-500 nm) and the anisotropic EPR spectra for the superoxide radical attached to Ti(IV) centers on different titano-silicates. In the presence of aqueous H₂O₂, however, the different EPR signals originating from non-equivalent Ti-environments seem to lose their inequality leading to the observation of two broad signals mainly due to the presence of water (coming from aqueous H₂O₂), which increases and/or equalizes the coordination number of different Ti-species during the formation of Ti-superoxo complexes.

Catalysis

- Comparable catalytic activities and product selectivities of Al-MCM-41 (in isopropylation of naphthalene by isopropanol) and Ti- and V-MCM-41 samples (in hydroxylation of 1-naphthol and epoxidation of cyclohexene using different peroxide sources e.g. aqueous H₂O₂, UHP and TBHP) prepared in the presence and the absence of promoters also indicate that the active Al-, Ti- and V-sites/species must be similar in nature present on these catalysts.
- Ce-MCM-41 samples show dual (acid as well as redox) catalytic properties. It is active as solid acid catalyst for the dehydration of cyclohexanol and chemoselective acylation of alcohols, amines and thiols including bulky steroidal molecules. Similarly, its activity towards the hydroxylation of bulky 1-naphthol shows its redox catalytic properties. Higher activity of Ce-MCM-41 samples in comparison to Ce-Ex-MCM-41, Ce-Im-MCM-41, and SiO₂-CeO₂ samples is indicative of the presence of highly dispersed tetra-coordinated Ce in Si-rich environments. Comparison of catalytic activity of Ce-MCM-41

with Lewis acidic Ti-MCM-41 and Zr-MCM-41 shows that Ce-MCM-41 is a better catalyst for chemoselective acylation reactions than the corresponding Ti- and Zr-analogues.

- A highly selective heterogeneous catalytic method for the preparation of epoxides from the corresponding olefins has been demonstrated using anhydrous urea-hydrogen peroxide adduct as the oxidizing agent in the presence of Ti-MCM-41, TS-1 and TS-2. A significant increase in the selectivity of the desired epoxides could be achieved when urea-hydrogen peroxide (UHP) and U+HP (urea and aqueous H₂O₂ added separately for the *in situ* formation of UHP) were used as oxidants instead of aqueous H₂O₂. The controlled release of *anhydrous* H₂O₂ from UHP is the main reason for enhanced epoxide selectivity. Urea present in UHP or added separately in aqueous hydrogen peroxide (U+HP) not only acts as a dehydrating agent but also as a buffer for the system, which minimizes further acid catalyzed isomerization and hydrolysis of the desired epoxide.

LIST OF PUBLICATIONS

1. Selective Epoxidation of Styrene to Styrene Oxide over TS-1 Using Urea-hydrogen Peroxide as Oxidizing Agent
S. C. Laha and R. Kumar, *J. Catal.* **204**, 64-70 (2001).
2. Cerium Containing MCM-41 Type Mesoporous Materials and Their Acidic and Redox Catalytic Properties
S. C. Laha, P. Mukherjee, S. R. Sainkar and R. Kumar, *J. Catal.* (in press).
3. Highly Selective epoxidation of Olefinic Compounds over TS-1 and TS-2 Redox Molecular Sieves using Anhydrous Urea-hydrogen Peroxide as Oxidizing Agent
S. C. Laha and R. Kumar, *J. Catal.* (in press).
4. Promoter induced synthesis of MCM-41 type mesoporous materials including Ti and V-MCM-41 and their catalytic properties in oxidation reactions
S. C. Laha and R. Kumar, *Microporous Mesoporous Mater.* (in press).
5. Synthesis and Characterization of Surface-modified and Organic-functionalized MCM-41 type Ordered Mesoporous Materials
S. C. Laha, P. Mukherjee and R. Kumar, *Bull. Mater. Sci.* **22**, 623-26 (1999).
6. Organo-functionalized Surface Modified MCM-41 type Mesoporous Materials having Various Organic Functional Groups
P. Mukherjee, **S. Laha**, D. Mandal and R. Kumar, *Stud. Surf. Sci. Catal.* **129**, 283-86 (2000).
7. Synthesis and characterization of mesoporous cerium silicate analogues of MCM-41 type molecular sieves
S. Laha, P. Mukherjee and R. Kumar, *Stud. Surf. Sci. Catal.* **135**, 254 (2001).
8. Promoter assisted efficient synthesis of MCM-41 type all-silica, Al- and Ti-silicate mesoporous materials under reflux conditions
S. C. Laha, C. R. Patra, S. R. Sainkar and R. Kumar, *Recent trends in Catalysis* 90-95 (1999).